Award Number: W81XWH-09-1-0391
(Enter Army Award number assigned to research, i.e., DAMD17-00-1-0296)

TITLE:
(Enter title of award)
Host Genes and Resistance/Sensitivity to Military Priority Pathogens

PRINCIPAL INVESTIGATOR:
(Enter the name and degree of Principal Investigator and any Associates)
Gerald I. Byrne, PhD

CONTRACTING ORGANIZATION:
(Enter the Name, City, State and Zip Code of the Contracting Organization)
University of Tennessee Health Science Center
62 South Dunlap, Suite 300
Memphis, Tennessee 38163-1201

REPORT DATE:
(Enter month and year, i.e., January 2001)
June 2010

TYPE OF REPORT:
(Enter type of report, i.e., annual, midterm, annual summary, final)
Annual

PREPARED FOR: U.S. Army Medical Research and Material Command
Fort Detrick, Maryland 21702-5012

DISTRIBUTION STATEMENT: (Check one)

- ✓ Approved for public release; distribution unlimited

REPORT DOCUMENTATION PAGE

Form Approved
OMB No. 0704-0188

1. REPORT DATE *(DD-MM-YYYY)*	2. REPORT TYPE	3. DATES COVERED *(From - To)*
01-06-2010	Annual	06/01/09 – 05/31/2010

4. TITLE AND SUBTITLE
Host Genes and Resistance/Sensitivity to Military Priority Pathogens

5a. CONTRACT NUMBER
W81XWH-09-1-0391

5b. GRANT NUMBER
08192004

5c. PROGRAM ELEMENT NUMBER

6. AUTHOR(S)
Gerald I. Byrne, James E. Bina, Yan Cui, Kui Li, Lu Lu, Mark A. Miller, Isao Miyairi, C. Re, Robert Williams, Mark Bix, Adrianus Boon

E

5e. TASK NUMBER

5f. WORK UNIT NUMBER

7. PERFORMING ORGANIZATION NAME(S) AND ADDRESS(ES)

University of Tennessee Health Science Center
65 S. Dunlap
Memphis TN 38163-1201

8. PERFORMING ORGANIZATION REPORT NUMBER

9. SPONSORING / MONITORING AGENCY NAME(S) AND ADDRESS(ES)
U.S. Army Medical Research and Material Command
Fort Detrick, MD 21702-5012

10. SPONSOR/MONITOR'S ACRONYM(S)

11. SPONSOR/MONITOR'S REPORT NUMBER(S)

12. DISTRIBUTION / AVAILABILITY STATEMENT
Approved for public release; distribution unlimited

13. SUPPLEMENTARY NOTES

14. ABSTRACT

The major objective of the award is to identify host genetic loci/pathways whose expression/lack of expression correlate with resistance vs. susceptibility to pathogenic challenge using recombinant inbred BXD mice. The DoD priority pathogens studied are *Francisella tularnsis* (FT), *Burhholderia*, *Acinetobacter*, *Leishmania major* (Lm), SARS, H5N1 avian influenza. The FT project has made progress with the IVS imaging of respiratory infections in mice, and generated and characterized attenuated mutant strains of FT LVS. The Acinetobacter project has generated a luminescence reporter vector, which facilitates *in vivo* IVIS imaging, and i*n vitro* studies suggest that *A. baumanii* activates TLR4 pathway. The Leishmania project revealed differences in the immunological and clinical response shown by C57BL/6 and DBA/2 parental strains to Lm. The influenza project has made progress with generating their congenic mouse lines. The mouse genomics core maintains the BXD mouse colonies and has produced full genome sequencing of the DBA/2 parental strains and collected gene expression data from the spleen. The bioinformatics core has developed and integrated the algorithms to model the genetic pathways underlying the host responses to pathogen infections, and tested the algorithm using BXD mice infected with *Chlamydia psittaci* to provide a model for infection with other DoD priority pathogens.

15. SUBJECT TERMS
Host genetics, Pathogens, Biodefense, Disease susceptibility, Humanized mice

16. SECURITY CLASSIFICATION OF:			17. LIMITATION OF ABSTRACT	18. NUMBER OF PAGES	19a. NAME OF RESPONSIBLE PERSON
a. REPORT	b. ABSTRACT	c. THIS PAGE	UU	82	USAMRMC
U	U	U			19b. TELEPHONE NUMBER *(include area code)*

Standard Form 298 (Rev. 8-98)
Prescribed by ANSI Std. Z39.18

Table of Contents

Introduction

This is our first annual progress report representing work done on the grant in the past year. Some of the data has already been reported in one of our three Quarterly Reports submitted since the grant was awarded. This report is more comprehensive and includes updates from previous reports as well as information from other investigators not previously reported. We will relate our work progress to the milestones outlined in the grant proposal.

We hypothesized that the differential susceptibility to DoD-priority pathogens is the result of host genetic variability, and that these discreet loci and/or gene pathways can be identified using BXD recombinant inbred mice. The DoD priority pathogens are naturally occurring endemic diseases, emerging infectious diseases, and potential biowarfare agents: *Leishmania major*, *Burkholderia pseudomallei*, Severe Acute Respiratory Syndrome (SARS-CoV), highly pathogenic H5N1 Avian Influenza virus, *Francisella tularensis* and multidrug resistant *Acinetobacter baumannii*.

We outlined a three-step sequence for studying each pathogen with the following specific aims:

Objective 1 (18 months): To identify specific phenotypic differences in the responses of the BXD parental strains following infection with each of the DoD-priority pathogens.

Objective 2 (6 to 30 months): To identify host genetic loci and pathways that correlate with the differential susceptibility/resistance phenotype(s) of the parental mouse strains to the DoD-prioirty pathogens.

Objective 3 (12 to 36 months): To define and validate candidate genes and gene networks responsible for differential susceptibility/resistance phenotype(s) of the parental mouse strains for each DoD-priority pathogen.

Each project is performed in parallel to achieve the milestones set forth in Objectives 1-3. As we stated in our proposal the infection models are at various levels of development, and therefore the timelines for the objectives differ according to the pathogen. We are reporting the progress of each pathogen model in the one-year period since the grant was initiated. In year 1, most of the work performed was related to Objective 1 under the following subheadings:

Objective 1a. Infection of parental strains with DoD-priority pathogens and sample collection.
We will report on ongoing studies for the different pathogens related to this objective.

Objective 1b. Infection of primary cells with DoD-priority pathogens and sample collection.
We will report on ongoing studies for the different pathogens related to this objective

The format of this report will present the data of the ongoing projects for the different pathogens, as well as reports from the animal core and bioinformatics core.

Key research accomplishments, reportable outcomes, conclusion, references

1. *Projects with DoD-priority Bacterial Pathogens*

Task 1: Infection of parental strains with DoD-priority pathogens and sample collection (Year 1: 12 months)

1.1 Studies with *Francisella tularensis* (FT)

1.1.1 Overview

We have been using the live vaccine strain (LVS) to identify phenotypic differences in the responsiveness of the two parental strains to Francisella infection. We have identified several phenotypic differences with the LVS strain that could be used as readouts for BxD analyses. Through a series of studies in which immune cell influx into the lungs of mice was determined following infection with FT we have found that FT delays neutrophil recruitment into the lung by several days (data not shown). We have also found that there is a significant difference in the number of neutrophils that are recruited into the lungs of B6 vs. D2 mice (**Figure 1**) that correlates well with the differences observed in the bacterial burdens measured in spleens and livers of infected mice (**Figure 2**). Interestingly, there appears to be an inverse correlation between the ability of D2 mice to recruit neutrophils (which in part is responsible for reduced bacterial burden in the spleen and liver) and susceptibility to infection. In our hands, D2 mice appear to be marginally more sensitive to FTLVS infection, especially when dosed with 5 x 10^4 CFU via the intranasal route (**Figure 3**).

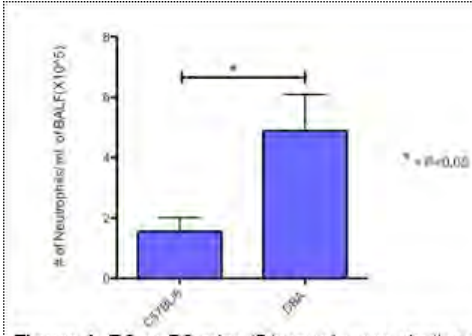

Figure 1. B6 or D2 mice (5/group) were challenged with 5 x 10e4 CFU FTLVS via the intranasal route. Five days later, brochioalveolar lavage was performed and the neutrophil populations were detected via flow cytometric analysis.

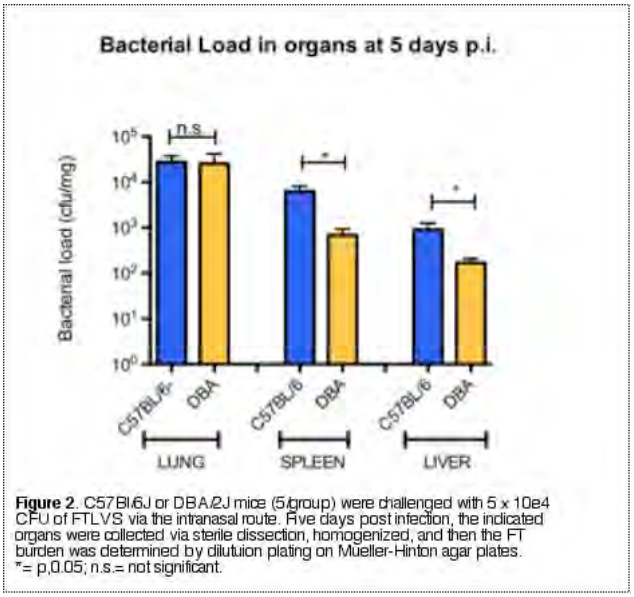

Figure 2. C57Bl/6J or DBA/2J mice (5/group) were challenged with 5 x 10e4 CFU of FTLVS via the intranasal route. Five days post infection, the indicated organs were collected via sterile dissection, homogenized, and then the FT burden was determined by dilutuion plating on Mueller-Hinton agar plates. *= p,0.05; n.s.= not significant.

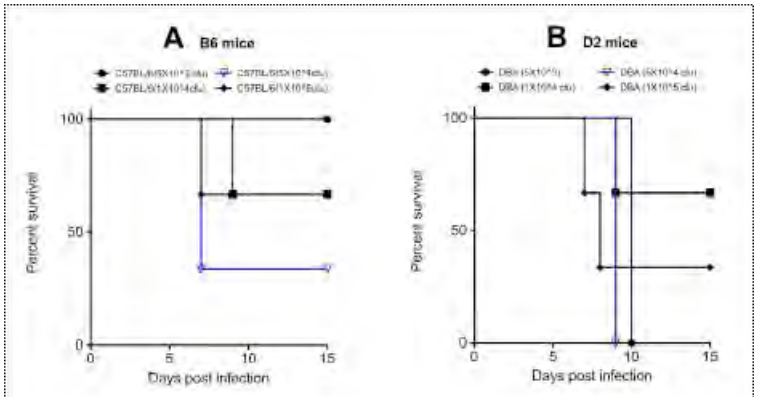

Figure 3. Female age-matched C57BL6 and DBA2J mice were infected intranasally with FTLVS at the indicated doses. Survival was recorded daily over a period of 20 days.

We have also performed several preliminary studies in an attempt to identify potential readouts of differences between B6 vs. D2 responsiveness to FT Schu S4. We have found that D2 mice express significantly higher amounts of TNF-α and SOCS3 than B6 mice, while B6 mice express larger quantities of both IFN-γ and MIP-2 than do D2 mice (**Figure 4**).

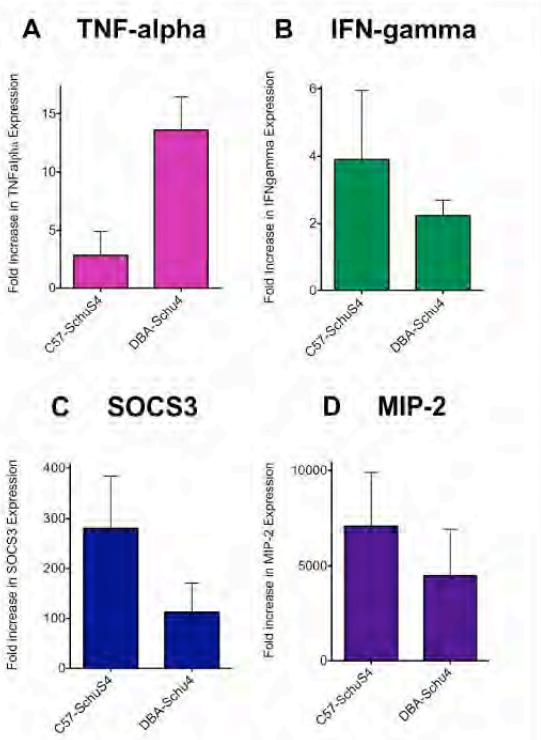

Figure 4. Age matched female mice were infected with 1X106 cfu of SchuS4 via the intraperitoneal route and sacrificed at 48 hours post infection. Total RNA was extracted from liver tissue and analyzed for gene expression. Relative levels of A) TNF alpha, B) IFN gamma, C) SOCS3 and D) MIP2 mRNA was analyzed by real-time PCR, normalized to β-actin levels and expressed as fold increase compared to RNA from PBS treated group. Data is derived from a single representative experiment and presented as mean $\pm$ SEM.

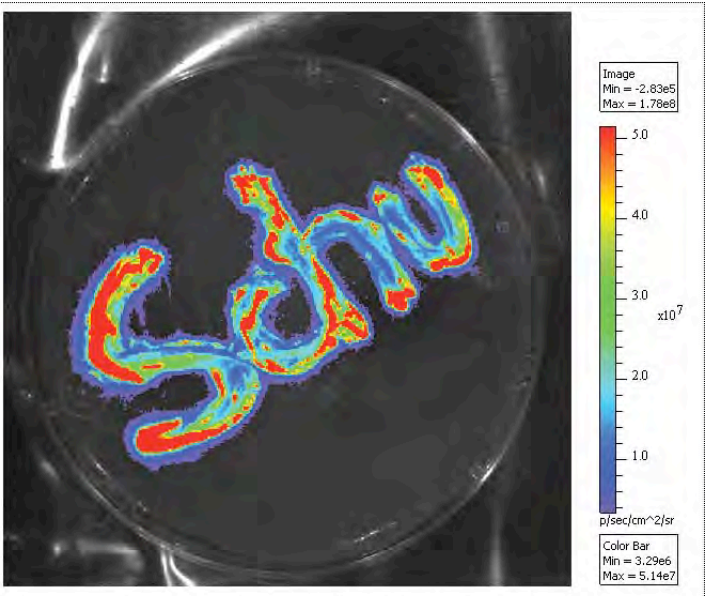

Figure 5. FT SchuS4 was transformed with pXB178-LUX and cultured overnight on modified Mueller-Hinton agar. The image was captured using an IVIS Spectrum whole animal imaging system.

We have also made progress in our efforts to monitor FT infection via whole animal IVIS imaging. First, we have verified that the pXB178-LUX reporter vector can be used to drive photon production in FT Schu S4 (**Figure 5**). In addition, using FTLVS transformed with the pXB178-LUX reporter vector, we are able to visualize dissemination of FT infection in real time following intranasal challenge (**Figure 6**). Each of the mice in this study were challenged with approximately 1 x 10^6 FTLVS in either 5µl, 10µl, 25µl, or 50µl/nare. The mice that received their challenge dose in only 5µl/nare each experienced a non-lethal upper airway/superficial cervical node/salivary gland infection that peaked in intensity between 48 and 72 hours post-infection and never disseminated to the lungs, spleen or liver. All of the other animals in the study experienced a fully disseminated infection that resulted in mortality 2-3 days after bacteria were detectable in the liver via IVIS imaging. We look forward to evaluating the ability of FT Schu S4 to disseminate from the upper airways following intranasal dosing in 5µl/nare (which fails to

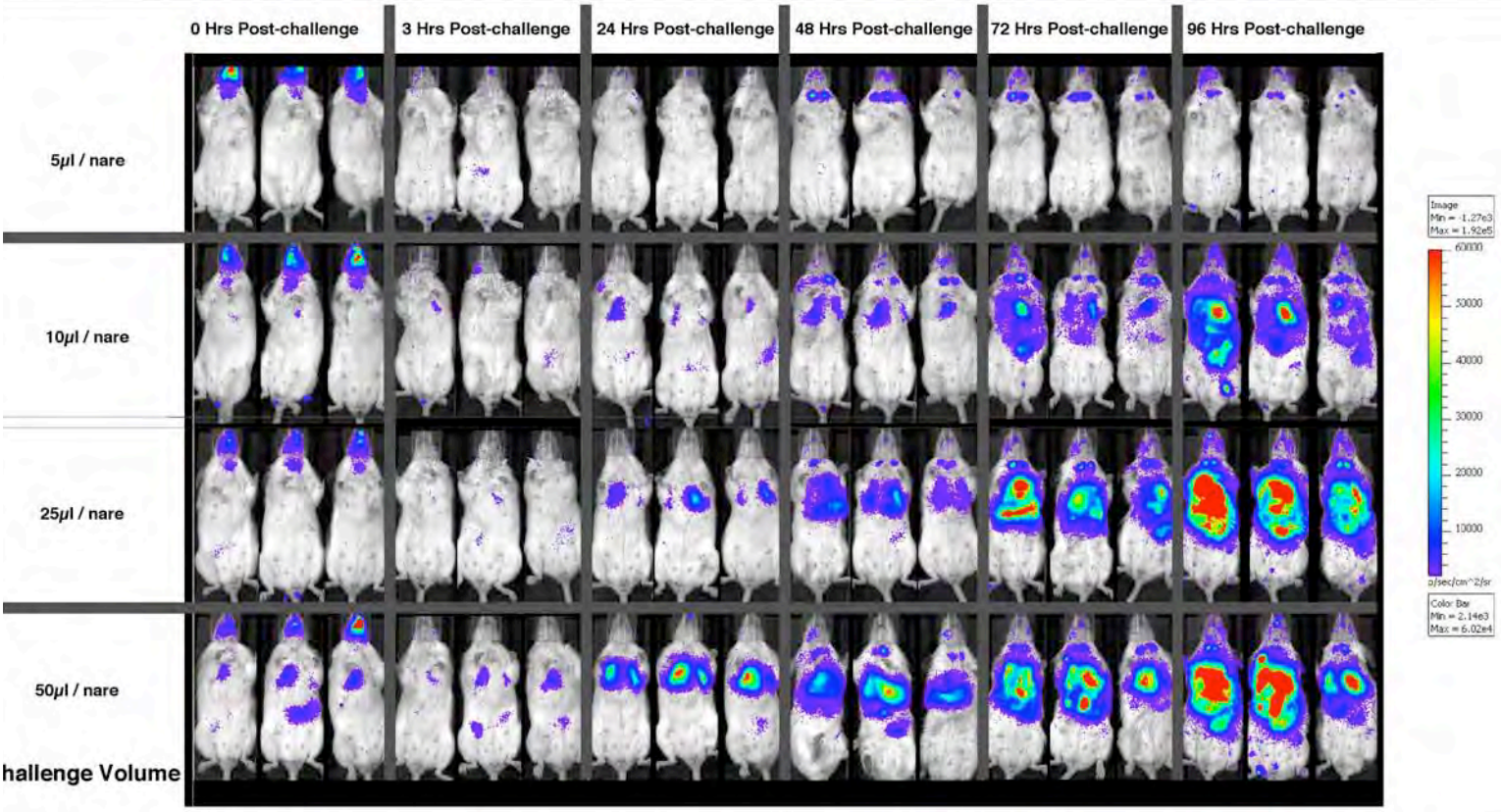

Figure 6. BALB/c mice (3/group) were challenged with 1 x 10e6 CFU of FTLVS bearing the pXB178-LUX reporter plasmid via the intranasal route in either 5µl, 10µl, 25µl, or 50µl/nare. Dissemination of FTLVS was then monitored using an IVIS Spectrum whole animal imaging system. Images were collected at the indicated timepoints post-infection. The images collected from all mice were normalizied to reflect photons per second per cm^2/sr.

deliver the bacteria efficiently to the lungs). These studies will be initiated as soon as we are able to begin FT work in the RBL. All indications are that the RBL will be available for these studies by the end of July at the latest.

We have also generated a number of attenuated mutant strains of FT LVS and have characterized a couple of them in some detail. We are currently working to generate clean deletions of the same genes (if possible) in the Schu S4 background. If the mutations are attenuating in the Schu S4 strain, we will be able to use these strains for additional BXD studies in FT. Their reduced virulence will likely make it possible for us to identify additional readouts of resistance/susceptibility differences between the parental mouse strains that would otherwise be masked by the extreme virulence of the wild-type Schu S4 strain. Any new readouts will increase our ability to identify host genetic elements that correlate with susceptibility to tularemia.

1.1.2 Reportable outcomes

Publications

1. Clinton, S. R., J. E. Bina, T. P. Hatch, M. A. Whitt, and M. A. Miller. **2010**. Binding and activation of host plasminogen on the surface of *Francisella tularensis*. *BMC Microbiol* 10:76.

1.2 Studies with *Burkholderia pseudomallei*.

We have not performed any experiments relating to the *Burkholderia* component of the project. We have received approval from the CDC to add *Burkholderia* to our select agent program, and we are in the process of acquiring the bacterium. Our efforts have been derailed to date due to a failure of UTHSC to reach a material transfer agreement with BEI Resources. We expect this to be rectified within the next month. As soon as we acquire the strain(s) we will begin studies to define resistance/susceptibility readouts in the parental strains, and then we will move into BXD stains to identify host genetic elements that correlate with strain-specific differences in disease phenotypes.

1.3 *Acinetobacter baumanii* project.

Our initial goals for the *in vivo Acinetobacter* work will include defining the baseline for challenge dosing in the two parental mouse strains. Ideally, we would identify a challenge dose that is lethal to one of the parental strains, but not lethal to the other strain. Our initial studies have suggested that survival as a readout for resistance/susceptibility differences of immunocompetent mice will not be possible with this pathogen. We are currently attempting to define more-subtle resistance/susceptibility readouts that can be used with this pathogen (influx of immune cell types into infected lungs, cytokine/chemokine production profiles, innate signaling differences, etc). Because *Acinetobacter*-related disease is typically observed as a nosocomial infection of immunologically suppressed patients, we have also begun to evaluate methods of immunosuppresion for the mouse model (cyclophosphamide treatment or gamma irradiation) prior to infection. Immunosuppression prior to challenge may enable us to more clearly define host genetic elements that relate to differences in resistance/susceptibility observed between BXD mouse strains.

We have generated a luminescence reporter vector for *Acinetobacter* and are now able to visualize the bacterium *in vivo* via IVIS imaging. In fact, we are currently using Acinetobacter-plux to develop our procedures for using our newly acquired aerosol delivery device. These studies will help us to define ideal inocula concentrations vs. exposure durations for reliable delivery of desired CFU to the lungs of mice.

We have also initiated the *in vitro* studies with Acinetobacter. In order to identify specific phenotypic differences in the response of the BXD parental strains to infection with the DOD-priority pathogen *Acinetobacter baumanii* we analyzed the innate immune response of bone marrow-derived dendritic cells of C57BL/6J and DBA/2J strains stimulated *in vitro* with live or heat killed *A. baumanii*. As shown in Figure 1, *A. baumanii* induced a pattern of cytokines characteristic of Gram-negative bacteria. In particular, induction of the chemokines RANTES and IP-10 suggests that *A. baumanii* activates the TLR4 pathway, which controls the expression of RANTES and IP-10 through the TRIF pathway. Most cytokine and chemokine transcripts were induced to the same extent in the two parental strains. The mRNA for IL-12p40 however, was induced more efficiently in the C57BL/6J cells than in DBA/2J. This effect may reflect the known polarization of the C57BL/6J strain toward the TH1 lineage.
In order to analyze whether *A. baumanii* is capable of activating the inflammasome leading to secretion of IL-1β, mouse bone marrow-derived dendritic cells were stimulated with *A. baumanii* for 18 hours and IL-1β was measured in supernatants by ELISA (figure 2). These experiments revealed that *A. baumanii* is a poor stimulator of the inflammasome. This result is consistent with the notion that the inflammasome is primarily activated by intracellular bacteria or bacteria that possess type three or type four secretion systems. Future experiments will determine whether inflammasome activation occurs *in vivo* during *A. baumanii* infection.

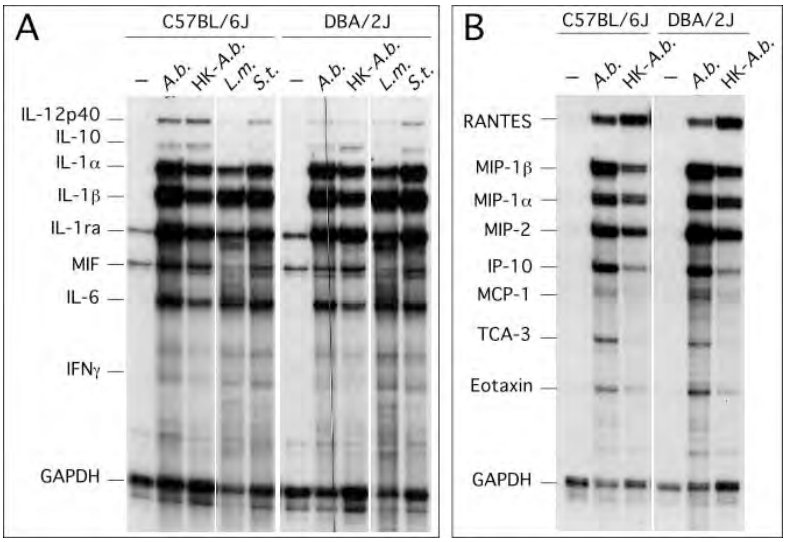

Figure 1. Comparison of innate immune response to *Acinetobacter baumanii* in C57BL/6j and DBA/2J bone marrow-derived DC. BM-DC were stimulated for four hours with live or heat-killed (HK) *Acinetobacter* (*A.b.*)(moi 10) or for 3 hours or with *Listeria monocytogenes* (*L.m.*)or *Salmonella thyphimurium* (*S.t.*). Total RNA was extracted from cells and expression of a panel of cytokines (A) and chemokines (B) was analyzed by RNase protection assay.

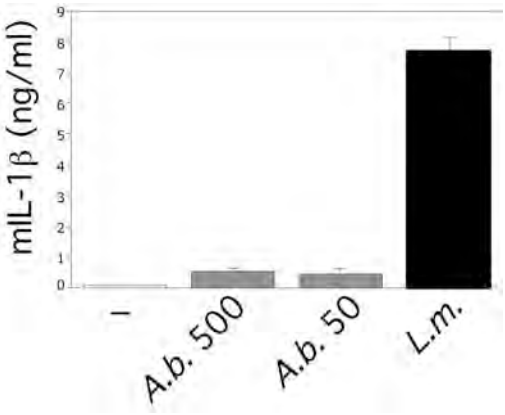

***Figure 2. A. baumanii* is a poor stimulator of the inflammasome.** BMDC were stimulated with *A. baumanii* (*A.b.*) at the indicated MOI for 18 hours or with *Listeria monocytogenes* (*L.m.*) and IL-1b was measured in supernatants by ELISA.

2. Influenza virus (H5N1) project

2.1 Conclusions reported in Quarterly report of December 2009

- Inbred mouse strains vary in their response to inoculation with highly pathogenic H5N1 influenza virus infection. Several strains are very susceptible with infection ultimately resulting in death, while other mouse strains overcome and survive the infection. The observed differences in pathogenicity are caused by the genetic differences between the mouse strains.
- Increased susceptibility to highly pathogenic H5N1 virus is associated with higher viral loads in the susceptible animals as well as increased production of pro-inflammatory cytokines. Both items are hallmarks of H5N1 infections in humans.
- Recombinant Inbred mouse strains, derived from a susceptible and a resistant mouse strain identified multiple genetic loci associated with resistance to H5N1 pathology. These loci will be referred to as QTL for influenza virus resistance (*Qivr*).
- RNA expression analysis in lungs of H5N1 infected susceptible and resistant mice also found increased pro-inflammatory cytokine mRNA expression in the susceptible strains. In addition, RNA profiling identified several candidate genes, located within the *Qivr*, linked to increased resistance following infection.

2.2 Research Accomplishments

Since the last quarterly progress report we have made significant progress with the congenic mouse lines. These lines are genetically almost identical to C57BL/6 (resistant) mice except for a small region that is derived from DBA/2. These regions correspond to the previously identified loci associated with susceptibility to H5N1 influenza virus infection. Three lines were obtained from various sources and expanded at our facility. The B6.D2.11D congenic line was homozygous upon arrival and after expansion was tested for its susceptibility to A/Puerto Rico/8/34, a mouse adapted H1N1 influenza A virus. Although we need to do larger numbers, the data suggests that there are no large difference in weight-loss and mortality of these mice compared to their wild-type controls (Figure 1). Future experiments will also determine the susceptibility to highly pathogenic H5N1 virus.

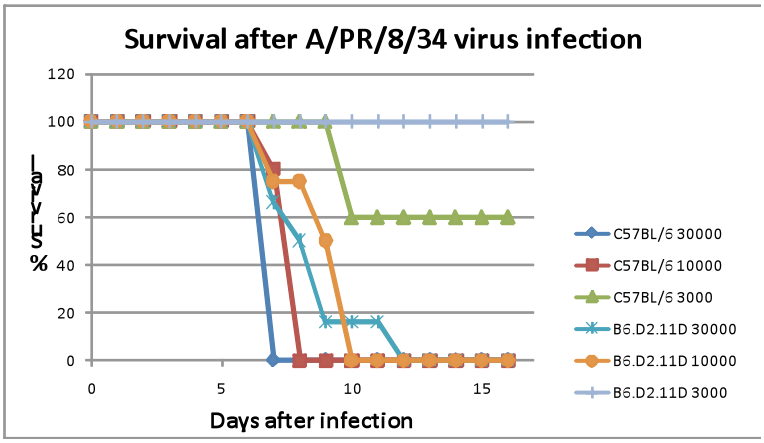

Figure 1: Survival curve after infection with different doses (EID_{50}) of A/Puerto Rico/8/34 virus.

Two other congenic mouse lines, B6.D2.7C and B6.D2.17D, arrived at our facility as heterozygous mice. After extensive breeding and genotyping we have been able to generate several breeding pairs of homozygous B6.D2.17D mice. The B6.D2.7C mice have been difficult to breed and therefore we have not been able to generate homozygous mice. Hopefully in the next progress report on H5N1 influenza we are able to report on these mice and show significant differences in disease progression for one or both of these congenic lines.

Because of the extreme susceptibility of DBA/2 mice to highly pathogenic H5N1 virus, we hypothesized that other influenza A viruses could also induce severe disease in these mice. A set of 18 different human or avian influenza A virus isolates belonging to 8 different subtypes of influenza virus were pathotyped in DBA/2 and C57BL/6 mice. We found that more than 70% of them were pathogenic for DBA/2 mice while only two viruses were pathogenic for C57BL/6 mice (Table 1).

Table 1: Mortality after intranasal inoculation of DBA/2 and C57BL/6 mice with various human and avian influenza A virus isolates

Influenza A virus isolate	Subtype	DBA/2		C57BL/6
		10^6 EID_{50}	10^4 EID_{50}	10^6 EID_{50}
A/Memphis/3/2008 [1]	H1N1	100	88	0
A/California/4/2009 [2]	H1N1	100	100	60
A/mallard/Alberta/79/2003	H2N3	33	0	ND [4]
A/mallard/Alberta/33/2004	H2N4	0	0	0
A/pintail duck/Alberta/66/2005	H4N1	20	0	0
A/mallard/Alberta/147/2007	H4N6	0	ND	ND
A/shorebird/Delaware/101/2004	H5N7	20	0	0
A/ruddy turnstone/Delaware/103/2007	H5N9	100	25	ND
A/teal/Hong Kong/W312/1997	H6N1	100	100	40
A/mallard/Alberta/154/2003	H6N5	100	40	0
A/shorebird/Delaware/22/2006	H7N3	100	100	0
A/mallard/Alberta/177/2004	H7N9	0	0	0
A/quail/Hong Kong/G1/1997	H9N2	100	0	0
A/duck/Hong Kong/Y280/1997	H9N2	100	20	0
A/mallard/Alberta/162/2007	H9N5	0	0	ND
A/mallard/Alberta/221/2006	H9N6	0	0	ND
A/blue-winged teal/Alberta/271/2007	H10N5	100	75	0
A/mallard/Alberta/56/2004	H10N7	100	75	0

[1] Human influenza A virus isolate, [2] Human 2009 pandemic H1N1 virus isolate, [4] ND, not done.

Because 2009 heralded the first influenza pandemic of the 21st century, we also pathotyped a pandemic H1N1 influenza virus strain called A/California/04/09. The DBA/2 mice were extremely susceptible to this virus with a LD_{50} of 30 infectious particles, while only a few C57BL/6 mice succumbed to infection with 10^6 particles. Combined these data show that DBA/2 mice are very susceptible to most natural non-adapted influenza A viruses, and therefore these mice can be used as a new small animal model in vaccine or therapeutic efficacy studies.

We used the model to understand one of the fundamental questions of the 2009 influenza pandemic; why are the elderly protected from infection with the pandemic H1N1 virus? *In vitro* hemagglutination inhibition and virus neutralization assays suggested that sera from elderly contain cross-reactive antibodies; however nobody had shown that these antibodies were fully functional *in vivo*. For our study we obtained human sera from 60-80 year old individuals and tested the sera for the presence of cross-reactive antibodies against the pandemic H1N1 virus. Sera that contained virus neutralizing antibodies were pooled and injected intraperitoneally prior to challenge with a lethal dose of A/California/04/09. As a control we used sera from aged matched individuals that lacked any detectable cross-reactive antibodies.

As shown in Figure 2, the cross-reactive antibodies in sera from unexposed individuals protected the mice from excess weight-loss and mortality compared to negative sera or PBS controls. Based on these findings we suggest that the elderly are partially protected against the pandemic virus and that these antibodies were most likely derived from a prior infection with a related H1N1 virus.

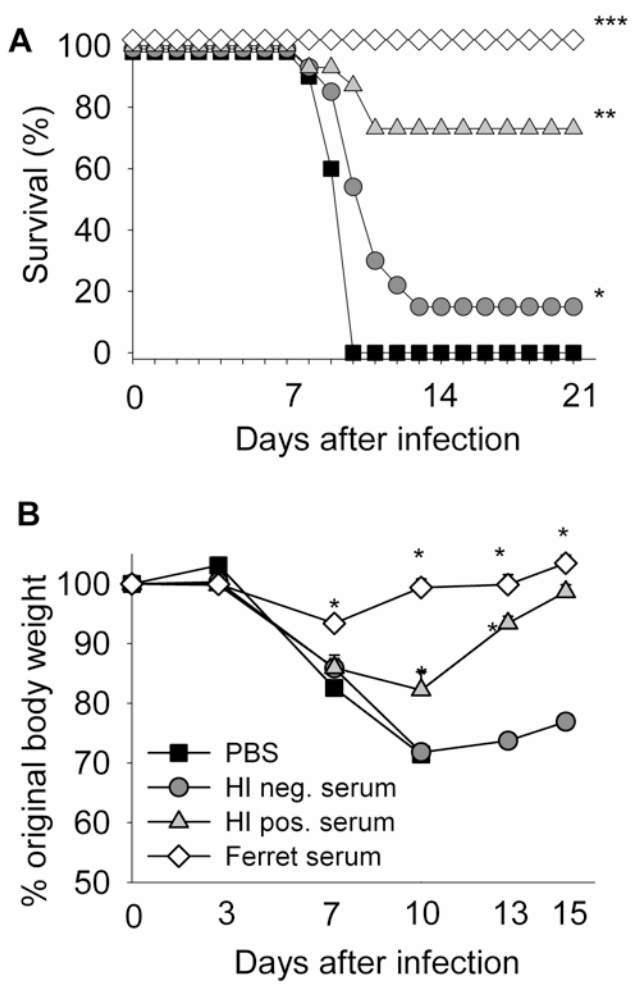

Figure 2 Survival curve (A) and weight loss (B) after intranasal challenge with a lethal dose of A/California/4/09 pandemic H1N1 virus.

2.3 Conclusions

- DBA/2 mice are highly susceptible to many non-adapted isolates of influenza A virus
- DBA/2 mice can be used as a sensitive small animal model in vaccine and therapeutic efficacy studies specific for influenza virus
- Cross-reactive antibodies identified in sera from elderly individuals is fully functional in vivo and protects against severe morbidity and mortality

2.4 Reportable outcomes

Publications

1. Boon AC, Debeauchamp J, Krauss S, Rubrum A, Webb AD, Webster RG, McElhaney J, Webby RJ. Cross-reactive neutralizing antibodies directed against pandemic H1N1 2009 virus are protective in a highly sensitive DBA/2 influenza mouse model. J Virol. 2010; in print.

Presentations

- Lectures at University of Maryland, College Park, Maryland and Washington University, St Louis, Missouri.
- Presentation at the BXD World meeting in Braunschweig, Germany 2009

Abstracts

- Abstract at the BXD World meeting in Braunschweig, Germany, 2009
- Abstract for the Options for the Control of Influenza VII, Hong Kong, 2010

Animal models

Developed a new sensitive small animal model to study human and avian influenza A viruses

3. *Leishmania major* project

3.1 Overview

We set out in year 1 of this study to determine the feasibility of using the BXD resource to study the host response to *Leishmania major* (*Lm*), a protozoal parasite that causes a disease in mice similar to cutaneous leishmaniasis in humans. The murine model of *Leishmania* infection has been very well characterized. For our studies purified metacyclic promastigote stage *Lm* (WHOM/IR/-/173) was injected at several different doses into both hind footpads (*ifp*) of cohorts of mice (aged 60±10 days). Just prior to and at weekly intervals post-infection, we followed the clinical infection course by using a metric caliper to monitor changes in the diameter of both hind footpads. In addition, at regular intervals we recovered ~50 µl of orbital sinus blood for analysis of serum Ig isotype and circulating cytokine levels. At selected intermediate times and at the endpoint of experiments (~8-11 weeks), animals were sacrificed and analyzed as follows. Local and disseminated parasite burdens were determined by scoring cultures of serially diluted spleen and footpad homogenates for outgrowth of parasites. Global gene expression profiles will be determined at a later date if additional funding is approved. This will utilize RNA recovered from snap-frozen draining popliteal lymph nodes stored in

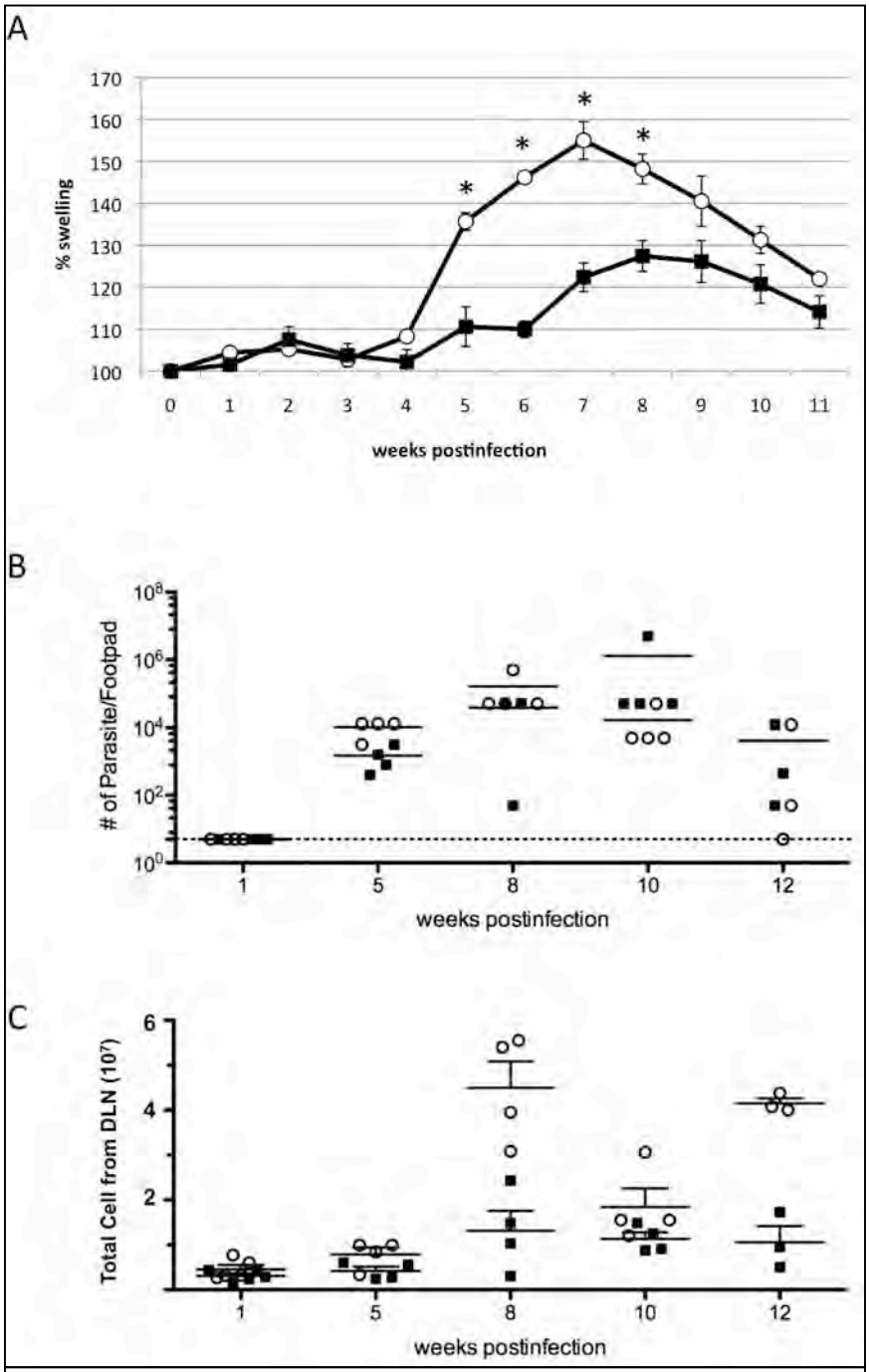

Figure 1. Pathology of *L. major* in C57BL/6 (open circles) and DBA/2 (solid squares). Mice were infected subcutaneously in hind footpads with 2 x 10^6 parasites. (A) Shown is weekly footpad thickness as measured by metric caliper. Error bars indicate standard error. (B) Shown are parasites recovered from the hind feet of infected mice as determined by serial dilution of feet homogenates cultured on blood agar plates for 7-10 days. (C) Shown are total mononuclear cell numbers per draining popliteal lymph node, as determined by trypan blue exclusion of single cell suspensions.

our tissue bank. Cell suspensions made from popliteal lymph node were used to determine antigen-specific recall cytokine responses to soluble *Lm* antigen (SLA). As shown in Figure 1A the data we obtained from clinical course we observed was consistent with published reports with DBA/2 being less resistant than C57BL/6. Despite the differential clinical course, parasite burdens were similar between the BXD parental strains (Figure 1B). These results suggested that differences in the inflammatory response to *Lm* might be responsible for the contrasting clinical outcomes. In support of this interpretation, draining popliteal lymph node cellularity was significantly higher in DBA/2 versus C57BL/6 (Figure 1C).

To investigate the nature of the differential inflammation exhibited by DBA/2 and C57BL/6 in response to *Lm* infection, we performed FACS analysis of draining popliteal lymph node cells. We found that the number of MHC class II positive cells (dendritic cells and macrophages) was significantly elevated in DBA/2 versus C57BL/6 (Figure 2A). By contrast, the number of CD4 positive cells (T helper and NKT cells) was similar between BXD parental strains, consistent with the similar kinetics of parasite clearance and the known dependence of this on the adaptive T helper immune response (Figure 2B). Interestingly, we also noted that the number of CD4/CD25/Foxp3 positive T regulatory cells was also significantly elevated in DBA/2 versus C57BL/6 (Figure 2C). The significance of this finding has yet to be determined.

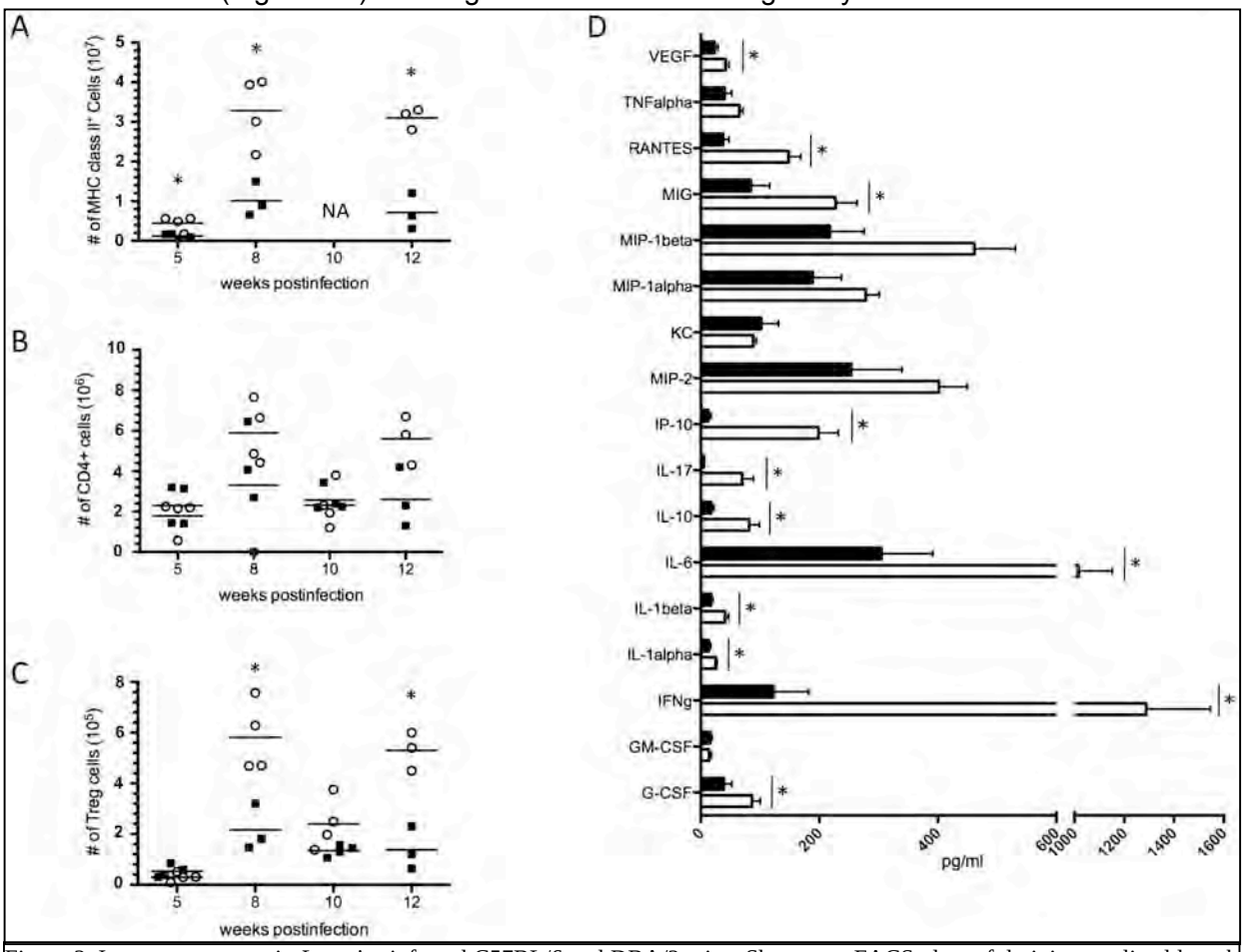

Figure 2. Immune response in *L. major* infected C57BL/6 and DBA/2 mice. Shown are FACS plots of draining popliteal lymph node cells. Each dot represents the number of (A) MHC class II+, (B) CD4+ and (C) CD4+CD25+Foxp3+ (Treg) cells per LN from individual C57BL/6 (open circles) and DBA/2 (closed squares) mice. (D) Shown is cytokine and chemokine content (as measured by Milliplex MAP kit) in the supernatant of draining popliteal lymph node cells cultured for 24 hours with soluble L. major antigen (SLA). Open bar: C57BL/6 mice, Closed bar: DBA/2. Asterisks indicate significant differences ($P < .05$).

Finally, to determine whether popliteal lymph node cells from infected DBA/2 and C57BL/6 mice exhibited functional differences that could potentially explain the differential inflammatory response, we cultured popliteal lymph node cells from mice infected for 8 weeks with soluble leishmania antigen (SLA) for 24 hours and then used a Milliplex bead assay to measure cytokine and chemokine content in culture supernatants. As shown in Figure 2D, with just a few exceptions, the soluble mediator response was significantly more vigorous from DBA/2 than from C57BL/6. Taken together, our results indicate that the BXD parental strains exhibit a very strong genetically programmed difference in their inflammatory response to *Lm*. Further, our results demonstrate that phenotypic analysis of the BXD resource will be a fruitful endeavor. Finally, our results establish the optimal conditions for reproducing a stereotypic infection course, optimal time points for phenotypic measurement and validation of an informative set of phenotypic measures with which to characterize the genetic contribution to the host response to *Lm* infection.

3.2 Key Research Accomplishments

1. Developed an optimal dosing regime for reproducible *Lm* infection-dependent clinical course.
2. Selected and optimized a set of *in vivo* and *ex vivo* phenotypic readouts with which to study the immunological, parasitological and clinical aspects of *Lm* infection in mice.
3. Identified optimal time points for phenotypic assessments.
4. Together, these accomplishments set the stage in year 2 for successful completion of the phenotypic analysis of the BXD resource.

3.3 Reportable Outcomes

Thus far, our studies have revealed that parental strains C57BL/6 and DBA/2 differ in their immunological and clinical responses to *Lm*. Interestingly, these differences are not correlated with parasitological score, suggesting underlying genetic differences in inflammatory responses to *Lm*. Thus, genetic dissection of these differences using the BXD resource is likely to be highly informative with regard to fundamental aspects of the inflammatory response.

3.4 Conclusions

Our initial studies have revealed that the host response to *Lm* is well suited for genetic analysis using the BXD mouse resource. Parental strains C57BL/6 and DBA/2 exhibit highly significant and reproducible differences in immunological and clinical scores. Interestingly, these are not correlated with parasitological score, suggesting that underlying genetic differences in the inflammatory response to *Lm* are responsible for differential clinical outcomes. We have established an optimal dosing regime for obtaining reproducible *Lm* infection courses, suitable for analysis of BXD mice in independent cohorts over a period of time. Further, we have selected and optimized an informative set of *in vivo* and *ex vivo* phenotypic readouts to study the immunological, parasitological and clinical aspects of *Lm* infection in mice. Finally, we have selected optimal time points for phenotypic assessments. With these preliminary studies now completed, we are well positioned to begin phenotypic scoring of the BXD mice. At this point, we request additional funding to support expression profiling of RNA collected from draining popliteal lymph nodes of uninfected and infected mice. Additional funding would cover the cost of preparing RNA from frozen tissue saved in our archive, preparing reverse translated DNA libraries suitable for Illumina deep sequencing and Illumina sequencing itself. The additional data we seek will permit detection of eQTLs that regulate the host response to *Lm*. Further by the application of Bayesian analysis, it may be possible to discern cause/effect relationships between specific DNA variants, expression and phenotype QTLs.

4. Severe Acute Respiratory Syndrome (SARS Co-V) project

We have fully executed the Material Transfer Agreements with CDC and NIH for transferring the wild-type (Urbani strain) and mouse adapted (MA-15) SARS coronaviruses to UTHSC and have obtained both viruses. The personnel engaged in the SARS project have gone through DOJ clearance and have been approved for access to select agents and/or toxins. They have also been enrolled in the UTHSC Animal Care and Use Occupational Health & Safety Program and fit-tested.

In a related project, we have further characterized the interferon (IFN) antagonism mediated by the papain-like proteases (PLPs) of two important human coronaviruses, SARS-CoV and NL63, in collaboration with S. Baker at Loyola University - Chicago. The results show that the PLP2 of NL63, like what we have previously demonstrated for the PLP of SARS-CoV, blocks IFN induction by inhibiting the activation of IFN regulatory factor-3, a latent transcription factor pivotal for type I IFN synthesis. Furthermore, the PLP IFN antagonism is enhanced by, but is not strictly dependent on, the catalytic activity of the PLP enzyme. A manuscript has been published to report these findings (see below).

Reportable outcomes

Publications

1. Clementz MA, Chen Z, Banach BS, Wang Y, Sun L, Ratia K, Baez-Santos YM, Wang J, Takayama J, Ghosh AK, **Li K**, Mesecar AD, Baker SC. Deubiquitinating and interferon antagonism activities of coronavirus papain-like proteases. *Journal of Virology* 2010; 84: 4619-4629.

5. Systems Genetics using a prototype model of *Chlamydia psittaci* genetic susceptibility.

5.1 Overview

In a previous study, we determined that polymorphisms in two genes *(Iigp2* and *Irgb10*) between B6 and D2 mice account for differential susceptibility (Difference in 100% Lethal dose >100,000 fold) to infection with *C. psittaci*. This model was investigated further to serve as a proof of concept system to perform systems genetic studies using the BXD mice in infectious diseases. We generated immune and disease phenotype data for 59 BXD strains infected with *Chlamydia* and microarray based transcriptional analysis in 40 BXD strains. These data were used to perform QTL analysis for each parameter and the correlation of each parameter was also investigated.

5.2 Multi-scale QTL analysis

BXD mice were infected and were assessed for pathogen load, immune parameters (32 cytokine and immune cell population), and disease outcome. Results indicate that while Chr11 locus influences variations in many parameters several other unique genetic loci control individual parameters (Figure 1). In particular, we found that some Th1/Th2 cytokines (IFNγ, IL10) were under the control of Chromosome 1 and 8. The chromosome 8 locus reached a statistically significant level with an LRS >20 and mapped to candidate genes Nod2 and Cyld that are known to be negative regulators of NFkB (Figure 2).

Figure 1 (LEFT). QTL analysis of disease phenotypes (weight loss day 6) and immune phenotypes (pathogen load, macrophage activation status, neutrophil recruitment, 20 cytokine levels:). X-axis represents various traits and Y-axis represents position of the genetic locus on the mouse genome (chromosome 1-19, X). Statistically significant association of a genetic locus with a given trait is given a color. Cold colors indicate that the B6 genotype increases trait value and warm colors indicate that D2 genotype increases value. Results indicate that the previously defined QTL on Chr 11 dictates immune responses observed. Multiple other genetic loci (Chr 1, 8, 9) .

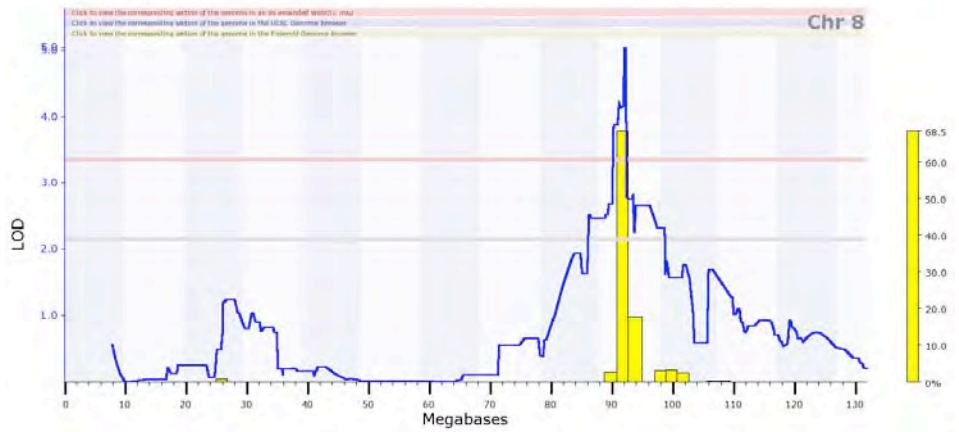

Figure 2. QTL analysis of IFNg level induced by Chlamydia. The X axis represents the position on the Chromosome 8 and blue line indicates level of association of IFNγ level with the genetic marker on the chromosome. The QTL at position 91MB includes 20 genes including Nod2 and Cyld.

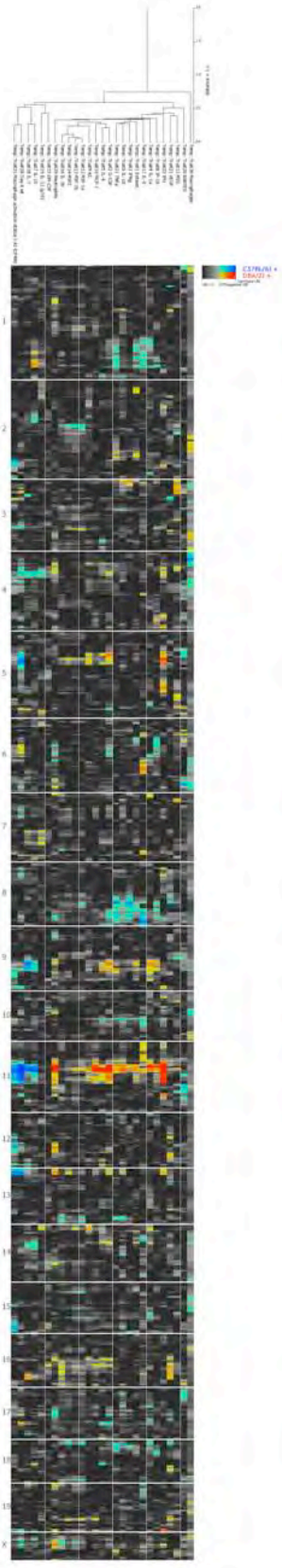

Figure 1.

5.3 Modeling Immune phenotypes

In order to generate a model of how individual immune phenotypes influence each other, a correlation analysis was performed for all immune phenotypes using Pearson and Spearman correlations. Strongest positive correlation with the disease phenotype (weight) was found with macrophage activation status, rather than *Chlamydia* load (Figure 3). The macrophage activation status itself had a strong negative correlation with *Chlamydia* load as well as percentage of neutrophils in the inflammatory cell population. The level of cytokines such as IFNγ and TNFα were not associated with the weight changes observed in this model.

In order to determine whether the phenotype was a direct consequence of the pathogen burden we examined the correlation of pathogen load with weights of individual mice according to the genotype at chromosome 11 encoding the IRGs. Results demonstrated that mice that have the B6 genotype at the locus are tolerant to increases in the pathogen load (Data not shown). Also, there was a significant overlap in the pathogen load between two genotypes. These findings suggest the IRGs encoded in chromosome 11 locus affect disease outcome by a mechanism of tolerance (ability to withstand increasing pathogen burden) rather than resistance (ability to restrict pathogen load).

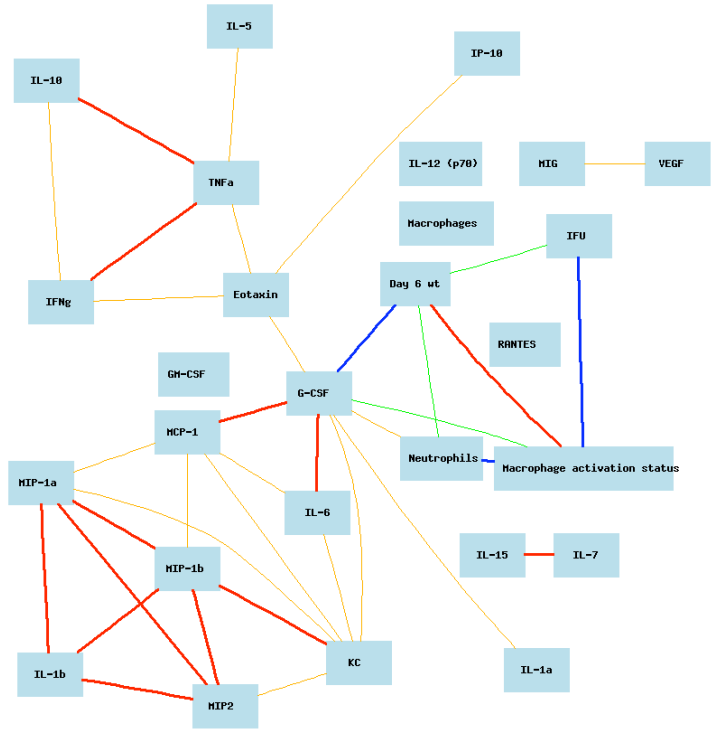

Figure 3: Graphical representation of the association among phenotypes .A line between the phenotypes indicate significant correlation. Warm colored lines represents a positive correlation. Cold colors represents a negative correlation. Thicker lines (R value >0.7). Thin lines (R value 0.5-0.7). The strongest positive correlation with the disease phenotype (weight) was found with macrophage activation status, rather than Chlamydia load. The macrophage activation status itself had a strong negative impact on Chlamydia load as well as percentage of neutrophils in the inflammatory cell population. The level of cytokines such as IFNγ and TNFα were not associated with the weight changes observed in this model suggesting cellular phenotypes drive pathogenesis.

5.4 Transcriptional analysis and eQTL mapping.

We have performed a microarray based transcriptional analysis of peritoneal lavage samples obtained from 40 BXD strains infected intraperitoneally with *Chlamydia* and an eQTL analysis using this data set. Consistent with other studies, eQTLs with the highest associations were primarily cis-acting QTLs, however the analysis also reproduced trans-acting QTLs that have been reported by others in the past (Figure 4).

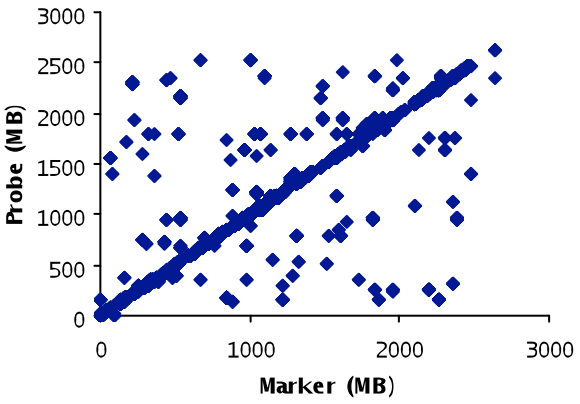

Figure 4: eQTL analysis of microarray transcriptional profiling from Chlamydia infected BXD strains. Position of the transcript on the Chromosome is indicated on the Y axis and position of the QTL that controls transcriptional l levels is indicated on X axis. Each dot represents transcript/QTL with LRS>24 with false discovery rate of 5%. Numerous cis-QTLs as well as trans-QTLs are represented.

5.5 Reportable outcomes

Publications

1. Miyairi I l, Laxton J, Ziebarth J, Williams R, Lu L, Byrne G, Cui Y. Systems Genetics Analysis of *Chlamydia psittaci* Infection*. 2010.* Proc. 12th Int. Symposium on Human Chlamydial Infections, Schachter et al eds, pp 197-200, June 20-25, Hof bei Salzburg, Austria.

(see Appendices)

5.5 Model construction

Data of high order traits and transcriptional analysis was combined to construct hierarchical model of how genotype at a particular QTL influences gene transcription and outcome of high order traits. Over 10 models were constructed. An example is shown in Figure 5. This model suggests that Chr8 locus (described in Figure 2) controls IFNγ levels through Prdx2. This is biologically plausible association given the presence of two candidate genes on Chr 8 (Nod2 and Cyld), and because Prdx2 is known to be a negative regulator of NFκB and control Th1 cytokine levels. This will require further validation.

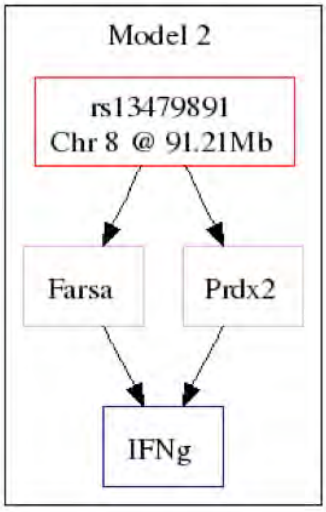

Figure 5. Model of how a genetic locus controls downstream gene and phenotype. This model indicates that a gene/or genes in the Chr 8 interval (described in Figure 2) controls IFN gamma levels through the regulation of Farsa or Prdx2.

6. Mouse genomics core

6.1 Gene expression data collection from BXD spleen

We plan to collect spleen gene expression data from 50~70 BXD strains and 20~30 inbred mouse strains (2 chips/strain) for genetic analysis of DoD priority pathogens. So far we have run the Affy mouse GENE 1.0 array for about 110 samples including 52 BXD strains and 27 inbred strains (see table below). The RNA has been extracted for the remaining samples. Most of them have passed QC and are in the queue to be run on the chip.

BXD strain	chip/strain	BXD strain	chip/strain	Inbred strain	chip/strain
BXD2	2	BXD55	1	129P3/J	2
BXD5	1	BXD60	2	129S1/SvImJ	2
BXD6	1	BXD61	1	129X1/SvJ	2
BXD8	1	BXD62	1	B6D2F1	1
BXD9	3	BXD64	1	BALB/cByJ	2
BXD11	1	BXD66	1	BALB/cJ	2
BXD12	1	BXD69	2	BTBR T+ tf/J	1
BXD13	2	BXD70	1	C57BL/6ByJ	2
BXD14	2	BXD71	1	C57BL/6J	2
BXD16	1	BXD73	2	C57BL/10J	1
BXD18	2	BXD75	2	C57BLKS/J	2
BXD21	2	BXD79	1	CBA/CaJ	1
BXD22	1	BXD80	2	DBA/2J	1
BXD24	1	BXD83	1	FVB/NJ	1
BXD25	1	BXD84	1	ILS	2
BXD27	2	BXD86	2	ISS	1
BXD32	1	BXD87	1	KK/HlJ	1
BXD33	1	BXD89	3	LG/J	2
BXD34	2	BXD90	2	LP/J	2
BXD39	2	BXD92	1	NOD/LtJ	1
BXD40	2	BXD95	1	NZB/BiNJ	1
BXD42	1	BXD96	1	NZO/HlLtJ	1
BXD43	1	BXD97	1	NZW/LacJ	2
BXD44	2	BXD98	1	PL/J	1
BXD48	2	BXD99	2	PWD/PhJ	1
BXD50	3	BXD101	1	PWK/PHJ	1
				SJL/J	1
				WSB/EiJ	1

6.2 BXD mice colony for DoD priority pathogens

We maintain more than 500 cages for DoD including most of Jax BXD strains and all of UT BXD strains, and BXD parental strains. During 2009-2010 year, we have provided about 1000 mice for DoD projects. Moreover, we are developing 50 new BXD strains in order to increase the power of genetic analysis. About 25 new strains have passed generation 4, and 20 strains are in generation 6~8.

6.3 Sequence of DBA/2J

The parental strains of BXD RI mice are C57BL/6J (B6) and DBA/2J (D2). The B6 sequence was completed by the NIH several years ago, but the D2 genome-wide sequence data is still missing. Though the BXD panel is widely used to find the gene loci that control many diseases and phenotypes, cloning the genes for these QTLs is quite challenging work, creating a bottleneck in the research process. The sequence polymorphisms between B6 and D2 are key information for QTL cloning, especially eQTL cloning. As such, we sequenced the D2 genome by co-operating with our colleagues.

Genomic DNA from littermate DBA/2J females (generation 224) was originally prepared from liver tissue. These fully inbred animals were born at UTHSC, their parents being DBA/2J F223 foundation stock obtained directly from the Jackson Laboratory in mid 2008 (date of birth 07/27/2008).

We sequenced the genome of DBA/2J using next-generation sequencing technology: ABI SOLiD in our campus and Illumina GA2 in UCLA. We produced 10.04 billion (6.66 billion from ABI SOLiD and 0.38 billion from Illumina GA2) of mate-paired reads that align to the B6 reference mouse genome, of which 3.41 billion (143.77 Gb nucleotides) have been mapped to the genome by MAQ program for reads from Illumina GA2, and by ABI Corona Lite pipeline for reads from ABI SOLiD. This indicates an average depth-coverage of ~55× (Table 1). However, the depth-coverage increases to ~79× when we use only MAQ program to map the short reads from both Illumina GA2 and ABI SOLiD.

Table 1: Summary of sequencing data for the D2 genome

Sequencing method	Clone insert size	# of total reads (Billion)	# of total nucleotides (Gb)	# of mappable reads (Billion)†	# of mappable nucleotides (Gb)†	Sequence depth (X)*
ABI SOLiD	1-2 kb	1.29	32.27	0.80/1.23	19.95/30.83	7.67 /11.86
	2-3 kb	4.32	163.89	1.92/3.09	72.39/114.87	27.84/44.18
	3-4 kb	1.05	46.06	0.34/0.52	16.28/24.98	6.26/9.61
Subtotal		6.66	242.22	3.06/4.84	108.62/170.23	41.77/65.47
Illumina GA2	200 bp	0.38	41.87	0.35	35.15	13.52
Total		10.04	284.09	3.41/5.19	143.77/205.38	55.29/78.99

*Assumed B6 reference genome size is 2.6 Gb. Read depth was determined through the calculation of all mappable nucleotides divided by the size of B6 reference genome.
† The number of mappable reads and nucleotides for data from ABI SOLiD using ABI Corona Lite (top) and MAQ (bottom) mapping tools.

We detected approximately 4.6 million SNPs variants between the DBA/2J and C57BL/6J reference genome, including 4,235,516 and 3,147,000 SNPs from ABI SOLiD by ABI Corona Lite pipeline and Illumina GA2 by MAQ program, respectively (Figure 1). Compared SNPs between ABI SOLiD and Illumina GA2, 2.72 million SNPs are shared between two platforms. Around 0.34 million SNPs were exclusively presented in GA2 and 1.3 million SNPs were exclusively presented in SOLiD platform (figure 2). The number of SNPs varied among chromosomes, with the highest rate on chromosome 1 and lowest rate on chromosome X (Figure 1). We observe long segments of either extremely high (40 SNPs per 10 kb) or extremely low (0.5 SNPs per 10 kb) polymorphism rates. According to the position of SNPs, we mapped all SNPs to the structure

of known reference genes. As a result, we identified 1,667,877 (36.4%) SNPs were located within gene regions (Figure 1). Of 1,667,877 SNPs, the vast majority (95.8%) of SNPs was located within intron regions, followed by exon (1.97%), 3'UTR (1.84%) and 5' UTR (0.33%). There are average 68 SNPs per gene according to the 24,341 reference genes from UCSC.

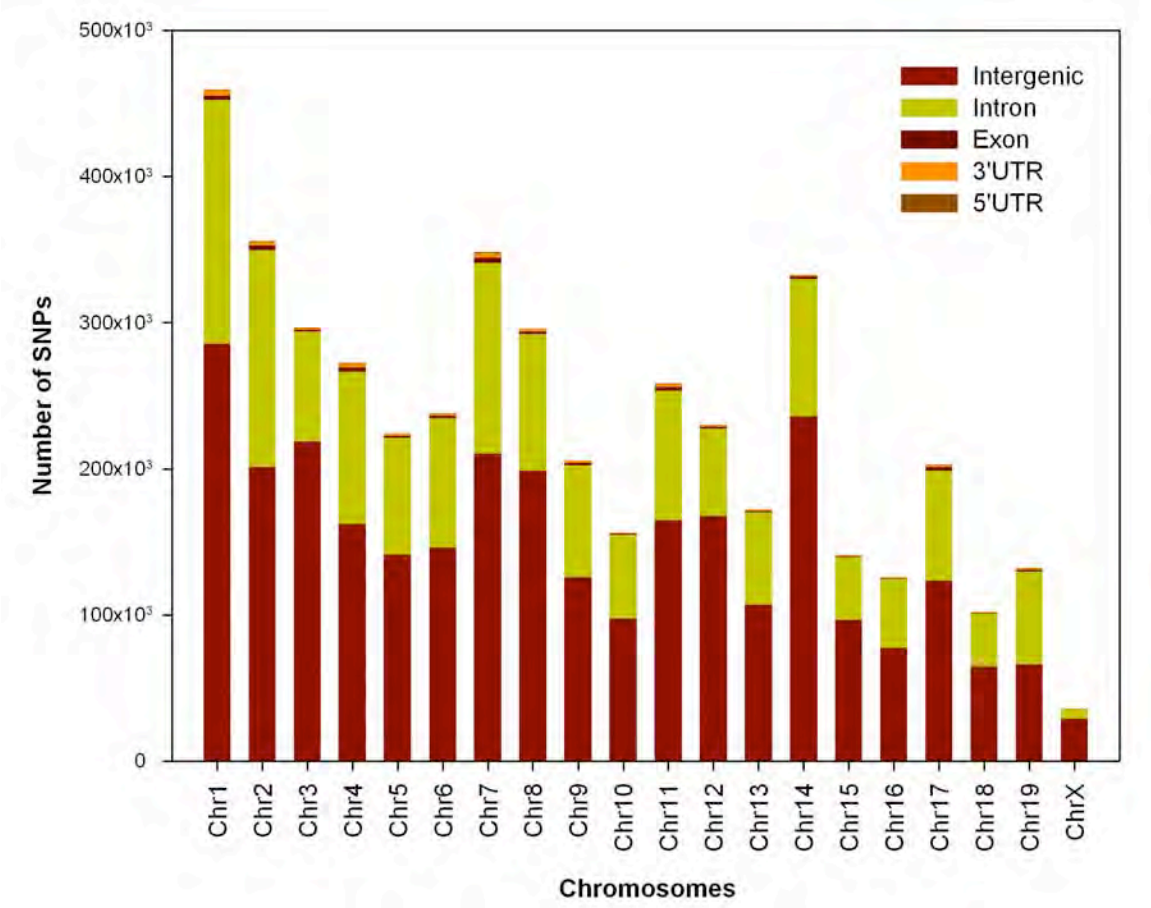

Figure 1. SNPs distribution across each chromosome from SOLiD and GA2.

To further assess our ability to call genotypes correctly by sequencing, we compared our data with 1.03 million SNPs from the public dbSNP database. Approximately, 0.93 million SNPs from public dbSNPs are shared with our SNPs. In addition, to confirm the new SNPs that we found, we randomly selected about 500 SNPs that are exclusively presented in SOLiD and GA2 platform and novel as indicated by an absence in public dbSNPs for experimental validation using Sanger capillary sequencing method. More than 90% of SNP have been validated in both SOLiD and GA2 platform.

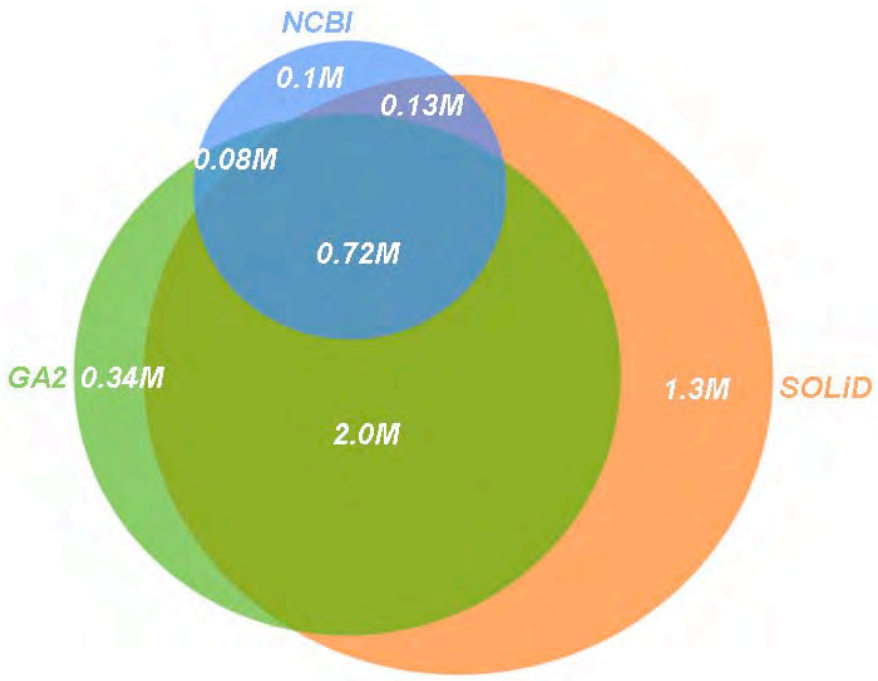

Figure 2. Comparison of SNPs between GA2, SOLiD and dbSNPs.

7. Construction of gene network models

7.1 Overview

During the first year of the grant support, we have developed and integrated algorithms (eQTL mapping, Bayesian network, SNP analysis etc.) to model the genetic pathways underlying the host responses to pathogen infections. We used BXD mice infected by *Chlamydia psittaci* to test our algorithm because the datasets for other pathogens are not yet available. The analysis of data from Chlamydia infected BXD mice will provide a model for the analysis of the analysis of data from BXD mice infected by other pathogens. B6 and D2 mice have significant differences in response to infection with Chlamydia [1]. Our goal is to determine the genetic variations between B6 and D2 mice that result in these differences to Chlamydia susceptibility and form genetic networks that link genotype to gene expression to phenotype. These networks provide testable hypotheses, which can be used to validate the networks and confirm the importance of the selected genomic and gene expression differences to disease outcomes.

7.2 Adjustment of microarray batch effects.

One common problem in evaluating microarray data is that all samples in a study cannot be analyzed simultaneously because of practical limits to the number of samples that can be prepared or analyzed at one time. The microarray data obtained will then contain non-biological experimental errors, termed batch effects, which are correlated with the time the sample was analyzed. Microarray data from 44 BXD strains were observed to contain batch effects, as clustering of the microarray data showed clusters were highly correlated with the batch. Initially, the microarray data was adjusted so that the averages of the different batches for each transcript were identical; however, clustering analysis showed that significant batch effects persisted. ComBat [2], an implementation of an empirical Bayes method, was then used to adjust the data, as it has been developed to reduce batch effects for data where the number of samples is much fewer than the number of measurements. ComBat has been successfully used to correct for batch effects in several previous microarray studies [3-4]. After adjustment with ComBat, clustering of the microarray data based on batch was greatly reduced.

7.3 eQTL mapping.

The eQTL mapping was performed with QTL Reaper, and 1000 permutations of the strain labels were used to adjust for multiple testing and provide a false discovery rate (FDR). Fig. 1 shows the eQTLs that were found for the infected mice with a likelihood-ratio statistic (LRS) > 24, corresponding to a FDR or 4%. The eQTLs fall into two groups: *cis*-eQTLs, which are located on a diagonal line through the origin with a slope of 1 and occur when the marker and gene are located less than 5 Mb apart, and *trans*-eQTLs, which are scattered throughout the remainder of the plot and occur when the gene and marker are not at the same location. A total of 6262 *cis*-eQTLs and 1343 *trans*-eQTLs were found for a FDR of 4%. Permutation of the strain labels also allows for an assessment of the FDR for eQTL hotspots [5], which can be seen in Fig. 1 by vertical bands of *trans*-eQTLs, and are locations on the genome where a marker controls several *trans*-genes. Using a FDR of 10%, 3 genomic locations were found to be eQTL hotspots: chromosome 13 near 21 Mb, chromosome 14 near 45 Mb, and chromosome 17 near 20 Mb. The next step in the analysis of the hotspots is determining candidate genes near the hotspot markers that result in the downstream gene expression changes.

7.4. Bayesian network modeling.

Small, causal networks have also been created for BXD mice infected with *Chlamydia* using Bayesian network (BN) modeling. The genetic network models link genotype to gene expression to higher order phenotypes, such as pathogen load and survival. Briefly, the BNs

are created by grouping genes and higher order phenotypes that map to the same genomic marker with standard QTL mapping procedures. Then, the hypothetical causal pathways, which link the QTL, gene, and phenotype are scored, and those groups in which the model where the QTL is causal to the gene and the gene is causal to the phenotype are selected. Models 1 and 2 in Fig. 2 show simple models in which a single gene influences the phenotype. Additional genes can be included in the models, as shown in Models 3 and 4 of Fig. 3, if they improve the accuracy of the phenotype prediction. Several of the genes included in the models of Fig. 2 have been associated with GO annotations [6] which are likely involved in response to *Chlamydia* infection, including *Prdx2*, which is involved in immune response, and *Gps2* and *Ndel1*, which are associated with GTPase activity, which has been previously linked to response to *Chlamydia* infection [1]. Fig. 3 shows a further investigation of Model 1. To create the BNs, gene expression and phenotype data are discretized into high and low values, and Fig.3 shows the probability distributions of B6 or D2 genotype and high and low gene expression and phenotype values if the QTL and gene are fixed to certain values. Strains with the B6 genotype at the rs13481068 marker on chromosome 11 have low expression of *Ndel1* and low weight 5 days after infection (Day5wt), while the D2 genotype at this marker results in higher expression of *Ndel1* and higher Day5wt. Additionally, Fig. 3 shows that fixing the value of *Ndel1* to being either low or high improves the prediction accuracy of the phenotype, in comparison to fixing the genotype at the rs13481068 marker. These genetic network models provide testable hypothesis that can be used to verify the networks. For example, if the *Ndel1* gene is silenced, Model 1 predicts that Day5wt should decrease regardless of the phenotype at the rs13481068 marker.

Figure 1. eQTL mapping of BXD mice infected with *Chlamydia psittaci*. The eQTLs shown have an LRS > 24, corresponding to a false discovery rate of 4%. The vertical lines indicate the separation of chromosomes, which are indicated with the numbers at the top of the figure.

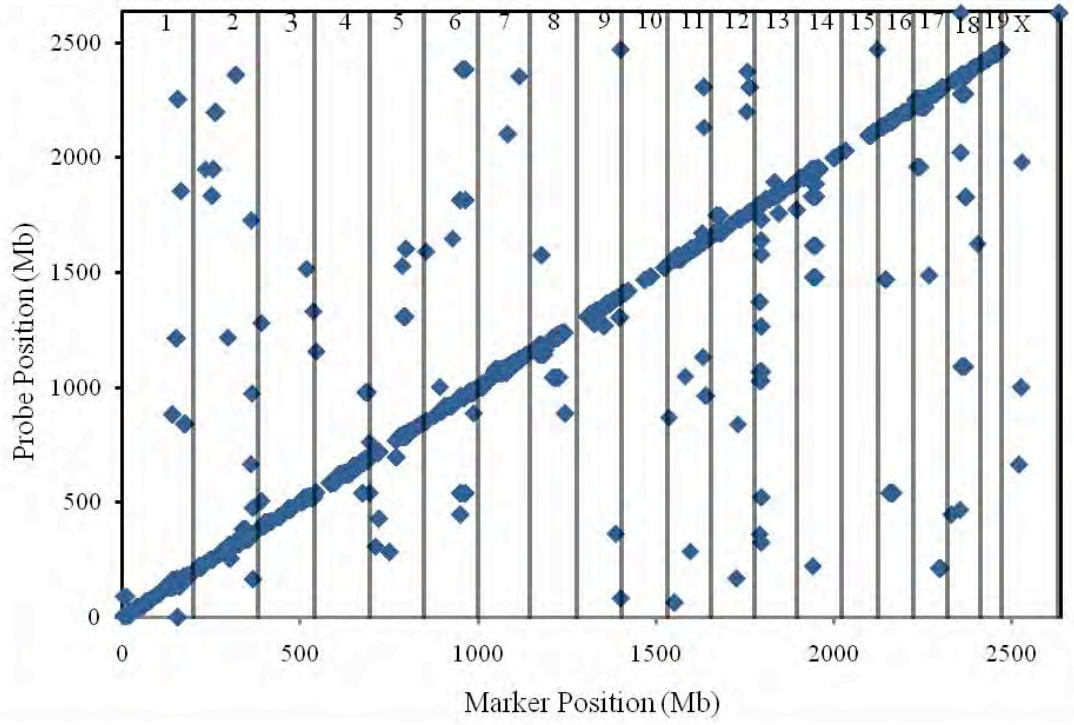

Figure 2. Causal pathways linking genotype SNPs to gene expression levels to phenotypes in BXD mice infected with *Chlamydia psittaci*. Nodes outlined in red are genotype marker, purple nodes are genes, and blue nodes are higher order phenotypes. Day5wt is the weight at 5 days after infection, IFNg is the amount of the the cytokine interferon-gamma 6 days after infection, and IFU is the pathogen load 6 days after infection.

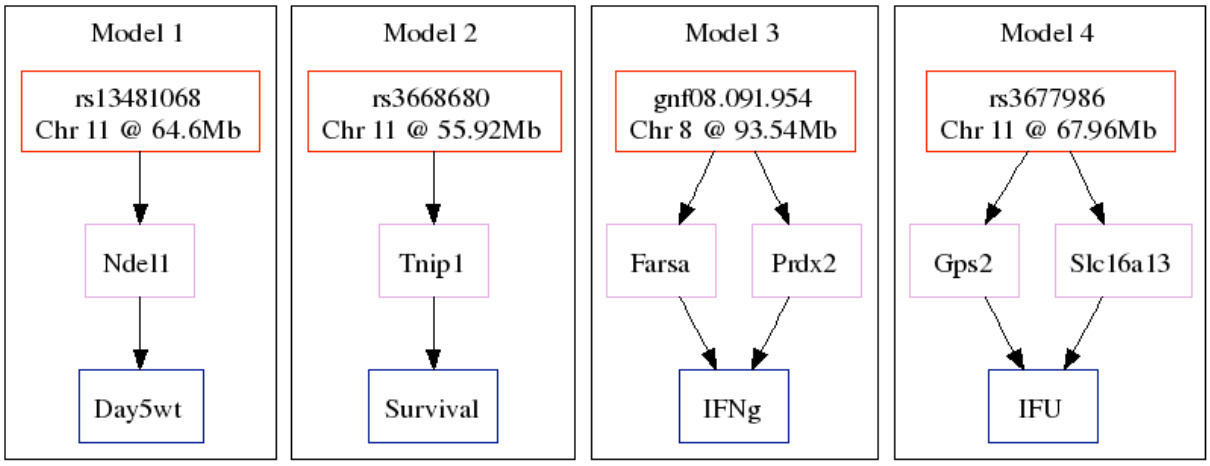

Figure 3. Further investigation into Model 1 of Fig. 2. The nodes shaded in yellow show the probability distributions of the variables after fixing the node shaded in grey to a certain value.

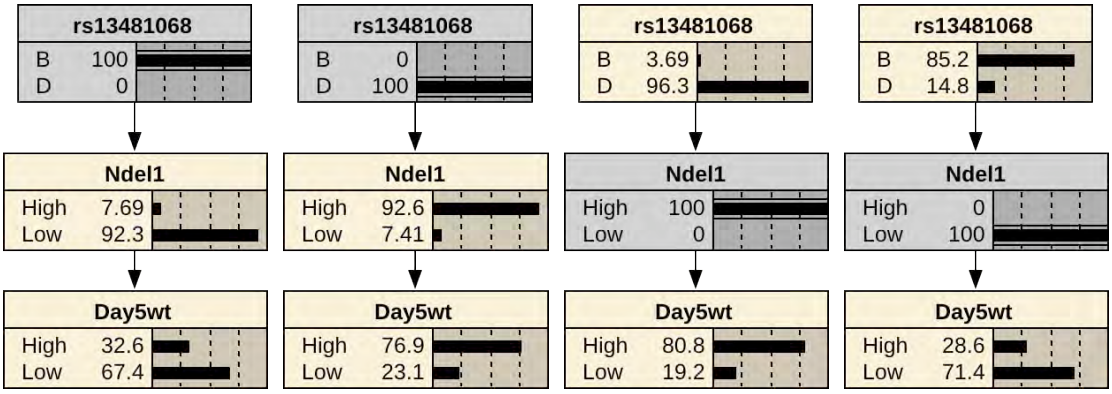

7.5. Key Research Accomplishments:

- Investigated methods to deal with batch effects in microarray data and used ComBat to reduce batch effects in microarray data of BXD mice infected with *Chlamydia*
- Performed eQTL mapping of *Chlamydia* infected BXD strains and found 3 QTL hotspots
- Constructed small Bayesian network models which link genotype to gene expression to higher order phenotypes associated with *Chlamydia* infection

7.6 Reportable Outcomes

Publications
Ziebarth, J., B. Li, I. Miyairi, and Y. Cui, *Linking genotype to phenotype with Bayesian network modeling of Chlamydia infection*.
Poster presentation at UT-ORNL-KBRIN Bioinformatics Summit 2010, March 20, 2010.
The Abstract (see appendices 2.1) will be published in *BMC Bioinformatics*.

7.7 Conclusion:

The analysis of the BXD strains infected with *Chlamydia* has currently provided two results that merit future investigation. eQTL mapping of microarray data showed that there are three potential QTL hotspots, where a single genome location effects many genes on several chromosomes. The next step in this analysis is to investigate the genes near the hotspot regions to select the genomic and gene expression differences at the hotspot that cause the downstream effects. Bayesian network modeling casual pathways from genotype to gene expression data to phenotype has yielded several interesting gene network models that require experimental validation. Additionally, the methods used to perform the eQTL mapping and Bayesian network modeling can be easily adapted for use with mice infected with other pathogens. We have made significant progress with respect to Objective 3 of the Statement of Work.

7.8 References:

2. Miyairi, I., et al., *The p47 GTPases Iigp2 and Irgb10 regulate innate immunity and inflammation to murine Chlamydia psittaci infection*. J Immunol, 2007. **179**(3): p 1814-24.
3. Johnson, W.E., A. Rabinovic, and C. Li, *Adjusting batch effects in microarray expression data using Emperical Bayes methods.* Biostatistics, 2007. **8**(1): p. 118-27.
4. Romanoski, C.E., et al., *Systems genetics analysis of gene-by-environment interactions in human cells*. Am J Hum Genet, 2010. **86**(3): p. 399-410.
5. Walker, W.L., et al., *Emperical Bayes accommodation of batch-effects in microarray data using identical replicate reference samples: application to RNA expression profiling of blood from Duchenne muscular dystrophy patients*. BMC Genomics, 2008. **9**: p. 494.
6. Breitling, R., et al., *Genetical genomics: spotlight on QTL hotspots*. PLoS Genet, 2008. **4**(10): p. e1000232.
7. Bult, C.J., et al., *The Mouse Genome Database (MGD): mouse biology and model systems.* Nucleic Acids Res, 2008. **36**(Database issue): p. D724-8.

Appendices:

1. Administrative and logistical matters

1.1 List of personnel with percent effort on the project

Personnel	**% Effort**
Gerald I. Byrne, PI	10
James E. Bina, Co-I	10
Yan Cui, Co-I	10
Kui Li, Co-I	10
Lu Lu, Co-I	10
Mark A. Miller, Co-I	10
Isao Miyairi, Co-I	10
Fabio C. Re, Co-I	10
Robert Williams, Co-I	5
Olaimatu Mahdi, Project Manager	25
Xiaowen Renee Bina, Research Faculty	75
Jonathan Laxton, Research Assistant	100
Baoming Lin, Postdoc	100
Jesse Dylan Ziebarth, Postdoc	100
Himangi R. Jayakar, Postdoc	**100**
Jyothi Pavathareddy, Research Technician	100
Li Lui, Postdoc	100
Sarah Hasty, Research Assistant	**25**
Lishi Wang, Postdoc	**100**

1.2 Request for changes in personnel and/or personnel efforts

The table above gives the list of all UTHSC personnel supported by the grant in year 1. Some of the personnel listed were not supported for the whole year (June 2009-May 2010) depending on when they started/stopped working on the grant. Personnel no longer supported by the grant are in bold.

We are requesting permission to make the following changes in personnel:

1. To hire two undergraduate students during the summer (July and August) to continue the work of Dr. Mark Miller's former postdoc Himangi Jayakar.
2. To increase the percentage support of the Project Manager from 25% to 50%, reflecting the increasing responsibility associated with managing the grant.

2. Publications

2.1 Linking genotype to phenotype with Bayesian network modeling of *Chlamydia* infection

Jesse D Ziebarth[1*], Bao Li[1], Isao Miyairi[1,2], Yan Cui[1,3]
[1]Department of Molecular Sciences and [2]Pediatrics, [3]Center of Integrative and Translational Genomics, University of Tennessee Health Science Center, Memphis TN, 38163, USA
*jziebart@uthsc.edu

Background
Understanding the causal pathways that link genotypes with gene expression and higher order phenotypes, such as disease susceptibility, has been a recent goal of systems genetic studies. Pairwise correlations can select genes and phenotypes that are associated with a common genetic locus; however, the directions of these links are more difficult to determine. We propose a method in which Bayesian networks are used to establish causal pathways from genotype to gene expression to phenotype and apply it to mice infected with *Chlamydia psittaci*.

Results
Recombinant inbred BXD mice strains have been previously used to study the genetic differences that cause a much greater resistance to *Chlamydia psittaci* infection in C57BL/6J mice compared with DBA/2J mice [1]. Gene expression levels and higher order phenotypes, such as pathogen load and survival, were collected for 44 BXD strains. Directed graphs linking SNPs [2] in the BXD genomes to this data were created with QTL mapping and the Bayesian network method. Figure 1 shows a selection of the resulting causal pathways; many of the genes in these pathways are knows to be associated with immune response or GTPase activity, which has been linked to *Chlamydia psittaci* infection [1].

Figure 1. Causal pathways linking genotype SNPs to gene expression levels to phenotypes in BXD mice infected with *Chlamydia psittaci*

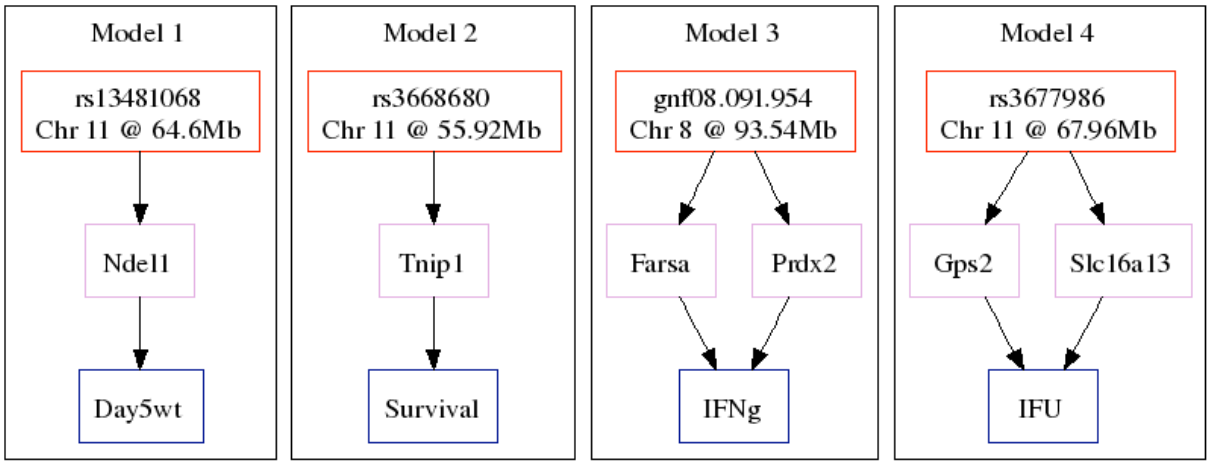

Acknowledgements
This work was support by NIH grant AI081050 and DOD grant W81XHW-05-01-0227.

References

1. Miyairi I, Tatireddigari VRRA, Mahdi OS, Rose LA, Belland RJ, Lu L, Williams RW, Byrne GI: **The p47 GTPases *Iigp2* and *Irgb10* regulate innate immunity and inflammation to murine *Chlamydia psittaci* infection**. *J Immunol* 2007, **179:**1814-1824.

2. **BXD Genotypes at the GeneNetwork** [http://www.genenetwork.org/genotypes/BXD.geno]

SYSTEMS GENETICS ANALYSIS OF CHLAMYDIA PSITTACI INFECTION

I. Miyairi[1, 2], J. Laxton[1], J. Ziebarth[1], R. Williams[3], L. Lu[3], G. Byrne[1], Y. Cui[1].

Department of Molecular Sciences[1], Pediatrics[2], and Anatomy and Neurobiology[3], University of Tennessee Health Science Center, Memphis, TN, USA.

Introduction

Individual differences in susceptibility to infectious diseases have been mapped to numerous disease defining genetic polymorphisms or quantitative trait loci (QTL) by forward genetics (1-3). However, such genotype-phenotype associations do not provide information on the causal pathways of how disease occurs. Inbred mouse models have been widely utilized for identification of susceptibility genes and systems genetics. Recombinant inbred (RI) strains contain unique, approximately equal proportions of genetic contributions from two progenitor inbred strains. A panel of 78 established BXD RI strains derived from C57BL/6J (B6) and DBA/2J (D2) strains have been genotyped over 13,377 SNP markers and are available for repeated testing. Combined with a web-based analytical tool (GeneNetwork.org) this allows high precision Quantitative trait loci (QTL) mapping. In a previous analysis, we determined that a QTL on chromosome 11 containing two polymorphic innate immune genes (Irgm3 and Irgb10) in the family of immunity-related GTPases (IRG) were responsible for the innate difference in susceptibility to a systemic infection to *C.psittaci* between the B6 and D2 mice (3). Characterization of the immunological differences between the B6 and D2 mice revealed significant differences in *Chlamydia* load, inflammatory responses, and cytokine profiles. While the IRGs were shown to control *Chlamydia* load (2), alternative immunomodulatory functions of this gene have been implicated (4-5). In our model it is unclear whether the various immunological differences are a function of pathogen load, immunomodulatory functions or yet unrelated to the IRGs.

We hypothesized that a multiscale analysis of BXD genotype, pathogen load, and immune parameters can be combined to define causative immune pathways induced by *Chlamydia psittaci* infection.

Methods

1. Infection and sample collection.

Chlamydia infection: 8-10 week old male mice (C57BL/6J, DBA/2J, and 57 BXD strains) were infected in groups of 2-5/strain for a total of 372 mice. *C. psittaci* 6BC strains were propagated in L cells, titrated and stored at -80C°. Intraperitoneal infection with *C.psittaci* 6BC (10^4 IFU) was performed using the same stock source to minimize variations across experiments.

Monitoring and sample collection: Infected mice were monitored daily for weight changes. On day 6-post infection, mice were euthanized to obtain peritoneal lavage samples for pathogen load, flow cytometry, and cytokine analysis.

2. Assessment of immune phenotypes.

Chlamydia load: Titration was performed by a cell culture based IFU assay.

Flow cytometry: Standard methods were used. Briefly, murine peritoneal exudates were blocked with Fc block and incubated with fluorochrome-conjugated Abs. The following Abs was used: (Macrophage) F4/80-APC, (Neutrophil) Ly6G-PE, (Class II) IA/AE-Alexa488, (Myeloid) and CD11b-PE-Cy7. Data was expressed as percent of macrophages or neutrophils in the CD11b expressing myeloid cells. Class II expression was used as a marker for macrophage activation status and data was expressed as percent of F4/80 expression cells that also expressed class II.

Cytokine analysis: Peritoneal lavage supernatants were stored in -80°C till assessment. We used the Mouse 32-plex kit to analyze levels of 32 cytokines.

3. Data analysis.

QTL analysis: We used interval mapping method available on the GeneNetwork.org interface to identify genetic loci regulating infection/immune phenotypes. Interval Mapping is a statistical test of association between trait values and the genotypes of marker loci through the genome. A significant association is interpreted as indicating the presence of a QTL linked to the marker that shows the association.

Correlation analysis: The correlation analysis was performed using Pearson and Spearman correlations and a network graph was drawn using a built in function in the GeneNetwork. This function enables graphical association among large groups of phenotypes.

Results

1. Immune phenotype data

Mice exhibited a range of disease manifestation ranging from 30 % weight reduction to 10 % weight increase in 6 days. *Chlamydia* load ranged from 4 to 6.5 log IFU/mouse. Neutrophils ranged 2-40% of the myeloid population. Of the macrophage population 2-80% expressed Class II. A measurable difference was observed in at 22 of the 32 cytokines examined.

2. QTL analysis

The majority of the variability observed in weight change, macrophage activation status, *Chlamydia* load, and neutrophil recruitment was attributed to the previously reported chromosome 11 locus. While many other traits were influenced by the chromosome 11 locus, subset of chemokines were controlled by a combination of minor QTLs on chromosomes 4, 5, 9, and 16 whereas IFNγ, TNFα, IL10 levels were under the primary control of a QTL on chromosome 8 (Table).

3. Correlation analysis

The strongest positive correlation with the disease phenotype (weight) was found with macrophage activation status, rather than *Chlamydia* load (Table). The macrophage activation status itself had a strong negative correlation with *Chlamydia* load as well as percentage of neutrophils in the inflammatory cell population. The level of cytokines such as IFNγ and TNFα were not associated with the weight changes observed in this model.

In order to determine whether the phenotype was a direct consequence of the pathogen burden we examined the correlation of pathogen load with weights of individual mice according to the genotype at chromosome 11 encoding the IRGs. Results demonstrated that mice that have the B6 genotype at the locus are tolerant to increases in the pathogen load. Also, there was a significant overlap in the pathogen load between two genotypes. These findings suggest the IRGs encoded in chromosome 11 locus affect disease outcome by a mechanism of tolerance (ability to withstand increasing pathogen burden) rather than resistance (ability to restrict pathogen load).

Discussion

Results indicate the involvement of multiple QTL in determining the immune phenotypes associated with a systemic *Chlamydia psittaci* infection. A systems approach utilized in this study allows us to infer immune responses and its hierarchy that contribute to disease process. Specifically, the disease status controlled by the chromosome 11, which is most likely the IRGs,

appeared to be a function of the macrophage activation status rather than direct *Chlamydia* load. In this model the macrophage activation status influences *Chlamydia* load as well as the inflammatory cell population. While, this will require further validation, this likely represents the multiple functions of the IRG. Cytokine levels that intuitively would be associated with disease severity such as IFNγ and TNFα were found to fluctuate independent of disease status and were controlled by other genetic loci. Candidate genes on the chromosome 8 interval are currently under investigation.

Table: QTL mapping results and Pearson correlation coefficient.

Phenotype	QTL (Chromosome)	Macro	Neutro	Weight	Chlamydia	TNFa	Mip2	IFNg
Mac activation status	Chr11	1						
Neutrophils	Chr11	-0.726	1					
Weight	Chr11	0.738	-0.673	1				
Chlamydia load	Chr11, 5	-0.736	0.556	-0.69	1			
TNFa	Chr 8, 11	-0.307	0.404	-0.25	0.374	1		
Mip2	Chr 4, 5, 9, 11, 16	-0.531	0.282	-0.354	0.269	0.149	1	
IFNg	Chr 1, 8	-0.261	0.356	-0.246	0.242	0.712	0.106	1

High positive correlations 0.7 to 1, Moderate positive correlation 0.5 to 0.7, High negative correlation –0.7 to -1.0, Moderate negative correlation –0.5 to –0.7.

Acknowledgements: This work was funded by AI081050 (IM, YC), 09GBIA2050135 (IM), BAA08-1 (GIB, IM), AI19782 (GIB), AI30040 (GIB).

References

1. Bernstein-Hanley, I., Z. R. Balsara, W. Ulmer, J. Coers, M. N. Starnbach, and W. F. Dietrich. 2006. Genetic analysis of susceptibility to Chlamydia trachomatis in mouse. Genes Immun 7:122-9.

2. Bernstein-Hanley, I., J. Coers, Z. R. Balsara, G. A. Taylor, M. N. Starnbach, and W. F. Dietrich. 2006. The p47 GTPases Igtp and Irgb10 map to the Chlamydia trachomatis susceptibility locus Ctrq-3 and mediate cellular resistance in mice. Proc Natl Acad Sci U S A 103:14092-7.

3. Miyairi, I., V. R. Tatireddigari, O. S. Mahdi, L. A. Rose, R. J. Belland, L. Lu, R. W. Williams, and G. I. Byrne. 2007. The p47 GTPases Iigp2 and Irgb10 regulate innate immunity and inflammation to murine Chlamydia psittaci infection. J Immunol 179:1814-24.

4. Howard J. 2008. The IRG proteins: a function in search of a mechanism. Immunobiology;213(3-4):367-75.

5. Taylor GA, Feng CG, Sher A. 2007. Control of IFN-gamma-mediated host resistance to intracellular pathogens by immunity-related GTPases (p47 GTPases). Microbes Infect. 9:1644-51.

Clinton et al. BMC Microbiology 2010, 10:76
http://www.biomedcentral.com/1471-2180/10/76

BMC Microbiology

RESEARCH ARTICLE Open Access

Binding and activation of host plasminogen on the surface of *Francisella tularensis*

Shawn R Clinton, James E Bina, Thomas P Hatch, Michael A Whitt, Mark A Miller*

Abstract

Background: *Francisella tularensis* (FT) is a gram-negative facultative intracellular coccobacillus and is the causal agent of a life-threatening zoonotic disease known as tularemia. Although FT preferentially infects phagocytic cells of the host, recent evidence suggests that a significant number of bacteria can be found extracellularly in the plasma fraction of the blood during active infection. This observation suggests that the interaction between FT and host plasma components may play an important role in survival and dissemination of the bacterium during the course of infection. Plasminogen (PLG) is a protein zymogen that is found in abundance in the blood of mammalian hosts. A number of both gram-positive and gram-negative bacterial pathogens have the ability to bind to PLG, giving them a survival advantage by increasing their ability to penetrate extracellular matrices and cross tissue barriers.

Results: We show that PLG binds to the surface of FT and that surface-bound PLG can be activated to plasmin in the presence of tissue PLG activator *in vitro*. In addition, using Far-Western blotting assays coupled with proteomic analyses of FT outer membrane preparations, we have identified several putative PLG-binding proteins of FT.

Conclusions: The ability of FT to acquire surface bound PLG that can be activated on its surface may be an important virulence mechanism that results in an increase in initial infectivity, survival, and/or dissemination of this bacterium *in vivo*.

Background

Francisella tularensis (FT) is a Gram-negative intracellular pathogen that is the etiological agent of a multi-syndromic disease with a high morbidity/mortality that is referred to as tularemia. The pneumonic form of tularemia is of particular concern because of the high mortality rate (up to 60%) following inhalation of as few as ten organisms [1-4]. *Francisella* species are found throughout the Northern Hemisphere and infect a variety of vertebrate and invertebrate hosts [5,6]. Infections with FT can be contracted from blood sucking insects, such as the deer fly [5,7], mosquitoes [8,9], and ticks [5,7,10], and by open-wound contact with infected animal tissue [5,11,12].

Upon entry into a susceptible vertebrate host, FT is readily phagocytized by resident macrophages and dendritic cells and quickly escapes into the cytoplasm [13,14] where it multiplies. Late in its replicative cycle, FT induces apoptotic death of the host phagocyte, resulting in release of progeny bacteria that can infect new host cells. Recent studies have shown that significant numbers of FT are found in the acellular plasma fraction of mice infected intradermally or intranasally with either FT Live Vaccine Strain (LVS) (Type B) or FT Schu S4 (Type A) [15], and intranasally with FT *novicida* [16]. These findings suggest that, in addition to utilizing the intracellular cytoplasmic niche for replication and protection from humoral immunity, FT may also have a significant extracellular phase. Several studies have shown that deposition of host complement component C3 on the surface of FT is required for opsonophagocytosis by activating CR3 and CR4-mediated phagocytosis by macrophages and dendritic cells [14,17,18]. It is also known that FT is relatively resistant to complement-mediated lysis [19]. A recent report suggested that resistance of FT to membrane attack complex-mediated lysis may be due (at least in part) to its ability to bind to factor H from host plasma [20]. It is possible that the ability of FT to bind to factor

* Correspondence: mamiller@uthsc.edu
Department of Molecular Sciences, The University of Tennessee Health Science Center, 858 Madison Avenue, Memphis, Tennessee 38163, USA

H and potentially to other host plasma components plays a significant role in its pathogenesis.

It has been long established that a broad spectrum of both gram-positive and gram-negative bacterial pathogens gain a survival advantage by interacting with components of the host coagulation/fibrinolytic system in humans [21-24]. For instance, the ability to acquire surface-associated plasmin has been documented as an important virulence mechanism in Group A streptococci [25], *Borrelia burgdorferi* [26], and *Yersinia pestis* [27] by aiding in the organism's ability to penetrate the extracellular matrix and to disseminate to distal sites in the host. Plasminogen (PLG) is a 92-kDa glycoprotein zymogen that is involved in fibrinolysis. This precursor protein is converted to an active serine protease (plasmin) by cleavage of the peptide bond between residues $R^{560}$and V^{561} *in vivo* via urokinase-type (uPA) and/or tissue-type (tPA) PLG activators. Plasmin has an important role in blood clot resolution because of its role in the degradation of fibrin polymers. Because plasmin has other substrates that include pro-collagenases, pro-metalloproteinases, and extracellular matrix proteins, such as fibronectin, laminin, and vitronectin, the ability of a bacterium to acquire surface-associated plasmin can result in an enhanced ability of the pathogen to penetrate the extracellular matrix and to disseminate to distal sites in the host [21,23,25]. In this report we show that PLG binds to the surface of FT *in vitro* and that surface-bound PLG can be converted to the active plasmin form. In addition, using a combination of Far-Western blotting analyses coupled with proteomic methodologies, we have identified several FT proteins that can bind to human PLG *in vitro*.

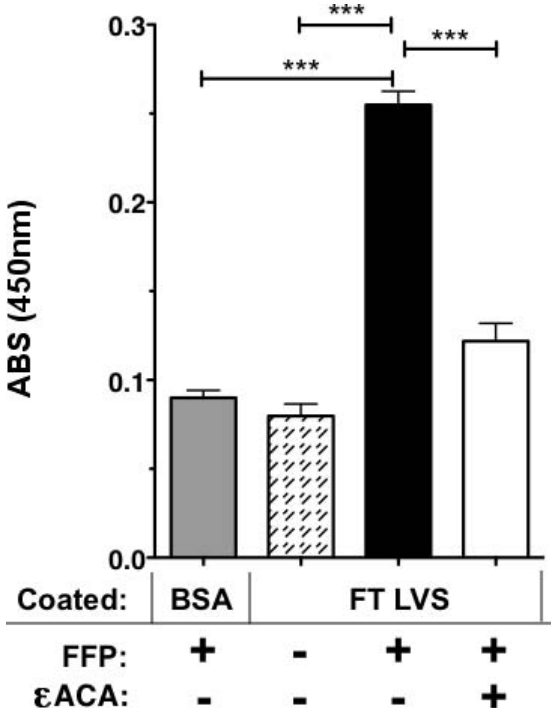

Figure 1 FT binds to PLG from human plasma. FTLVS cultured to mid-log phase in BHI broth were bound to wells of microtiter plates and then incubated for 1 hour with fresh frozen human plasma (FFP) in the presence or absence of 100 mM ε-amino caproic acid (εACA), a PLG-binding inhibitor. A modified ELISA was performed to measure FTLVS-bound PLG. The results shown are representative of 3 experiments of similar design. Bars indicate +/- SEM in triplicate. Statistical analysis was performed via one-way ANOVA using a Dunnett's Multiple Comparison post-test (*** P < .001).

Results

Binding of PLG from fresh human plasma to the surface of FTLVS

We used an ELISA assay to determine that PLG in fresh frozen plasma (FFP) binds to FTLVS grown to mid-log phase in BHI (Figure 1). Binding was inhibited when ε-aminocaproic acid (εACA), known to inhibit binding of PLG to lysine groups in proteins, was included in the incubation mixture. To help eliminate the possibility of non-specific binding of PLG due to its high concentrations in human plasma and also to rule out the contributions of other plasma proteins, we used purified human Glu-PLG (huPLG) and noted similar results to those observed when FFP was used (Figure 2A). We also found that huPLG binds to the highly virulent Schu S4 strain of FT at moderately higher levels than observed with FTLVS (Figure 2B). We confirmed that binding of huPLG to FT is a lysine-dependent interaction by showing that increasing concentrations of εACA can inhibit binding of huPLG to FTLVS in a dose-dependent fashion (Figure 3). When similar concentrations of glycine were used as an inhibitor control, no inhibition of huPLG binding was observed (data not shown). Confocal microscopic analyses suggested that huPLG binds to the surface of FT (Figure 4); however, it is possible that some of the staining observed was the result of huPLG penetration into the outer envelope of FT. Although is has been reported that culture media composition can have a significant impact of the surface properties and virulence characteristics of FTLVS [28], we observed no differences in the ability of PLG to bind to the surface of FTLVS grown in modified Mueller-Hinton medium vs. brain-heart infusion broth (data not shown).

Plasmin activation on the surface of FT LVS *in vitro* by a PLG activator

In other bacterial systems, surface-bound PLG can be converted to its proteolytically active plasmin form that contributes to the organism's virulence [21-24]. To test whether huPLG bound to FTLVS can be converted to plasmin, we used a chromogenic plasmin substrate

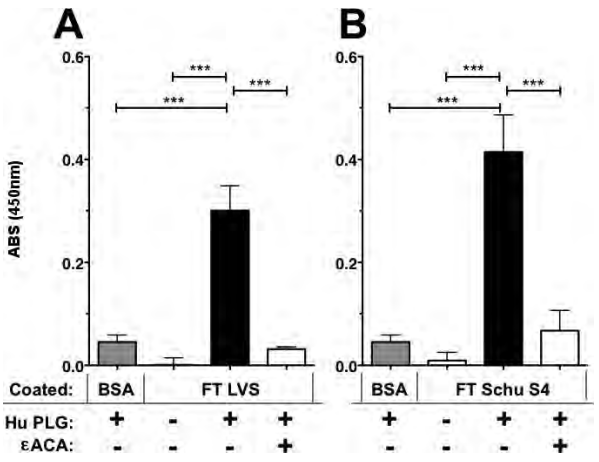

Figure 2 Purified huPLG binds to FTLVS and FTSchuS4. FTLVS (**Panel A**) and FTSchuS4 (**Panel B**) were bound to microtiter wells and incubated for 2 hours with purified huPLG (3 μg/ml) in the presence or absence of 10 mM εACA). A modified ELISA was performed to measure FTLVS-bound huPLG. The results shown are representative of four (**Panel A**) and one (**Panel B**) experiments, respectively, of similar design. Bars indicate +/- SEM in triplicate. Statistical analysis was performed via one-way ANOVA using a Dunnett's Multiple Comparison post-test (*** $P < .001$).

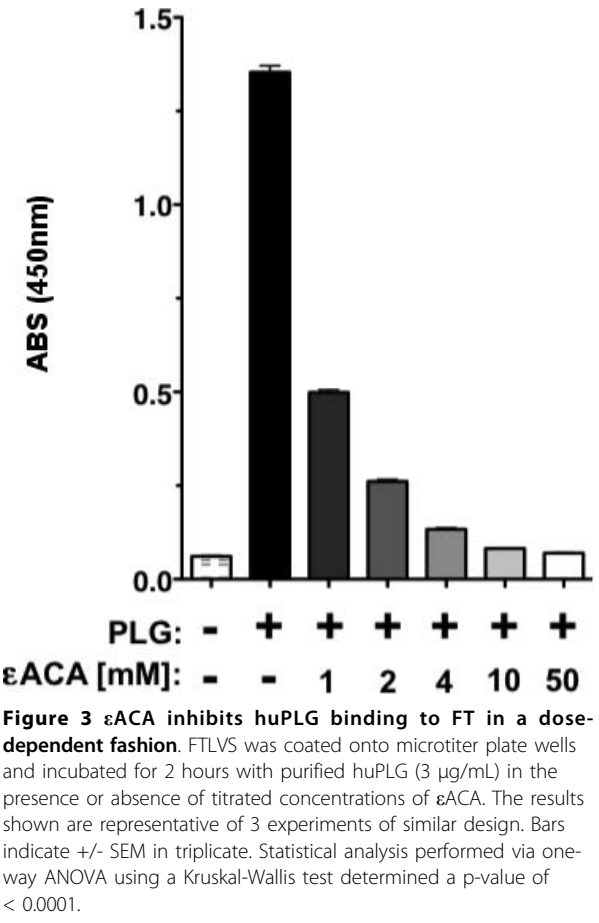

Figure 3 εACA inhibits huPLG binding to FT in a dose-dependent fashion. FTLVS was coated onto microtiter plate wells and incubated for 2 hours with purified huPLG (3 μg/mL) in the presence or absence of titrated concentrations of εACA. The results shown are representative of 3 experiments of similar design. Bars indicate +/- SEM in triplicate. Statistical analysis performed via one-way ANOVA using a Kruskal-Wallis test determined a p-value of < 0.0001.

(H-D-Val-Leu-Lys-pNA) to detect proteolytic activity following the addition of tissue PLG activator (tPA) (Figure 5). We also found that plasmin on the surface of FT can break down fibronectin (Figure 6), suggesting that FT-bound plasmin can potentially participate in the degradation of extracellular matrices.

Identification of putative *Francisella* PLG-binding membrane proteins

We used Far-Western Blot methodology and mass spectrometry to identify potential PLG receptors in the Sarkosyl soluble and insoluble FTLVS membrane fractions (Figure 7). Sarkosyl is a weak anionic detergent in which many outer membrane proteins of Gram-negative bacteria are insoluble [29]. We transferred the Sarkosyl-treated proteins to a PVDF membrane and incubated the membrane with PLG and identified bound PLG by reaction with anti-PLG mAbs (Figure 7a). We used the relative migration rates of the reactive bands to identify the reactive proteins on a duplicate Coomassie-stained polyacrylamide gel (Figure 7b), which were then excised for proteomic analysis by mass spectrometry. Several prominent PLG-binding proteins were noted in the total membrane fraction of FTLVS, all but one of which was found in the Sarkosyl insoluble fraction (Figure 7b). The identity of the prominent proteins from this assay (Figure 7c) are the products of the following genes: FTL_1328 (outer membrane associated protein, fopA1), FTL_1042 (FKBP-type peptidyl-prolyl cis-trans isomerase family protein), FTL_0336 (peptidoglycan-associated lipoprotein), FTL_0421 (hypothetical lipoprotein, lpn-A), and FTL_0645 (hypothetical lipoprotein).

Discussion

Until recently FT has been considered an intracellular pathogen whose dissemination to tissues distal to the site of initial infection was highly dependent on its ability survive within host macrophages. The observation that FT can be found in relatively high numbers in the acellular plasma fraction of its mammalian host [15,16] suggested that FT may have a significant extracellular component to its life cycle and that interactions between FT and one or more plasma proteins could contribute to its ability to disseminate within the host. There are a number of examples of bacterial pathogens that utilize interactions with host plasma components to enhance their ability to colonize and to penetrate the extracellular matrices of host cells/tissues. A wide range of bacterial pathogens (including *Francisella*) subvert the destructive mechanisms of the complement cascade by acquiring surface-bound complement control proteins [20,30-34]. Moreover, a number of Gram-positive bacterial pathogens including *streptococcal* spp. [35,36], *staphylococcal* spp. [37-40], and *Bacillus anthracis* [41,42],

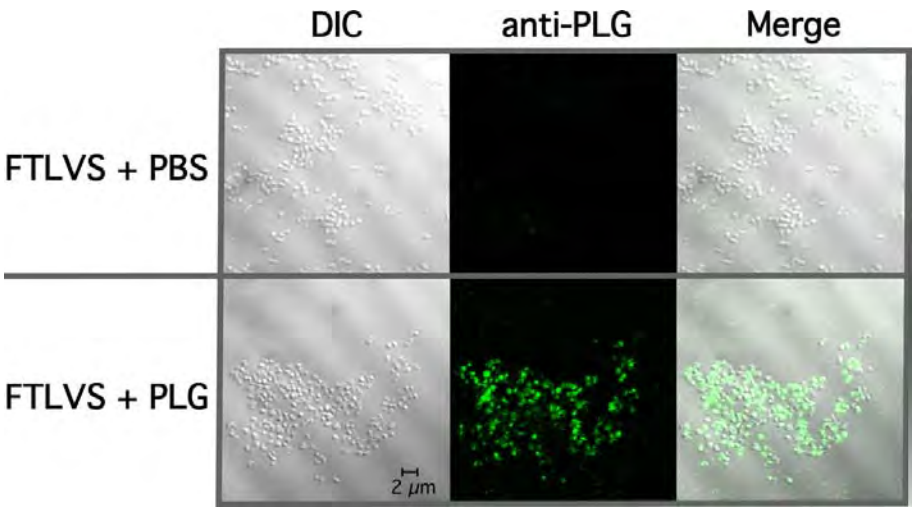

Figure 4 PLG binds to the outer envelope of FT. Laser scanning confocal microscopy of PLG-associated FTLVS was performed as described in "Materials and Methods". Bound huPLG ligand was detected using sheep anti-human PLG antibody followed by incubation with Dylight-488 conjugated donkey, anti-sheep/goat IgG secondary antibody. Samples were visualized using a Zeiss LSM 510 confocal microscope.

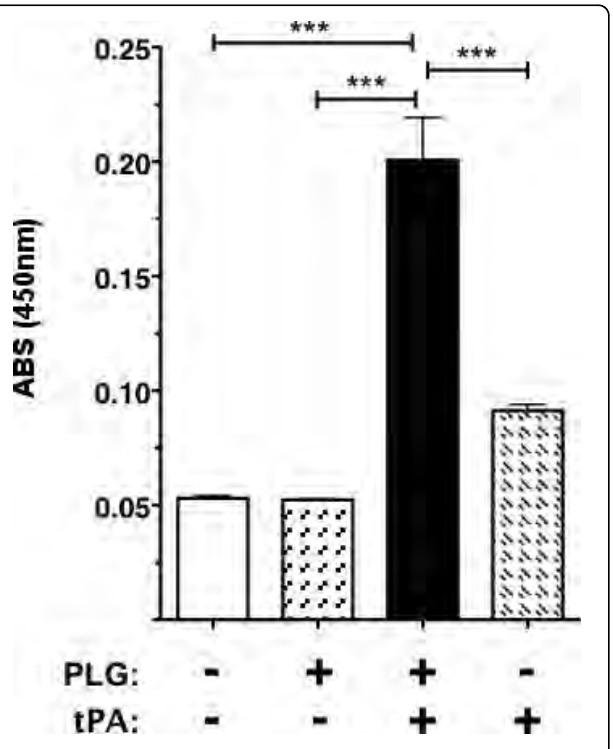

Figure 5 FT surface-bound huPLG can be converted to plasmin. FTLVS was incubated with huPLG at a concentration of 96 μg/mL. After removal of unbound huPLG, a chromogenic plasmin substrate (D-VLK-pNA), tissue PLG activator (tPA), or both were then added to test the proteolytic ability of each sample preparation. Conversion of the chromogenic substrate was measured by comparison of Δ405 nm. The results shown are representative of 3 experiments of similar design. Bars indicate +/- SEM in triplicate. Statistical analysis was performed via one-way ANOVA using a Dunnett's Multiple Comparison post-test (*** $P < .001$).

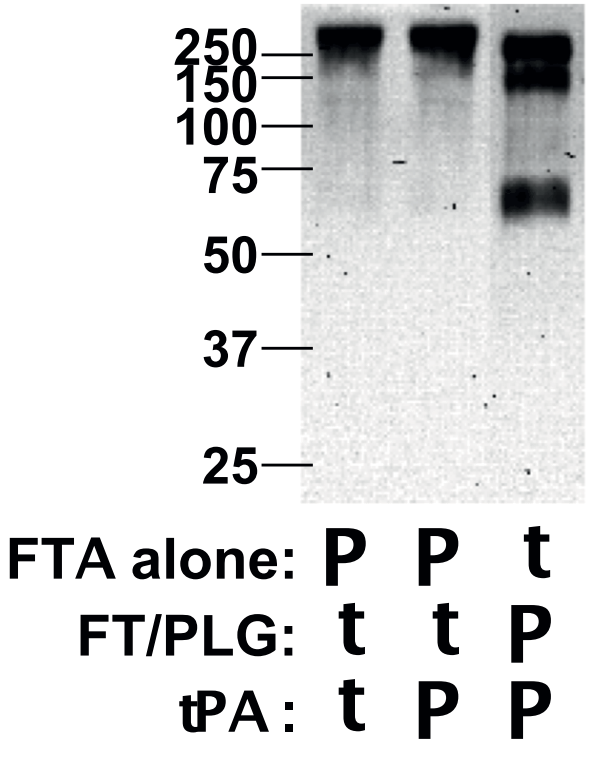

Figure 6 Fibronectin is a substrate for plasmin bound to FT. FTLVS (10^9 CFU) were incubated with 100 μg of huPLG and 0.5 μg tissue tPA for 1 hour at 37°C. After removal of unbound huPLG and tPA, 3 μg fibronectin was added and allowed to incubate for 24 hours at 37°C. Supernatant from each preparation were separated by SDS-PAGE and transferred to PVDF membrane. Degradation of fibronectin was detected by Western blot analysis as described in "Materials and Methods".

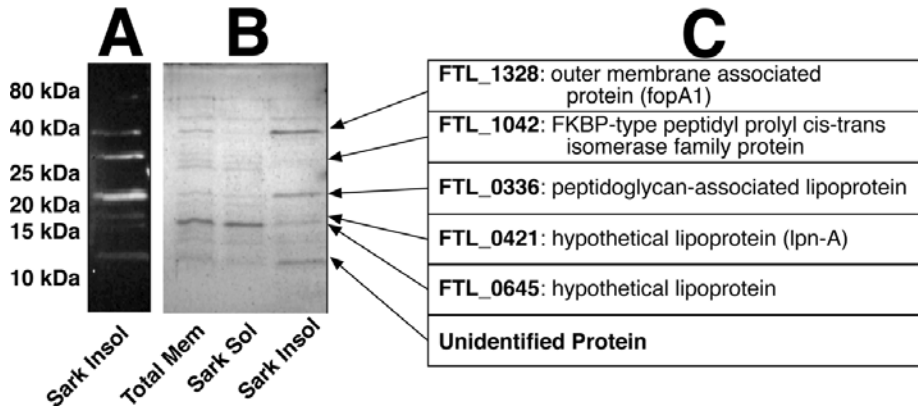

Figure 7 Identification of putative PLG-binding proteins of FT. Sarkosyl-soluble and insoluble protein fractions of FTLVS were separated by SDS-PAGE and transferred to PVDF membrane. Membranes were then blotted with huPLG (3 ug/mL) followed by anti-PLG antibody and HRP-conjugated secondary antibody to detect PLG-binding proteins (**Panel A**). Protein bands on an identical Coomassie Blue-stained SDS-PAGE gel corresponding to those identified via blotting (**Panel B**) were excised and identified using proteomic methodologies (**Panel C**).

as well as Gram-negative bacteria such as *Pseudomonas aeruginosa* [43] have been shown to augment their invasive capacity by interacting with fibrinogen, fibronectin, and/or PLG. *Yersinia pestis* is probably the best-characterized example of a pathogen that exploits the host fibrinolytic system to penetrate host tissues. *Yersinia* expresses a surface serine protease (designated Pla) whose substrates include several complement components, PLG, and alpha2-antiplasmin (the primary circulating inhibitor of plasmin). Pla also has adhesin activity and binds to laminin (a glycoprotein of mammalian basement membranes). Because Pla upregulates plasmin activity, and because laminin is a substrate of plasmin, *Yersinia* can very efficiently penetrate basement membranes of host tissues [for review, see Suomalainen et. al. [44]]. Clearly, interaction with plasma components is a strategy that is used by many bacterial pathogens to gain a survival advantage within their hosts.

The goal of the studies described here was to determine whether FT has the potential to use the host fibrinolytic system (specifically PLG) to enhance its ability to penetrate/disseminate following infection of a mammalian host. Our results indicate that both FTLVS and FTSchuS4 are able to acquire surface bound PLG *in vitro* and that this zymogen can be converted by a host-derived PLG activator into its active serine protease form (plasmin) while bound to FTLVS. The ability of PLG to bind its ligands typically involves its lysine-binding kringle domains. This specific interaction between PLG and exposed lysine residues can be inhibited with the lysine-analogue εACA and, to a lesser extent, with free lysine. Our findings revealed that binding of PLG to the surface of FTLVS could be inhibited by εACA in a dose-dependent fashion. Moreover, we showed that plasmin bound to the surface of FT could degrade fibronectin. This finding supports our hypothesis that the ability of FT to bind to serum plasmin may enhance its ability to penetrate extracellular matrices, enhancing its ability to disseminate *in vivo*.

Using a ligand-blotting technique coupled with proteomic methodologies we identified five FTLVS proteins that were able to bind to PLG, each of which are highly conserved among the various FT type A and B strains. Three of these proteins are lipoproteins (gene products of FTL_0336, FTL_0421, and FTL_0645). Two of the lipoproteins are unique to FT, while the third, peptidoglycan-associated lipoprotein (PAL), is highly conserved among gram-negative bacteria. The specific use of surface-exposed lipoproteins as receptors for host PLG is not unusual and has been well documented in other human bacterial pathogens, such as some members of the genus *Borrelia* and *Treponema*. Several members of the genus *Borrelia* use complement regulator-acquiring surface proteins (CRASP) to bind both PLG and complement factor H to aid in the ability of the organism to both disseminate and to resist innate immunity [45-50]. An additional example of a PLG-binding lipoprotein is OppA of *Treponema denticola*, which has been suggested to play a role in periodontal disease in humans [51]. With this in mind, there lies the possibility that lipoproteins of *Francisella* species may have the capacity to bind multiple host-derived proteins in addition to PLG.

Here we have shown that FT can bind to PLG and that surface-bound PLG can be activated by tPA to its proteolytic form (plasmin). The binding of PLG on the surface of FT could play a role in several phases of tularemia, including the initial entry into the host through insect bites and/or broken skin where active fibrinolytic processes would provide an early

opportunity for FT to acquire proteolytic activity that might augment the establishment or dissemination of infection. During later phases of tularemia the acquisition of plasmin on the cell surface may contribute to its pathogenicity by degrading host innate effector molecules and extracellular matrix components. Based on the new report that FT-bound plasmin can degrade immunoglobulins [52], as well as the established ability of FT to acquire surface-bound factor H [20], it also appears likely that FT uses plasma components to interfere with host humoral immune mechanisms throughout the course of FT infection. Future studies to identify additional plasma components that can be surface acquired by FT may uncover additional virulence mechanisms used by this pathogen during its extracellular life cycle.

Conclusions

FT interacts with at least two serum components (plasmin, and complement factor H), and it seems likely that FT also uses interactions with additional host serum components to gain a survival advantage. Our lab is examining FT interactions with additional targets, including fibrinogen and fibronectin, both of which are substrates for plasmin and are host components that are known to be exploited by numerous pathogens for adhesion to and penetration of extracellular matrix layers. The interaction of FT with host serum components may play a significant role in the survival and dissemination of this highly pathogenic bacterium. Gaining a better understanding of these interactions could be a critical step in the development of therapeutic and prophylactic interventions for tularemic disease.

Methods

Bacterial strains and culture

F. tularensis Live Vaccine Strain (FTLVS) was a kind gift of Dr. Karen Elkins (FDA, Bethesda, MD). FT Schu S4 was obtained from the CDC. All bacterial cultures were grown overnight in Brain-Heart Infusion broth (37 g/L, pH 6.8) from frozen stocks at 37°C with shaking to mid-log phase (OD_{600} = ~0.7) before use.

Reagents

Human fresh frozen plasma (FFP) was purchased from Lifeblood Mid-South Regional Blood Center (Memphis, TN). Purified human Glu-PLG (huPLG), human single-chain tissue PLG activator (tPA), and the plasmin colorimetric substrate (H-D-Val-Leu-Lys-pNA) were purchased from Molecular Innovations (Novi, MI). Bovine serum albumin (fraction V) was purchased from Thermo-Fisher Scientific (Pittsburgh, PA). Polyclonal sheep anti-human PLG, anti-human fibronectin, and donkey anti-sheep/goat IgG:Dylight-488 antibody preparations purchased from AbD Serotec (Raleigh, NC). Monoclonal anti-goat/sheep IgG-horseradish peroxidase conjugated secondary antibody (clone GT-34) and ε-aminocaproic acid (A7824) were purchased from Sigma-Aldrich (St. Louis, MO). Ninety-six well MAXISORP ELISA plates were purchased from Nunc (Rochester, NY).

PLG binding ELISA assays

FTLVS was cultured overnight to mid-log phase, pelleted at 6,400 × g for 30 minutes, washed twice with phosphate-buffered saline (PBS), and resuspended in PBS with 0.1% Na azide to an OD_{600} = 0.1. The resulting bacterial suspension was added to microtiter plates (100 μL/well; approximately 2.5×10^8 bacterial cells) before being incubated overnight at 4°C to facilitate binding. The wells were then washed twice with 200 μL of Tris-buffered saline (TBS) pH 7.45 containing 0.05% Tween-20 (TBST) to remove unbound bacteria and then pre-blocked with 200 μL of TBST containing 1% bovine serum albumin (1% BSA-TBST) for 1 hour at RT° to prevent non-specific protein binding. After removal of the blocking solution, 90% citrated human plasma or 3 μg/mL huPLG in 1% BSA-TBST was added to each well (100 μL), with or without the indicated concentrations of ε-amino caproic acid (εACA), and incubated for 1-2 hours at 37°C with gentle rocking. Wells were washed three times with TBST and then sheep anti-human PLG-specific antibody (1:2,000 dilution in 1% BSA-TBST) was added (100 μL/well) and allowed to incubate for 1 hour at 37°C. Unbound primary antibodies were removed by washing three times with TBST, followed by the addition of HRP-conjugated anti-sheep/goat IgG mAb (GT-34, 1:5,000 dilution in 1% BSA-TBST; 100 μL/well) and incubation for 1 hour at 37°C. Unbound secondary antibodies were removed by washing four times with TBST, and OptEIA TMB colorimetric substrate solution (Becton-Dickenson, Franklin Lakes, NJ) was added to each well (100 μL/well) and incubated at 37°C for 20 min. to allow color development. Absorbance at 450 nm was determined using a SpectraMAX 340 plate reader (Molecular Devices, Sunnyvale, CA).

Indirect immunofluorescence assays

FTLVS was cultured and washed as described above. After diluting the washed bacteria to OD_{600} = 0.1, 1 mL aliquots were incubated with a total of 40 μgs of PLG or PBS (negative control) for 30 minutes at 37°C with gentle rotation. Bacteria were then washed three times with PBS by centrifugation, resuspended in 100 μL of PBS, followed by spotting 20 μL of each sample onto glass coverslips. The samples were then air-dried overnight at 37°C. After methanol fixation, the coverslips were blocked with 1% BSA-PBS at room temperature before adding sheep anti-human PLG (1:100 diluted in 1%

BSA-PBS) for 30 minutes at room temperature. The coverslips were gently washed with PBS before adding donkey anti-sheep/goat IgG:Dylight-488 (1:100 diluted in 1% BSA-PBS), followed by incubation for 30 minutes at room temperature. After washing again with PBS, coverslips were mounted onto glass slides using 100% glycerol containing 0.1 M n-propyl gallate and images were collected on a Zeiss LSM 510 confocal microscope with an Axiovert 100 M base with a 100× Plan Apochromat 1.4 NA oil DIC objective using the argon laser for 488 nm excitation and 505-530 nm bandpass emission filter for imaging Dylight488 fluorescence and the HeNe1 543 nm laser for illumination of the DIC images. Both images were collected using identical detector gain and amplifier offset settings, and the images shown are 1.0 μm optical slices. Digital images were visualized using Zeiss AxioVision LE software.

Chromogenic plasmin activation assay

FTLVS was cultured overnight to mid-log phase, washed twice with TBS and then resuspended in TBS to an OD_{600} of 0.7. Aliquots of the bacterial suspension (50 μL) was added to 50 μL of TBS alone or TBS containing huPLG (192 μg/mL) and incubated for 1 hour at 37°C. The cells were washed 3× with TBST containing 0.1% BSA, and pellets were resuspended in 200 μL of TBS and then split into two 100 μL aliquots. 50 μL of 50 mM Tris-HCl (pH 7.45) with or without 333 μM of the chromogenic plasmin substrate (H-D-Val-Leu-Lys-pNA) and 50 μL 1.2 μg of tPA or TBS alone was added to each sample and incubated at 37°C for 3 h. Bacteria were pelleted via centrifugation and 150 μL of each supernatant was pipetted into a 96-well plate and absorbance at 405 nm was determined as a measure of plasmin activity.

Membrane protein fractionation

Outer membrane enriched fractions were isolated by a procedure adapted from de Bruin, et al [53]. FTLVS were grown in BHI broth (500 ml) to mid-log phase and then were pelleted via centrifugation at 6,400 × g for 30 minutes. Cells were resuspended in cold PBS and then lysed by sonication. Unlysed bacterial cells were separated from the whole-cell lysate by centrifugation at 10,000 × g for 20 minutes at 4°C. The insoluble membrane fraction was then isolated by ultracentrifugation for 1 hour at 100,000 × g at 4°C. After removal of the soluble protein fraction, the pelleted total membrane fraction was resuspended in 1% sarkosyl with vortexing and subjected to a second round of ultracentrifugation for 1 hour at 100,000 × g at 4°C. The Sarkosyl-insoluble pellet was resuspended in 50 mM Tris pH 8. The protein concentration of both the Sarkosyl-soluble and Sarkosyl-insoluble fractions was determined using the DC protein assay (Bio-Rad, Hercules, CA) according to manufacturer directions. Samples were stored at -20°C until use.

Fibronectin degradation assay

Overnight cultures of FTLVS were washed three times with PBS, 10^9 CFU were pipetted into 1.5 mL tubes, and bacteria were pelleted via centrifugation at 18,900 × g for 10 minutes. Bacterial pellets were then resuspended in 50 μl of PBS with or without PLG (2 mg/ml), followed by the addition of 50 μl of tPA (10 μg/mL) and incubation at 37°C with gentle shaking for 1 hour. The bacterial suspensions were pelleted via centrifugation at 18,900 × g, washed 3× with PBS and resuspended with 100 μl of 50 mM Tris, 100 mM NaCl, 5 mM $CaCl_2$) with 3 μg fibronectin (BD Biosciences) and incubation at 37°C with gentle shaking for 24 hours. After the incubation was complete, bacteria were pelleted via centrifugation at 18,900 × g and the supernatants were solublized by boiling in 2× SDS-PAGE sample buffer containing 2-mercaptoethanol. Samples were subjected to 10% SDS-PAGE and then electrophoretically transferred to a PVDF membrane (Immobilon-P, Millipore). The PVDF membrane was pre-blocked with 1% BSA-TBST for 1 hour at RT to minimize non-specific protein binding, and was then incubated with sheep anti-human fibronectin-specific antibody (diluted 1:2000 in 1% BSA-TBST) for 1 hour at RT with gentle rocking. The PVDF membrane was washed three times with TBST to remove unbound primary antibody. The membrane was then incubated in a solution of anti-sheep/goat IgG monoclonal antibody (GT-34, diluted 1:5000 in 1%BSA-TBST) with rocking for 1 hr at RT. The PVDF membranes were washed 3 times with TBST to remove unbound secondary antibody. The blot was developed using Pierce PicoWest chemiluminescence reagents and images were captured using a Bio-Rad ChemiDoc XRS system.

Far-Western blotting analysis

Approximately 100 μg of each protein fraction was precipitated using ice-cold acetone, pelleted via centrifugation at 18,900 × g for 15 minutes, and air-dried at room temperature. The samples were then solublized by boiling in 1× SDS-PAGE sample buffer containing 2-mercaptoethanol. Duplicate 20 μL aliquots of each sample were subjected to 15% SDS-PAGE to separate the proteins based on their size. One set of the samples was then electrophoretically transferred to a PVDF membrane (Immobilon-Psq, Millipore). The PVDF membrane was pre-blocked with 1% BSA-TBST for 1 hour at room temperature to minimize non-specific protein binding and was then incubated in a solution of huPLG (3 ug/mL in 1% BSA-TBST) for one hour with rocking

at 37°C. Unbound PLG was removed by washing three times with TBST. Sheep anti-human PLG-specific antibody (diluted 1:2,000 in 1% BSA-TBST) was added (100 μL/well) and allowed to incubate for 1 hour at RT° with rocking. The PVDF membrane was washed three times with TBST to remove unbound primary antibody. The membrane was then incubated in a solution of anti-sheep/goat IgG monoclonal antibody (GT-34, diluted 1:5,000 in 1%BSA-TBST) with rocking for 1 hr at room temperature. The PVDF membranes were washed three times with TBST to remove unbound secondary antibody. The blot was developed using Pierce PicoWest chemiluminescence reagents and imaged using a Bio-Rad ChemiDoc XRS system.

Proteomic identification of PLG-binding FT proteins

Protein bands were excised from Coomassie-stained SDS-PAGE gels, cut into small pieces, incubated in 50% acetonitrile/100 mM ammonium bicarbonate until colorless, and dried via vacuum centrifugation. The protein was digested by adding 20 μl of a 20 ng/μl trypsin solution and incubating overnight at 37°C. Peptides were extracted from the gel slices via sonication in 50 μl 60% acetonitrile/5%TFA, dried via vacuum centrifugation, and reconstituted in 15 μl 0.1% TFA. Tryptic peptides were desalted/enriched using a C18 ZipTip column (Millipore, Billerica, MA) according to manufacturer's instructions and the eluant was spotted on a MALDI plate and dried. Samples were analyzed using a MALDI-LTQ mass spectrometer (ThermoFinnigan, San Jose, CA). A full MS scan in high-mass range (m/z 600-4000, 5 microscans) was performed. The 50 most intense peaks in the full MS spectrum were selected, and MSMS scans were performed for those ions in high-mass range (m/z 50-4000, 5 microscans), the normalized collision energy for MSMS was 35. Xcalibur software was used to process the mass spectrometric data, and the NCBInr database and the Bioworks 3.2 search engine software were used for database searching.

Acknowledgements

The project described was supported by NIH grant #U54 AI057157 from Southeastern Regional Center of Excellence for Emerging Infections and Biodefense, by NIH grants AI074582 and AI079482 (to JEB) and AI061260 (to MAM), and by Department of Defense Army grant W81XHW-05-1-0227. The authors also thank Cory Blackwell and Himangi Jayakar for helpful discussions. We also thank Jyothi Parvathareddy, and Janice Collum for their technical assistance.

Authors' contributions

SRC conceived and performed all of the experimental work for the study and drafted the manuscript. JEB, TPH, and MAW both participated in the design of the study and played an important role in drafting the manuscript. MAM participated in the design and coordination of all studies, performed the statistical analyses, and helped to draft the manuscript. All authors read and approved the final manuscript.

Received: 10 August 2009 Accepted: 12 March 2010
Published: 12 March 2010

References

1. Hoel T, Scheel O, Nordahl SH, Sandvik T: **Water- and airborne Francisella tularensis biovar palaearctica isolated from human blood.** *Infection* 1991, **19(5)**:348-350.
2. Siret V, Barataud D, Prat M, Vaillant V, Ansart S, Le Coustumier A, Vaissaire J, Raffi F, Garre M, Capek I: **An outbreak of airborne tularaemia in France, August 2004.** *Euro Surveill* 2006, **11(2)**:58-60.
3. Feldman KA, Enscore RE, Lathrop SL, Matyas BT, McGuill M, Schriefer ME, Stiles-Enos D, Dennis DT, Petersen LR, Hayes EB: **An outbreak of primary pneumonic tularemia on Martha's Vineyard.** *N Engl J Med* 2001, **345(22)**:1601-1606.
4. Syrjala H, Kujala P, Myllyla V, Salminen A: **Airborne transmission of tularemia in farmers.** *Scand J Infect Dis* 1985, **17(4)**:371-375.
5. Francis E: **Landmark article April 25, 1925: Tularemia. By Edward Francis.** *JAMA* 1983, **250(23)**:3216-3224.
6. Hopla CE: **The ecology of tularemia.** *Adv Vet Sci Comp Med* 1974, **18(0)**:25-53.
7. **Tularemia transmitted by insect bites–Wyoming, 2001-2003.** *MMWR Morb Mortal Wkly Rep* , 2005/02/25 2005, **54**:170-173.
8. Eliasson H, Lindback J, Nuorti JP, Arneborn M, Giesecke J, Tegnell A: **The 2000 tularemia outbreak: a case-control study of risk factors in disease-endemic and emergent areas, Sweden.** *Emerg Infect Dis* 2002, **8(9)**:956-960.
9. Skierska B: **[Mosquitoes in the northern part of Szczecin region and their role in epidemiology of tularemia.].** *Biul Panstw Inst Med Morsk Trop J W Gdansku* 1955, **6**:267-275.
10. Hubalek Z, Treml F, Halouzka J, Juricova Z, Hunady M, Janik V: **Frequent isolation of Francisella tularensis from Dermacentor reticulatus ticks in an enzootic focus of tularaemia.** *Med Vet Entomol* 1996, **10(3)**:241-246.
11. Emmons RW, Ruskin J, Bissett ML, Uyeda DA, Wood RM, Lear CL: **Tularemia in a mule deer.** *J Wildl Dis* 1976, **12(3)**:459-463.
12. Greco D, Ninu E: **A family outbreak of tularemia.** *Eur J Epidemiol* 1985, **1(3)**:232-233.
13. Golovliov I, Baranov V, Krocova Z, Kovarova H, Sjostedt A: **An attenuated strain of the facultative intracellular bacterium Francisella tularensis can escape the phagosome of monocytic cells.** *Infect Immun* 2003, **71(10)**:5940-5950.
14. Clemens DL, Lee BY, Horwitz MA: **Francisella tularensis enters macrophages via a novel process involving pseudopod loops.** *Infect Immun* 2005, **73(9)**:5892-5902.
15. Forestal CA, Malik M, Catlett SV, Savitt AG, Benach JL, Sellati TJ, Furie MB: **Francisella tularensis has a significant extracellular phase in infected mice.** *J Infect Dis* 2007, **196(1)**:134-137.
16. Yu JJ, Raulie EK, Murthy AK, Guentzel MN, Klose KE, Arulanandam BP: **The presence of infectious extracellular Francisella tularensis subsp. novicida in murine plasma after pulmonary challenge.** *Eur J Clin Microbiol Infect Dis* 2008, **27(4)**:323-325.
17. Ben Nasr A, Haithcoat J, Masterson JE, Gunn JS, Eaves-Pyles T, Klimpel GR: **Critical role for serum opsonins and complement receptors CR3 (CD11b/CD18) and CR4 (CD11c/CD18) in phagocytosis of Francisella tularensis by human dendritic cells (DC): uptake of Francisella leads to activation of immature DC and intracellular survival of the bacteria.** *J Leukoc Biol* 2006, **80(4)**:774-786.
18. Barker JH, McCaffrey RL, Baman NK, Allen LA, Weiss JP, Nauseef WM: **The role of complement opsonization in interactions between F. tularensis subsp. novicida and human neutrophils.** *Microbes Infect* 2009, **11(8-9)**:762-9.
19. Sandstrom G, Lofgren S, Tarnvik A: **A capsule-deficient mutant of Francisella tularensis LVS exhibits enhanced sensitivity to killing by serum but diminished sensitivity to killing by polymorphonuclear leukocytes.** *Infect Immun* 1988, **56(5)**:1194-1202.
20. Ben Nasr A, Klimpel GR: **Subversion of complement activation at the bacterial surface promotes serum resistance and opsonophagocytosis of Francisella tularensis.** *J Leukoc Biol* 2008, **84(1)**:77-85.
21. Lahteenmaki K, Kuusela P, Korhonen TK: **Bacterial plasminogen activators and receptors.** *FEMS Microbiol Rev* 2001, **25(5)**:531-552.
22. Sun H: **The interaction between pathogens and the host coagulation system.** *Physiology (Bethesda)* 2006, **21**:281-288.

23. Lahteenmaki K, Edelman S, Korhonen TK: **Bacterial metastasis: the host plasminogen system in bacterial invasion.** *Trends Microbiol* 2005, **13(2)**:79-85.
24. Degen JL, Bugge TH, Goguen JD: **Fibrin and fibrinolysis in infection and host defense.** *J Thromb Haemost* 2007, **5(Suppl 1)**:24-31.
25. Li Z, Ploplis VA, French EL, Boyle MD: **Interaction between group A streptococci and the plasmin(ogen) system promotes virulence in a mouse skin infection model.** *J Infect Dis* 1999, **179(4)**:907-914.
26. Coleman JL, Gebbia JA, Piesman J, Degen JL, Bugge TH, Benach JL: **Plasminogen is required for efficient dissemination of B. burgdorferi in ticks and for enhancement of spirochetemia in mice.** *Cell* 1997, **89(7)**:1111-1119.
27. Sodeinde OA, Subrahmanyam YV, Stark K, Quan T, Bao Y, Goguen JD: **A surface protease and the invasive character of plague.** *Science* 1992, **258(5084)**:1004-1007.
28. Hazlett KR, Caldon SD, McArthur DG, Cirillo KA, Kirimanjeswara GS, Magguilli ML, Malik M, Shah A, Broderick S, Golovliov I, *et al*: **Adaptation of Francisella tularensis to the mammalian environment is governed by cues which can be mimicked in vitro.** *Infect Immun* 2008, **76(10)**:4479-4488.
29. Filip C, Fletcher G, Wulff JL, Earhart CF: **Solubilization of the cytoplasmic membrane of Escherichia coli by the ionic detergent sodium-lauryl sarcosinate.** *J Bacteriol* 1973, **115(3)**:717-722.
30. Friberg N, Carlson P, Kentala E, Mattila PS, Kuusela P, Meri S, Jarva H: **Factor H binding as a complement evasion mechanism for an anaerobic pathogen, Fusobacterium necrophorum.** *J Immunol* 2008, **181(12)**:8624-8632.
31. Verma A, Hellwage J, Artiushin S, Zipfel PF, Kraiczy P, Timoney JF, Stevenson B: **LfhA, a novel factor H-binding protein of Leptospira interrogans.** *Infect Immun* 2006, **74(5)**:2659-2666.
32. Hellwage J, Meri T, Heikkila T, Alitalo A, Panelius J, Lahdenne P, Seppala IJ, Meri S: **The complement regulator factor H binds to the surface protein OspE of Borrelia burgdorferi.** *J Biol Chem* 2001, **276(11)**:8427-8435.
33. Horstmann RD, Sievertsen HJ, Knobloch J, Fischetti VA: **Antiphagocytic activity of streptococcal M protein: selective binding of complement control protein factor H.** *Proc Natl Acad Sci USA* 1988, **85(5)**:1657-1661.
34. Ram S, Sharma AK, Simpson SD, Gulati S, McQuillen DP, Pangburn MK, Rice PA: **A novel sialic acid binding site on factor H mediates serum resistance of sialylated Neisseria gonorrhoeae.** *J Exp Med* 1998, **187(5)**:743-752.
35. Bergmann S, Rohde M, Chhatwal GS, Hammerschmidt S: **Characterization of plasmin(ogen) binding to Streptococcus pneumoniae.** *Indian J Med Res* 2004, **119(Suppl)**:29-32.
36. Sun H, Ringdahl U, Homeister JW, Fay WP, Engleberg NC, Yang AY, Rozek LS, Wang X, Sjobring U, Ginsburg D: **Plasminogen is a critical host pathogenicity factor for group A streptococcal infection.** *Science* 2004, **305(5688)**:1283-1286.
37. Espersen F: **Interactions between human plasma proteins and cell wall components of Staphylococcus aureus.** *Dan Med Bull* 1987, **34(2)**:59-69.
38. Hauck CR, Ohlsen K: **Sticky connections: extracellular matrix protein recognition and integrin-mediated cellular invasion by Staphylococcus aureus.** *Curr Opin Microbiol* 2006, **9(1)**:5-11.
39. Josefsson E, Higgins J, Foster TJ, Tarkowski A: **Fibrinogen binding sites P336 and Y338 of clumping factor A are crucial for Staphylococcus aureus virulence.** *PLoS ONE* 2008, **3(5)**:e2206.
40. Menzies BE: **The role of fibronectin binding proteins in the pathogenesis of Staphylococcus aureus infections.** *Curr Opin Infect Dis* 2003, **16(3)**:225-229.
41. Agarwal S, Kulshreshtha P, Bambah Mukku D, Bhatnagar R: **alpha-Enolase binds to human plasminogen on the surface of Bacillus anthracis.** *Biochim Biophys Acta* 2008, **1784(7-8)**:986-994.
42. Fricke B, Drossler K, Willhardt I, Schierhorn A, Menge S, Rucknagel P: **The cell envelope-bound metalloprotease (camelysin) from Bacillus cereus is a possible pathogenic factor.** *Biochim Biophys Acta* 2001, **1537(2)**:132-146.
43. Kunert A, Losse J, Gruszin C, Huhn M, Kaendler K, Mikkat S, Volke D, Hoffmann R, Jokiranta TS, Seeberger H, *et al*: **Immune evasion of the human pathogen Pseudomonas aeruginosa: elongation factor Tuf is a factor H and plasminogen binding protein.** *J Immunol* 2007, **179(5)**:2979-2988.
44. Suomalainen M, Haiko J, Ramu P, Lobo L, Kukkonen M, Westerlund-Wikstrom B, Virkola R, Lahteenmaki K, Korhonen TK: **Using every trick in the book: the Pla surface protease of Yersinia pestis.** *Adv Exp Med Biol* 2007, **603**:268-278.
45. Kraiczy P, Hartmann K, Hellwage J, Skerka C, Kirschfink M, Brade V, Zipfel PF, Wallich R, Stevenson B: **Immunological characterization of the complement regulator factor H-binding CRASP and Erp proteins of Borrelia burgdorferi.** *Int J Med Microbiol* 2004, **293(Suppl 37)**:152-157.
46. Kraiczy P, Hellwage J, Skerka C, Becker H, Kirschfink M, Simon MM, Brade V, Zipfel PF, Wallich R: **Complement resistance of Borrelia burgdorferi correlates with the expression of BbCRASP-1, a novel linear plasmid-encoded surface protein that interacts with human factor H and FHL-1 and is unrelated to Erp proteins.** *J Biol Chem* 2004, **279(4)**:2421-2429.
47. Kraiczy P, Hellwage J, Skerka C, Kirschfink M, Brade V, Zipfel PF, Wallich R: **Immune evasion of Borrelia burgdorferi: mapping of a complement-inhibitor factor H-binding site of BbCRASP-3, a novel member of the Erp protein family.** *Eur J Immunol* 2003, **33(3)**:697-707.
48. Kraiczy P, Skerka C, Brade V, Zipfel PF: **Further characterization of complement regulator-acquiring surface proteins of Borrelia burgdorferi.** *Infect Immun* 2001, **69(12)**:7800-7809.
49. Kraiczy P, Skerka C, Zipfel PF, Brade V: **Complement regulator-acquiring surface proteins of Borrelia burgdorferi: a new protein family involved in complement resistance.** *Wien Klin Wochenschr* 2002, **114(13-14)**:568-573.
50. Wallich R, Pattathu J, Kitiratschky V, Brenner C, Zipfel PF, Brade V, Simon MM, Kraiczy P: **Identification and functional characterization of complement regulator-acquiring surface protein 1 of the Lyme disease spirochetes Borrelia afzelii and Borrelia garinii.** *Infect Immun* 2005, **73(4)**:2351-2359.
51. Fenno JC, Tamura M, Hannam PM, Wong GW, Chan RA, McBride BC: **Identification of a Treponema denticola OppA homologue that binds host proteins present in the subgingival environment.** *Infect Immun* 2000, **68(4)**:1884-1892.
52. Crane DD, Warner SL, Bosio CM: **A novel role for plasmin-mediated degradation of opsonizing antibody in the evasion of host immunity by virulent, but not attenuated, Francisella tularensis.** *J Immunol* 2009, **183(7)**:4593-4600.
53. de Bruin OM, Ludu JS, Nano FE: **The Francisella pathogenicity island protein IglA localizes to the bacterial cytoplasm and is needed for intracellular growth.** *BMC Microbiol* 2007, **7**:1.

doi:10.1186/1471-2180-10-76
Cite this article as: Clinton *et al.*: Binding and activation of host plasminogen on the surface of *Francisella tularensis*. *BMC Microbiology* 2010 **10**:76.

JVI Accepts, published online ahead of print on 19 May 2010
J. Virol. doi:10.1128/JVI.02444-09

Cross-reactive neutralizing antibodies directed against pandemic H1N1 2009 virus are protective in a highly sensitive DBA/2 influenza mouse model

Adrianus CM Boon[1], Jennifer deBeauchamp[1], Scott Krauss[1], Adam Rubrum[1], Ashley D Webb[1], Robert G Webster[1], Janet McElhaney[2], Richard J Webby[1,*]

[1] Department of Infectious Diseases, St. Jude Children's Research Hospital, Memphis TN 38105, USA. [2] Department of Medicine, University of British Columbia, Vancouver, BC, Canada

Running Title: Improving preclinical models for influenza

* Corresponding author
St. Jude Children's Research Hospital
Department of Infectious Diseases
Mailstop 330
262 Danny Thomas Place
Memphis, TN 38105
Phone: 901-595 3014
Fax: 901-595 8559
Email: Richard.Webby@stjude.org

Word count Abstract: 177
Word count Main text: 3786

Abstract

Our ability to rapidly respond to emerging influenza is hampered somewhat by the lack of a susceptible small animal model. To develop a more sensitive model we pathotyped eighteen low-pathogenic non-mouse-adapted influenza A viruses of human and avian origin in DBA/2 and C57BL/6 mice. The majority of the isolates (13/18) induced severe morbidity and mortality in DBA/2 mice upon intranasal challenge with one million infectious doses. Also, at a 100-fold lower dose, more than 50% of the viruses induced severe weight loss and mice succumbed to the infection. In contrast, only two virus strains were pathogenic for C57BL/6 mice upon high dose inoculation. Therefore DBA/2 mice are a suitable model to validate influenza A virus vaccines and antiviral therapies without the need for extensive viral adaptation. Correspondingly, we used the DBA/2 model to assess the level of protection afforded by pre-existing pandemic H1N1 2009 virus (H1N1pdm) cross-reactive human antibodies detected by hemagglutination inhibition assay. Passive transfer of these antibodies prior to infection protected mice from H1N1pdm-induced pathogenicity, demonstrating the effectiveness of these cross-reactive neutralizing antibodies *in vivo*.

Keywords: Pandemic, Influenza, Animal Model, DBA/2, Pandemic H1N1 2009 virus

Introduction

Respiratory tract infections are the third leading cause of mortality in the world [28]. Influenza, a disease of the airways caused by influenza viruses, is responsible for approximately half a million deaths and 3–5 million hospitalizations per year [29]. In addition to the annual disease burden, influenza A virus is more notoriously known for its ability to cause pandemics. Three pandemics have been reported in the twentieth century: the first that occurred in 1918 (Spanish influenza) killed 20–50 million individuals [15]; the other 2 in 1957 and 1968, although less lethal, killed millions due to the lack of preexisting immunity. In April 2009, 2 cases of febrile illness were confirmed to be caused by swine-origin influenza A virus (H1N1) [3,7]. Continuous spread within North America and other parts of the world has signaled the first influenza pandemic of this century.

To study the pathogenicity of influenza A viruses, including the current pandemic A (H1N1) 2009 virus (H1N1pdm), in mammalian hosts and to determine the effectiveness of pharmaceutical interventions, it is essential to have a sensitive animal model. Although influenza has some important differences in mice and humans, a murine model is the only animal model thus far described that allows for relatively high group numbers and any relatively high throughput. Unfortunately, only few strains of influenza A virus – almost exclusively belonging to the highly pathogenic avian influenza virus isolates of the H5 and H7 subtype – are pathogenic in most commonly used mouse strains without adaptation through serial passaging. The hemagglutinin proteins of these H5 and H7 viruses contain a basic amino-acid cleavage site, allowing them to spread systemically [12,20,27]. Most other subtypes of influenza virus, including H1N1 and H3N2, either do not infect or cause very mild disease in mice. The requirement for adaptation of a pandemic virus to commonly used mouse strains can lead to a delay in the gathering of important data to help guide public health control strategies. As such, the lack of a sensitive small animal model to study the infection dynamics of various subtypes of avian influenza viruses severely hampers the rapid and effective response required during a pandemic or prepandemic situation.

This study was designed to demonstrate the utility of DBA/2 mice, previously reported to be susceptible to highly pathogenic influenza viruses [1], to study infections caused by several influenza A virus subtypes isolated from birds or humans without the need for prior adaptation. To assess the utility of the model to respond to emerging strains, we used DBA/2 mice to examine the functional activity of sera from individuals previously shown to have pre-existing cross-reactive H1N1pdm antibodies. It is hypothesized that these individuals may be partially protected from infection because of the presence of cross-reactive neutralizing antibodies produced after infection with a different but related H1N1 virus. This hypothesis is supported by *in vitro* microneutralization and hemagglutination inhibition assays [10,18]; however, it is not yet known whether these antibodies are also functional *in vivo*.

Material and Methods

Mice and viruses

Six- to ten-week-old female C57BL/6 and DBA/2 mice were purchased from Jackson Laboratories (Bar Harbor, ME) and housed in the Animal Resource Center at St. Jude Children's Research Hospital (St. Jude). The mice received food and water *ad libitum,* and all experiments were conducted in accordance with rules of the Institutional Animal Control and Use Committee of St. Jude.

Twenty-three influenza A viruses (Table 1) from 9 different hemagglutinin subtypes (H1–H7, H9 and H10) were propagated in the chorioallantoic cavity of 10-day-old embryonated chicken eggs. The allantoic fluid containing infectious particles was harvested 48 h after inoculation and the infectious virus titer (egg infectious dose 50, EID_{50}) was determined. All virus stocks had a minimum titer of $10^{8.5}$ EID_{50}/ml.

Inoculation of mice with influenza A virus

C57BL/6 and DBA/2 mice were inoculated with influenza A viruses intranasally in 30 µl of sterile PBS after sedation with avertin (2,2,2-tribromoethanol, Sigma-Aldrich, MO, USA). The mouse lethal dose 50 (MLD_{50}) was determined after infecting mice with 10-fold serial dilutions of the viruses from 10^6 EID_{50} to 10^1 EID_{50}. Morbidity and mortality were monitored for 21 days and the MLD_{50} values were calculated by the Reed-Munch method [21]. Groups of 5 mice per inoculum size per isolate were tested with the exception of seasonal H1N1 (10^6 EID_{50}, n = 6 and 10^4 EID_{50}, n = 8), H1N1pdm (10^4 EID_{50}, n = 9), H2N3 (10^6 EID_{50}, n = 3 and 10^4 EID_{50}, n = 4), H2N4 (10^4 EID_{50}, n = 4), H4N6 (10^6 EID_{50}, n = 3), H5N9 (10^6 EID_{50}, n = 6 and 10^4 EID_{50}, n = 4), H5N7 (10^6 EID_{50}, n = 10), H7N3 (10^6 EID_{50}, n = 9 and 10^4 EID_{50}, n = 4), H7N9 (10^4 EID_{50}, n = 4), H9N2/Y280 (10^6 EID_{50}, n = 10), H9N5 (10^6 and 10^4 EID_{50}, n = 4), H10N5 (10^6 EID_{50}, n = 6 and 10^4 EID_{50}, n = 8) and H10N7 (10^4 EID_{50}, n = 4) for DBA/2 mice and H5N7 (10^6 EID_{50}, n = 8), H6N5 (10^6 EID_{50}, n = 6), H7N3 (10^6 EID_{50}, n = 10), H7N9 (10^6 EID_{50}, n = 4) and H9N2 (10^6 EID_{50}, n = 4) for C57BL/6.

Lung viral titers

Lungs were collected on days 2 and 7 postinoculation with 10^4 EID_{50} of influenza A virus and stored at –80°C. They were homogenized in 1.0 ml of minimal essential medium, and homogenates were spun for 5 min at 1000*g* to remove cellular debris. The supernatant was used to quantify the amount of infectious virus present in the lungs. Depending on the virus isolate, viral titers were determined in eggs or Madin-Darby Canine Kidney (MDCK) cells as described previously [1].

Hemagglutination inhibition and virus neutralization assays

Influenza A virus neutralizing activity in serum was quantified by hemagglutination inhibition (HI) and virus microneutralization (VN) assay. Sera were first treated with receptor destroying enzyme (RDE) (RDE (II) "Seiken", Denka Seiken UK Ltd, UK) for 18 h at 37°C followed by 30 minutes inactivation at 56°C. HI assays were done with 4 hemagglutination units of the virus and 0.5% turkey red blood cells (H1N1pdm) or 0.5% chicken red blood cells (avian virus isolates) as described previously [9]. For a VN assay the sera were diluted two-fold starting at 1:10 dilution in PBS and incubated for 1h at 37°C with 100 $TCID_{50}$ of A/California/4/09 virus. Next, 100µl of the mixture of virus and sera were added to MDCK cells for 1 h at 37°C. Following the aspiration of the supernatant, cells were washed with PBS and fresh 200µl of minimal essential medium supplemented with 0.1% bovine serum albumin (A8412, Sigma-Aldrich), antibiotics (Invitrogen, NY, USA), vitamins (Invitrogen) and 1µg/ml TPCK trypsin (Worthington, NJ, USA) was added. After 3-4 days at 37°C, the assay was developed by HA assay using turkey red blood cells. The average HI and VN titer was calculated following $\log_2$ transformation of the highest serum dilution able to inhibit hemagglutination or virus replication respectively.

Passive antibody transfer

Human sera were collected as part of a clinical trial conducted during the 2007-08 and 2008-09 influenza seasons in the Greater Vancouver Area of British Columbia, Canada or in the vicinity of the Greater Hartford Area of Connecticut. All participants received the standard dose of the licensed trivalent split-virus influenza vaccine

containing A/Solomon Islands/3/2006-like (H1N1), A/Wisconsin/67/2005-like (H3N2), and B/Malaysia/2506/2004-like viruses in 2007-08 or A/Brisbane/59/2007 (H1N1)-like, A/Brisbane/10/2007 (H3N2)-like, and B/Florida/4/2006-like viruses in 2008-09. Sera were collected before vaccination and 4 weeks after vaccination. Post-vaccination sera from individuals, aged 65 years and older, with a detectable HI and VN titer toward H1N1pdm (A/California/4/2009) were pooled and heat-inactivated for 30 min at 56°C. To study the effect of neutralizing antibodies we used age-matched pooled human sera without a detectable HI and VN titer to H1N1pdm (A/California/4/2009), seasonal H1N1 (A/Brisbane/59/2007) and H7N3 (A/shorebird/Delaware/22/2006) virus. Ferret polyclonal serum obtained from ferrets 14 days after inoculation with the H1N1pdm virus (HI titer of 2560, VN titer of 320) or PBS were used as a positive and negative control respectively. Four hundred micro liters of pooled human sera, diluted 1:1 in PBS, were injected intraperitoneally into 10 mice 24 h prior to inoculation with a lethal dose of virus. The positive and negative controls were also injected into 10 mice each for the H1N1pdm experiment, while 5 PBS control mice were included in the H7N3 and seasonal H1N1 follow-up experiment.

Cytokine analysis

Lungs were collected on days 2 and 7 postinoculation with 10^4 EID_{50} of influenza A virus and concentrations of CCL2, CCL5, interleukin-6 (IL-6), tumor necrosis factor-alpha (TNF-α) and interferon-gamma (IFN-γ) were determined as described previously [1]. ELISA was performed according to manufacturer's instructions (Quantikine kits, R&D Systems, Minneapolis, MN). At least 4 animals infected with a particular strain of influenza A virus were tested for 1 cytokine at a given time point.

Statistical analysis

Statistical analyses of differences in mortality were determined by using the log-rank test. The Student's T-test was used to analyze differences in lung virus titers between the different strains of mice following ln-transformation of the data as well as to determine statistical significance in cytokine and chemokine production and weight loss after influenza A virus infection.

Results

Increased susceptibility of DBA/2 mice to influenza A virus isolates

To assess the utility of DBA/2 mice as a more universal small animal model for influenza, we tested a range of different viral subtypes for their ability to induce morbidity and mortality in this host. A set of twenty-three viruses belonging to 9 different hemagglutinin subtypes was selected and used to inoculate DBA/2 mice. At a dose of 10^6 EID_{50}, 18 or 78% of the viruses were pathogenic and mice succumbed to infection 5–12 days postinoculation, depending on the virus isolate (Table 1). Inoculation with a lower dose of virus (10^4 EID_{50}) caused severe weight loss and death of DBA/2 mice in 14 of 22 (64%) virus isolates tested (Table 1). These isolates included a seasonal human H1N1 virus from 2008 and both H10 viruses. The ability to induce severe disease, as measured by weight loss and mortality, in DBA/2 mice was not limited to certain subtypes of influenza; however, virus isolates of the H2 and H4 subtype were only mildly pathogenic. Few isolates were pathogenic at 10^2 EID_{50}, and these included the 2 mouse-adapted influenza A viruses (A/Puerto Rico/8/1934 (100% mortality) and X31 (60% mortality)), 2 highly pathogenic H5N1 influenza A viruses (A/Hong Kong/213/2003 (84% mortality) and A/Vietnam/1203/2004 (100% mortality)), a low pathogenic H7N3 (A/shorebird/Delaware/22/2006, 45% mortality) virus, and the H1N1pdm (100% mortality). Eighteen isolates were also tested in C57BL/6 mice at a dose of 10^6 EID_{50}. Only the mouse-adapted virus A/Puerto Rico/8/1934 virus, 3 highly pathogenic viruses, a H6N1 virus (A/teal/Hong Kong/W312/1997), and the H1N1pdm virus caused severe disease and mortality (Table 1).

Nonadapted avian influenza A viruses can replicate to high titers in C57BL/6 and DBA/2 mice

We hypothesize that the large difference in pathogenicity of avian influenza A viruses between DBA/2 and C57BL/6 mice may be due to increased replication efficiency. To test this, we measured day 2 and 7 postinoculation pulmonary viral loads in mice infected with 10^4 EID_{50} of H7N3 or H10N5 virus (Figure 1). These avian virus isolates were selected for their exceptionally large difference in pathology score between DBA/2 and

C57BL/6 mice. High dose inoculation (10^6 EID_{50}) with H7N3 or H10N5 virus induced 7% and 4% maximum weight loss in C57BL/6 mice, while DBA/2 mice succumbed to infection with 10^2 or 10^4 EID_{50} respectively. On day 2 postinoculation, lung viral titers of DBA/2 and C57BL/6 mice were similar for both H7N3 ($10^{6.25}$ vs. $10^{6.75}$ EID_{50}/ml, respectively) and H10N5 virus ($10^{5.3}$ vs. $10^{6.0}$ EID_{50}/ml, respectively, Figure 1). Interestingly, titers in H7N3-infected lungs were approximately 1-log_{10} higher than those of H10N5-infected lungs. Day 7 postinoculation, H7N3-infected lungs of DBA/2 mice had higher virus loads than that of C57BL/6 mice ($P < 0.05$, Figure 1). Lungs of H10N5-infected DBA/2 mice also contained more virus than those of C57BL/6 mice, however this difference was not significant ($P = 0.07$).

To assess the ability of other non- or low-pathogenic avian influenza A virus isolates to infect mice, we measured the serological response against the challenge virus in convalescent sera as a surrogate marker for viral replication. In C57BL/6 mice, an HI titer was detected postinoculation with 5 of the 8 virus isolates studied, suggesting that the majority of the isolates replicate in the respiratory tract of mice (Table 2). Inoculation of 3 viruses, an H4N1, H6N5 and an H5N7 virus did not cause seroconversion in C57BL/6 mice. Because DBA/2 mice are generally more susceptible to influenza virus infection and fewer isolates were non- or low-pathogenic, we tested convalescent sera following inoculation with only 5 virus isolates. Of the 5 convalescent sera tested, 3 contained a detectable HI titer whereas 2 (an H4N6 and an H9N6 virus) did not (Table 2). This data suggests that most influenza virus isolates are capable of replicating in the respiratory tract of mice, but the outcome after infection depends entirely on the mouse strain, virus strain, or a combination of both.

Pandemic H1N1 2009 virus A/California/4/2009 is highly pathogenic in DBA/2 mice

Based on the results presented above, we next looked at the replication of the H1N1pdm viruses in DBA/2 and C57BL/6 mice. Inoculation of mice with 10^6–10^2 EID_{50} of A/California/4/09, a representative H1N1pdm virus, resulted in 100% mortality after 8–12 days, and that with 10^1 EID_{50} caused significant weight loss in 100% and mortality in 50% of DBA/2 mice (Table 1). In contrast, C57BL/6 mice lost a significant amount of weight (14%, $P<0.05$) by day 7 when inoculated with 10^6 EID_{50} and 60% of the mice

died. Inoculation with 10^5 to 10^4 EID_{50} did not cause death of C57BL/6 mice. Therefore, the MLD_{50} for A/California/4/2009 was 10^5-fold lower in DBA/2 than C57BL/6 mice, a finding consistent with other viral strains.

Increased pathogenicity is often associated with higher viral loads and increased levels of proinflammatory cytokines such as CCL2, IL6, and TNFα. At Day 2 postinoculation with 10^4 EID_{50} of H1N1pdm, lung viral titers of DBA/2 mice and C57BL/6 mice were similar (Figure 1a). There were also no significant differences in the levels of CCL2, CCL5, and IL6 between both strains (Table 3), but levels of TNFα were significantly higher in DBA/2 than C57BL/6 mice ($P < 0.01$). At Day 7 postinfection, lung homogenates of DBA/2 mice had higher viral loads than C57BL/6 mice ($P < 0.01$, Figure 2b) as well as significantly higher concentrations of CCL2 and IL6 ($P < 0.01$, Table 3).

Passive transfer of cross-reactive human neutralizing antibodies protects against H1N1pdm-induced pathogenicity

To assess the functionality of human cross-reactive polyclonal antibodies, passive antibody transfer experiments were performed using the highly susceptible DBA/2 mice. Human sera were obtained from individuals not previously exposed to the H1N1pdm virus but who had cross-reactive neutralizing antibodies to it with HI titer of 160 and VN titer of 95. Twenty-four hours after passive transfer, mice were inoculated with 10^2 EID_{50} (3–5 LD_{50}) of A/California/4/2009 virus and morbidity and mortality were assessed. As expected, all control mice treated with PBS died within 10 days of inoculation (Figure 2a). Mice treated with ferret sera containing high levels of H1N1pdm-specific neutralizing antibodies did not succumb to infection ($P < 0.001$) and lost significantly less weight on days 7, 10, 13, and 15 than mice in all other groups ($P < 0.01$, Figure 2). DBA/2 mice injected with pooled human serum containing cross-reactive antibodies had a higher survival rate (75%) than mice in the PBS control group (0%, $P < 0.01$) and mice receiving human sera without detectable cross-neutralizing antibodies (15%, $P < 0.05$). Increased survival of the mice injected with cross-neutralizing antibodies was accompanied by a decrease in percent weight loss on days 10 (11%) and 13 (20%) postinfection ($P < 0.01$, Figure 2b). These data indicate that H1N1pdm-specific

neutralizing antibodies induced after infection with a related H1N1 virus can protect DBA/2 mice from a lethal challenge and are likely responsible for the age related attack rates seen in humans. The protective effect of human sera without any neutralizing antibodies was validated using two additional challenge models, a seasonal H1N1 (A/Memphis/33/2008) and an avian H7N3 (A/shorebird/Delaware/22/2006) virus isolate. The survival rates increased significantly for the seasonal H1N1 virus (90%, $P < 0.01$) but not for H7N3 (17%, $P > 0.05$) suggesting that *in vitro* HI or MN assays underestimate the levels of pre-existing neutralizing immunity to influenza A virus strain in humans.

Discussion

The present study establishes that DBA/2 mice are very susceptible to most influenza A virus isolates and that infection often results in debilitating pneumonia and subsequent death. This sensitivity of DBA/2 mice was used to demonstrate that H1N1pdm is more pathogenic than the circulating seasonal H1N1 viruses and that pre-existing human cross-reactive neutralizing antibodies can prevent H1N1pdm-induced mortality and morbidity.

Small animal models, like the mouse, have frequently been used for influenza virus research including areas such as pathogenesis, vaccine efficacy, and antiviral therapies. The preferred strains, C57BL/6 and Balb/c, display few clinical symptoms upon high dose inoculation with most influenza A virus isolates and only highly pathogenic or mouse-adapted viruses cause severe morbidity and mortality at low doses. As such, it was generally believed that mice are resistant to most human and avian influenza A viruses. The current study, as well as a recent report by Driksell *et al* [5], provide substantial evidence to suggest that Balb/c and C57BL/6 mice are susceptible to infection with many different influenza A virus isolates (H1-H7, H9-H11); albeit that the infection does not cause significant disease. In contrast, DBA/2 mice become sick and often succumb to infection with the majority of the tested isolates. This enhanced susceptibility of DBA/2 mice was previously reported for highly pathogenic and mouse-adapted influenza viruses [1,24] and now includes many non-adapted avian influenza isolates.

The mechanism for the difference in susceptibility between C57BL/6 and DBA/2 is not yet fully understood but involves multiple genetic differences between the two mouse lineages affecting several pathways and processes [1]. Certain influenza viruses grow to higher titers in DBA/2 mice (A/Hong Kong/213/2003 (H5N1) or A/Memphis/33/2008 (H1N1, data not shown)), while others do not (H7N3 and H10N5, this study). Irrespective of the difference in viral load, DBA/2 mice respond more vigorously producing larger quantities of certain pro-inflammatory molecules like TNF-α which was shown to correlate with increased morbidity and mortality in humans [4]. Previous work has shown that the lack of a functional Hc in DBA/2 mice may result in a less effective adaptive immune response increasing the viral load during later stages of the infection [1,11]. In the same study, histopathologic evaluation DBA/2 and C57BL/6 mice after H5N1 virus infection was able to clearly show more extensive involvement of the entire lung as

well as necrotic epithelium on day 4 in the DBA/2 mice. At day 7 there was a dramatic difference in the number of cells that stain positive for influenza between the two strains. In the C57BL/6 mice, an inflammatory response was observed in the parenchyma with multifocal macrophages within the infiltrate that stain positive for influenza. In contrast, the DBA/2 mice maintain widespread intensely positive staining of the airway epithelium, alveolar macrophages, Type I and Type II cells in the alveolar wall. Overall, the combined effect of poor clearance, excessive inflammation, and elevated virus titers likely creates a highly pathogenic environment in DBA/2 mice.

The exceptional susceptibility of DBA/2 mice for influenza virus infections was used to demonstrate the effectiveness of H1N1pdm cross-neutralizing human antibodies in reducing H1N1pdm driven mortality. Approximately 50% of the US population over 75 years of age have low levels of pre-exposure cross-reactive antibodies to H1N1pdm [13]. The age of these individuals suggests that these antibodies were generated between 1918 and 1930 when an antigenically similar H1N1 virus was possibly circulating among humans. We show in this study that these cross-reactive antibodies are also fully functional *in vivo*, and may offer some degree of protection to an otherwise at-risk elderly population against the current H1N1pdm. The identity of the neutralizing epitopes has yet to be identified but could be located within the antigenic site Sa [30]. Interestingly, there was a small but significant level of protection when mice were injected with human serum without detectable levels of virus neutralizing antibodies. The protection was specific for H1N1 viruses since the transfer of HI negative sera did not affect the survival after challenge with a H7N3 virus. The protection is possibly mediated by antibodies specific for the M2 protein [19,25,26] or to non-neutralizing epitopes on the HA or NA [16,22,2,14,23]. These data also suggest that the current *in vitro* assays (HI and VN) are underestimating the level of pre-existing protective immunity in the human population. Addition of serum factors, like C1q, have been shown to increase the sensitivity of these assays [6,17]. The limited capacity of HI or VN assays to detect neutralizing antibodies was previously noted in pre-clinical H5N1 ferret vaccine studies. A single dose of inactivated H5N1 vaccine did not induce a detectable HI or VN titer, however the animals were protected from a lethal challenge with highly pathogenic H5N1 virus [8].

Although the DBA/2 mouse model will provide a useful analytical tool to study viruses and antiviral therapies, the model may not necessarily reflect the natural response to influenza viruses in humans. With the exception of highly pathogenic H5N1 viruses, one should be careful interpreting pathogenesis data upon infection with these avian isolates as described in the current study.

To summarize, we have confirmed that the DBA/2 mouse model is a suitable and highly susceptible animal model to study infection of influenza A viruses of various subtypes, including those previously known to infect humans. Also, this model will allow us to define the requirements of viruses of avian origin to infect mammalian hosts and rapidly evaluate vaccines or antiviral therapies in the event of a pandemic emergency.

Acknowledgements

We thank David Walker for isolating and propagating influenza A virus isolates. We also acknowledge Drs. Nancy Cox, Sasha Klimov, and Ruben Donis (Centers of Disease Control), Dr. Ron Fouchier (Erasmus Medical Center), Drs. Malik Peiris and Guan Yi (University of Hong Kong), and the World Health Organization Global Influenza Surveillance Network as a source of influenza A viruses. Finally, we thank Drs. M Ducatez and S. Schultz-Cherry for critically reviewing the paper. This project was funded in part by grants from the National Institute Allergy and Infectious Diseases, National Institutes of Health, Department of Health and Human Services under contract no. HHSN266200700005C, by the Department of Defense award W81XWH-09-1-0391, by the Centers of Infectious Diseases Control at St Jude Children's Research Hospital and the American Lebanese Syrian Associated Charities (ALSAC).

Reference List

1. **Boon, A. C., J. Debeauchamp, A. Hollmann, J. Luke, M. Kotb, S. Rowe, D. Finkelstein, G. Neale, L. Lu, R. W. Williams, and R. J. Webby**. 2009. Host Genetic Variation Affects Resistance to Infection with a Highly Pathogenic H5N1 Influenza A Virus in Mice. J. Virol. **83**:10417-26

2. **Chen, Z., S. Kadowaki, Y. Hagiwara, T. Yoshikawa, K. Matsuo, T. Kurata, and S. Tamura**. 2000. Cross-protection against a lethal influenza virus infection by DNA vaccine to neuraminidase. Vaccine. **18**:3214-3222.

3. **Dawood, F. S., S. Jain, L. Finelli, M. W. Shaw, S. Lindstrom, R. J. Garten, L. V. Gubareva, X. Xu, C. B. Bridges, and T. M. Uyeki**. 2009. Emergence of a novel swine-origin influenza A (H1N1) virus in humans. N. Engl. J. Med. **360**:2605-2615.

4. **de Jong, M. D., C. P. Simmons, T. T. Thanh, V. M. Hien, G. J. Smith, T. N. Chau, D. M. Hoang, N. V. Chau, T. H. Khanh, V. C. Dong, P. T. Qui, B. V. Cam, d. Q. Ha, Y. Guan, J. S. Peiris, N. T. Chinh, T. T. Hien, and J. Farrar**. 2006. Fatal outcome of human influenza A (H5N1) is associated with high viral load and hypercytokinemia. Nat. Med. **12**:1203-1207.

5. **Driskell, E. A., C. A. Jones, D. E. Stallknecht, E. W. Howerth, and S. M. Tompkins**. 2010. Avian influenza virus isolates from wild birds replicate and cause disease in a mouse model of infection. Virology. **399**:280-289.

6. **Feng, J. Q., K. Mozdzanowska, and W. Gerhard**. 2002. Complement component C1q enhances the biological activity of influenza virus hemagglutinin-specific antibodies depending on their fine antigen specificity and heavy-chain isotype. J. Virol. **76**:1369-1378.

7. **Garten, R. J., C. T. Davis, C. A. Russell, B. Shu, S. Lindstrom, A. Balish, W. M. Sessions, X. Xu, E. Skepner, V. Deyde, M. Okomo-Adhiambo, L. Gubareva, J. Barnes, C. B. Smith, S. L. Emery, M. J. Hillman, P. Rivailler, J. Smagala, G. M. de, D. F. Burke, R. A. Fouchier, C. Pappas, C. M. puche-Aranda, H. Lopez-Gatell, H. Olivera, I. Lopez, C. A. Myers, D. Faix, P. J. Blair, C. Yu, K. M. Keene, P. D. Dotson, Jr., D. Boxrud, A. R. Sambol, S. H. Abid, G. K. St, T. Bannerman, A. L. Moore, D. J. Stringer, P. Blevins, G. J. mmler-Harrison, M. Ginsberg, P. Kriner, S. Waterman, S. Smole, H. F. Guevara, E. A. Belongia, P. A. Clark, S. T. Beatrice, R. Donis, J. Katz, L. Finelli, C. B. Bridges, M. Shaw, D. B. Jernigan, T. M. Uyeki, D. J. Smith, A. I. Klimov, and N. J. Cox**. 2009. Antigenic and genetic characteristics of swine-origin 2009 A(H1N1) influenza viruses circulating in humans. Science. **325**:197-201.

8. **Govorkova, E. A., R. J. Webby, J. Humberd, J. P. Seiler, and R. G. Webster**. 2006. Immunization with reverse-genetics-produced H5N1 influenza vaccine

protects ferrets against homologous and heterologous challenge. J. Infect. Dis. **194**:159-167.

9. **Hancock, K., V. Veguilla, X. Lu, W. Zhong, E. N. Butler, H. Sun, F. Liu, L. Dong, J. R. Devos, P. M. Gargiullo, T. L. Brammer, N. J. Cox, T. M. Tumpey, and J. M. Katz**. 2009. Cross-Reactive Antibody Responses to the 2009 Pandemic H1N1 Influenza Virus. N. Engl. J. Med.

10. **Hancock, K., V. Veguilla, X. Lu, W. Zhong, E. N. Butler, H. Sun, F. Liu, L. Dong, J. R. Devos, P. M. Gargiullo, T. L. Brammer, N. J. Cox, T. M. Tumpey, and J. M. Katz**. 2009. Cross-Reactive Antibody Responses to the 2009 Pandemic H1N1 Influenza Virus. N. Engl. J. Med.

11. **Hicks, J. T., F. A. Ennis, E. Kim, and M. Verbonitz**. 1978. The importance of an intact complement pathway in recovery from a primary viral infection: influenza in decomplemented and in C5-deficient mice. J. Immunol. **121**:1437-1445.

12. **Horimoto, T. and Y. Kawaoka**. 1994. Reverse genetics provides direct evidence for a correlation of hemagglutinin cleavability and virulence of an avian influenza A virus. J. Virol. **68**:3120-3128.

13. **Itoh, Y., K. Shinya, M. Kiso, T. Watanabe, Y. Sakoda, M. Hatta, Y. Muramoto, D. Tamura, Y. Sakai-Tagawa, T. Noda, S. Sakabe, M. Imai, Y. Hatta, S. Watanabe, C. Li, S. Yamada, K. Fujii, S. Murakami, H. Imai, S. Kakugawa, M. Ito, R. Takano, K. Iwatsuki-Horimoto, M. Shimojima, T. Horimoto, H. Goto, K. Takahashi, A. Makino, H. Ishigaki, M. Nakayama, M. Okamatsu, K. Takahashi, D. Warshauer, P. A. Shult, R. Saito, H. Suzuki, Y. Furuta, M. Yamashita, K. Mitamura, K. Nakano, M. Nakamura, R. Brockman-Schneider, H. Mitamura, M. Yamazaki, N. Sugaya, M. Suresh, M. Ozawa, G. Neumann, J. Gern, H. Kida, K. Ogasawara, and Y. Kawaoka**. 2009. In vitro and in vivo characterization of new swine-origin H1N1 influenza viruses. Nature. **20;460**:1021-1025.

14. **Johansson, B. E., D. J. Bucher, and E. D. Kilbourne**. 1989. Purified influenza virus hemagglutinin and neuraminidase are equivalent in stimulation of antibody response but induce contrasting types of immunity to infection. J. Virol. **63**:1239-1246.

15. **Johnson, N. P. and J. Mueller**. 2002. Updating the accounts: global mortality of the 1918-1920 "Spanish" influenza pandemic. Bull. Hist Med. **76**:105-115.

16. **McLain, L. and N. J. Dimmock**. 1989. Protection of mice from lethal influenza by adoptive transfer of non-neutralizing haemagglutination-inhibiting IgG obtained from the lungs of infected animals treated with defective interfering virus. J. Gen. Virol. **70**:2615-2624.

17. **Mehlhop, E., S. Nelson, C. A. Jost, S. Gorlatov, S. Johnson, D. H. Fremont, M. S. Diamond, and T. C. Pierson**. 2009. Complement protein C1q reduces the

stoichiometric threshold for antibody-mediated neutralization of West Nile virus. Cell Host. Microbe. **6**:381-391.

18. **MMWR**. 2009. Serum cross-reactive antibody response to a novel influenza A (H1N1) virus after vaccination with seasonal influenza vaccine. MMWR Morb. Mortal. Wkly. Rep. **58**:521-524.

19. **Mozdzanowska, K., K. Maiese, M. Furchner, and W. Gerhard**. 1999. Treatment of influenza virus-infected SCID mice with nonneutralizing antibodies specific for the transmembrane proteins matrix 2 and neuraminidase reduces the pulmonary virus titer but fails to clear the infection. Virology. **254**:138-146.

20. **Ohuchi, M., M. Orlich, R. Ohuchi, B. E. Simpson, W. Garten, H. D. Klenk, and R. Rott**. 1989. Mutations at the cleavage site of the hemagglutinin after the pathogenicity of influenza virus A/chick/Penn/83 (H5N2). Virology. **168**:274-280.

21. **Reed, L. J. and H. Muench**. 1938. A simple method for estimating fifty percent endpoints. Am. J. Hyg. **27**:493-497.

22. **Sambhara, S., A. Kurichh, R. Miranda, T. Tumpey, T. Rowe, M. Renshaw, R. Arpino, A. Tamane, A. Kandil, O. James, B. Underdown, M. Klein, J. Katz, and D. Burt**. 2001. Heterosubtypic immunity against human influenza A viruses, including recently emerged avian H5 and H9 viruses, induced by FLU-ISCOM vaccine in mice requires both cytotoxic T-lymphocyte and macrophage function. Cell Immunol. **211**:143-153.

23. **Sandbulte, M. R., G. S. Jimenez, A. C. Boon, L. R. Smith, J. J. Treanor, and R. J. Webby**. 2007. Cross-reactive neuraminidase antibodies afford partial protection against H5N1 in mice and are present in unexposed humans. PLoS. Med. **4**:e59.

24. **Srivastava, B., P. Blazejewska, M. Hessmann, D. Bruder, R. Geffers, S. Mauel, A. D. Gruber, and K. Schughart**. 2009. Host genetic background strongly influences the response to influenza a virus infections. PLoS. One. **4**:e4857.

25. **Tompkins, S. M., Z. S. Zhao, C. Y. Lo, J. A. Misplon, T. Liu, Z. Ye, R. J. Hogan, Z. Wu, K. A. Benton, T. M. Tumpey, and S. L. Epstein**. 2007. Matrix protein 2 vaccination and protection against influenza viruses, including subtype H5N1. Emerg. Infect. Dis. **13**:426-435.

26. **Treanor, J. J., E. L. Tierney, S. L. Zebedee, R. A. Lamb, and B. R. Murphy**. 1990. Passively transferred monoclonal antibody to the M2 protein inhibits influenza A virus replication in mice. J. Virol. **64**:1375-1377.

27. **Vey, M., M. Orlich, S. Adler, H. D. Klenk, R. Rott, and W. Garten**. 1992. Hemagglutinin activation of pathogenic avian influenza viruses of serotype H7 requires the protease recognition motif R-X-K/R-R. Virology. **188**:408-413.

28. **World Health Organization**. The Global Burden of Disease: 2004 update. 2008. Ref Type: Report

29. **World Health Organization**. Fact sheet Number 211. Influenza (Seasonal). Fact sheet Number 211.Influenza (Seasonal) . 2009. Ref Type: Report

30. **Xu, R., D. C. Ekiert, J. C. Krause, R. Hai, J. E. Crowe, Jr., and I. A. Wilson**. 2010. Structural basis of preexisting immunity to the 2009 H1N1 pandemic influenza virus. Science. **328**:357-360.

Figure Legends

Figure 1

Virus titer in lungs of C57BL/6 (●) and DBA/2 (▽) mice 2 and 7 days post inoculation with with 10^4 EID_{50} of A/shorebird/Delaware/22/2006 (H7N3), A/blue winged-teal/Alberta/271/2007 (H10N5) and A/California/4/2009 (H1N1pdm). * $P < 0.01$. [1] Infectious titer in EID_{50}/ml for H7N3 and H10N5, and in $TCID_{50}$/ml for H1N1pdm

Figure 2

Human cross-reactive 2009 pandemic H1N1 neutralizing antibodies are functional *in vivo.* Human serum pools with (△) or without (●) a detectable cross-reactive 2009 pandemic H1N1 (A/California/4/2009) neutralizing antibody titer were injected intraperitoneally 24 h prior to intranasal lethal challenge. Control mice were injected with PBS (■) or convalescent serum obtained from 2009 pandemic H1N1 virus–infected ferrets (◇). Survival was monitored for 21 days (A) and weight loss for 16 days (B). Data shown in (A) are the cumulative results of 2 experiments and those in (B) represent the average weight loss of 1 indicative experiment. $^{*, **, ***}$ $P < 0.01$.

Tables

Table 1 Percent mortality in DBA/2 and C57BL/6 mice inoculated with various isolates of influenza A virus

Influenza A virus isolate	Subtype	DBA/2		C57BL/6
		10^6 EID_{50}	10^4 EID_{50}	10^6 EID_{50}
A/Puerto Rico/8/1934	H1N1	100	100	100
A/Memphis/3/2008 [1]	H1N1	100	88	0
A/California/4/2009 [2]	H1N1	100	100	60
A/mallard/Alberta/79/2003	H2N3	33	0	ND [4]
A/mallard/Alberta/33/2004	H2N4	0	0	0
X31 (A/Hong Kong/1/1968) [3]	H3N2	100	100	0
A/pintail duck/Alberta/66/2005	H4N1	20	0	0
A/mallard/Alberta/147/2007	H4N6	0	ND	ND
A/Hong Kong/213/2003 [1]	H5N1	100	100	76
A/Vietnam/1203/2004 [1]	H5N1	100	100	100
A/shorebird/Delaware/101/2004	H5N7	20	0	0
A/ruddy turnstone/Delaware/103/2007	H5N9	100	25	ND
A/teal/Hong Kong/W312/1997	H6N1	100	100	40
A/mallard/Alberta/154/2003	H6N5	100	40	0
A/shorebird/Delaware/22/2006	H7N3	100	100	0
A/Netherlands/33/2003 [1]	H7N7	100	100	100
A/mallard/Alberta/177/2004	H7N9	0	0	0
A/quail/Hong Kong/G1/1997	H9N2	100	0	0
A/duck/Hong Kong/Y280/1997	H9N2	100	20	0
A/mallard/Alberta/162/2007	H9N5	0	0	ND
A/mallard/Alberta/221/2006	H9N6	0	0	ND
A/blue-winged teal/Alberta/271/2007	H10N5	100	75	0
A/mallard/Alberta/56/2004	H10N7	100	75	0

[1] Human influenza A virus isolate.

[2] Human 2009 pandemic H1N1 virus isolate.

[3] X31 is a 6 + 2 reassortant virus containing the *HA* and *NA* gene segments from A/Hong Kong/1/68 and 6 gene segments from A/Puerto Rico/8/1934 virus.

[4] ND, not done.

Table 2 Serum antibody responses in mice infected with 10^6 EID_{50} of non- or low-pathogenic influenza A viruses

Influenza A virus isolate	Subtype	Hemagglutination Inhibition titer [1]	
		DBA/2	C57BL/6
A/Memphis/3/2008	H1N1	ND[2]	40
A/mallard/Alberta/33/2004	H2N4	40	20
A/pintail duck/Alberta/66/2005	H4N1	ND	<10
A/mallard/Alberta/147/2007	H4N6	<10	ND
A/shorebird/Delaware/101/2004	H5N7	40	<10
A/mallard/Alberta/154/2003	H6N5	ND	<10
A/mallard/Alberta/177/2004	H7N9	40	80
A/mallard/Alberta/221/2006	H9N6	<10	ND
A/blue-winged teal/Alberta/271/2007	H10N5	ND	160
A/mallard/Alberta/56/2004	H10N7	ND	40

[1] Average geometric mean titer as measured by the HI assay.

[2] ND, not done. HI titer < 10 is undetectable.

Table 3. Concentrations of proinflammatory cytokines in lungs of C57BL/6 and DBA/2 mice infected with 10^4 EID_{50} of pandemic H1N1 2009 virus

Cytokine	Day 2		Day 7	
(pg/ml)	DBA/2	C57BL/6	DBA/2	C57BL/6
CCL2	4013	3387	10145 *	4520
CCL5	4212	2924	5703	7060
IL-6	710	950	1057 *	735
TNFα	236 *	102	96	109
IFNγ	46	42	1097	900

* Significant difference ($P<0.05$) in cytokine concentration between C57BL/6 and DBA/2 mice on day 2 or 7 after infection.

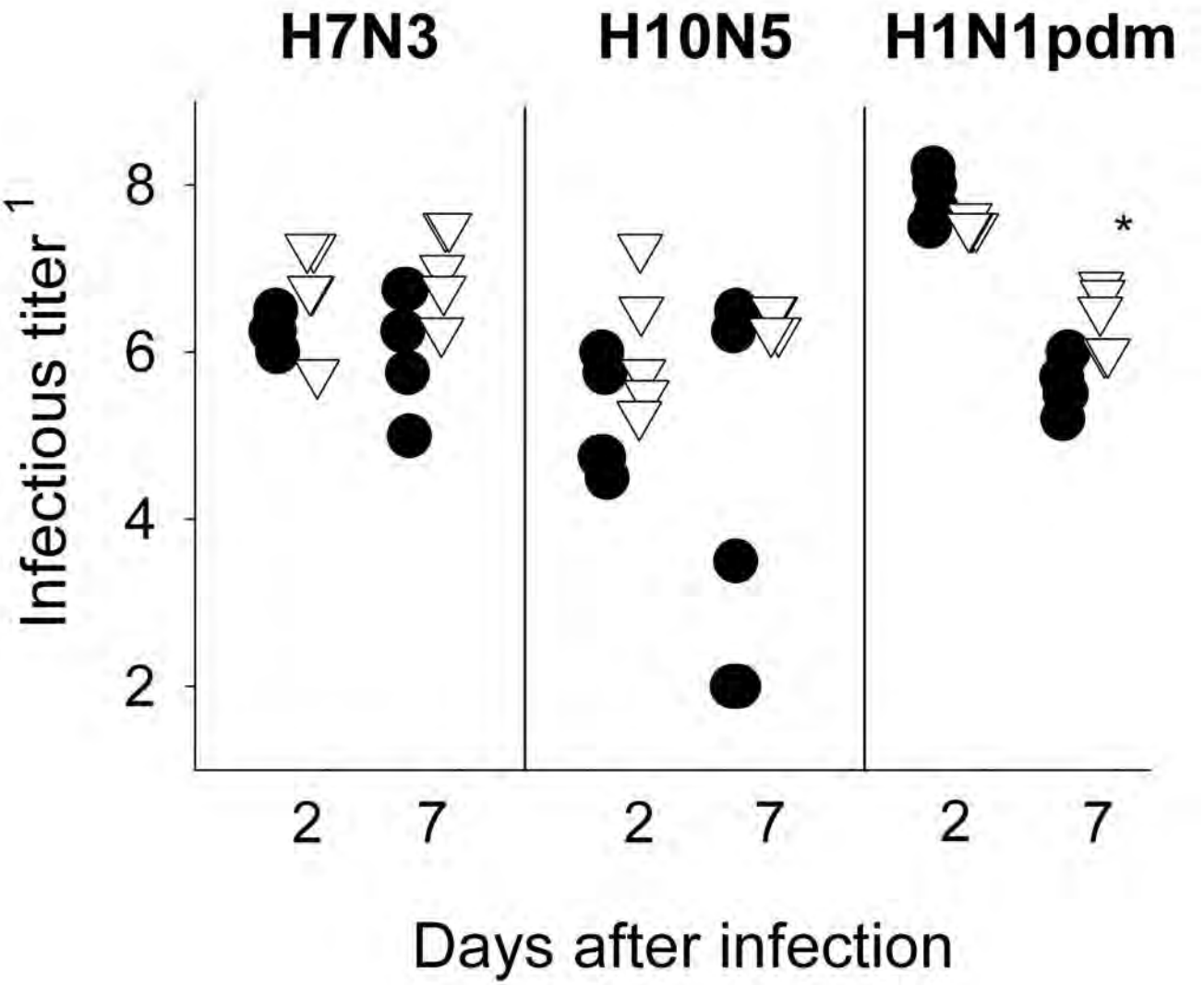

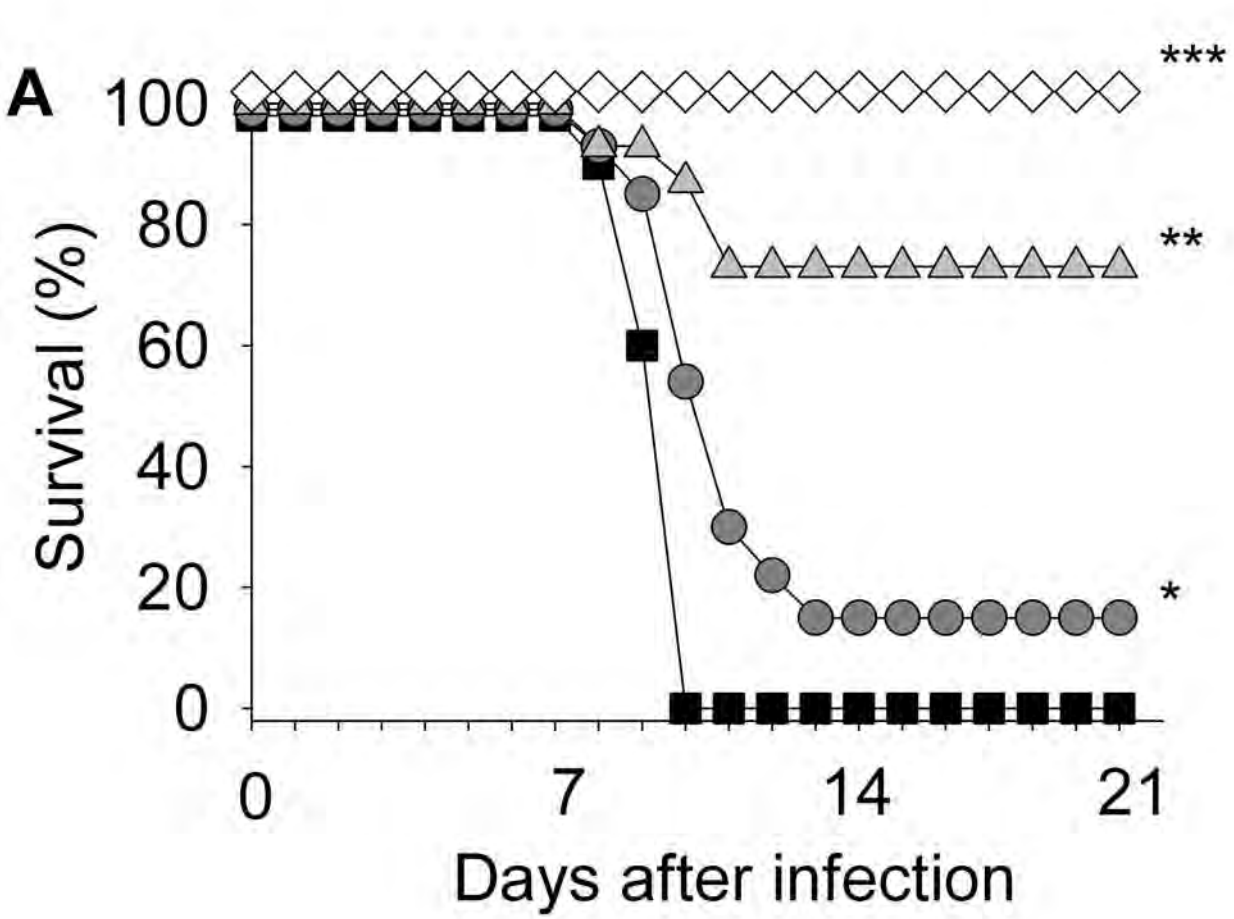

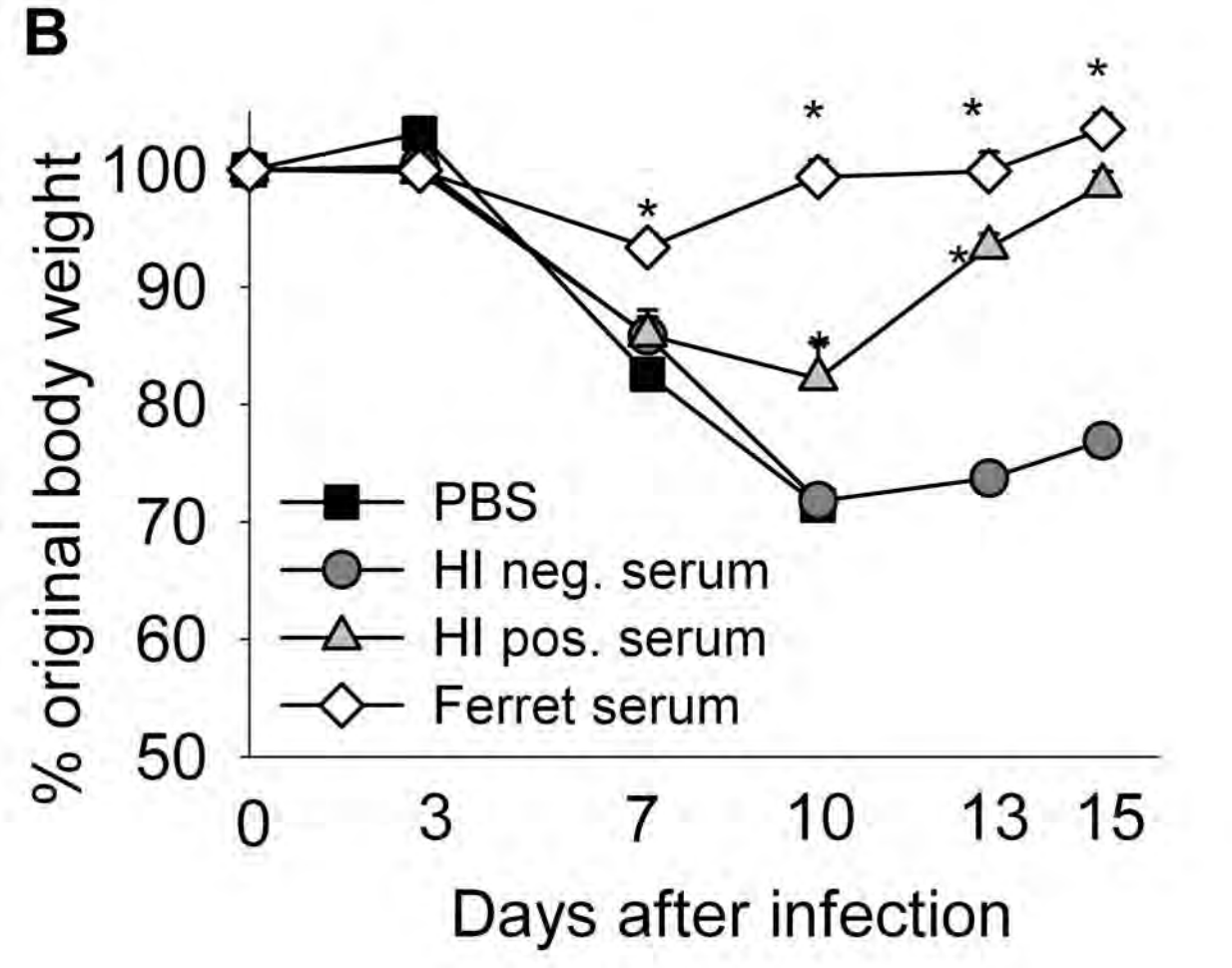

JOURNAL OF VIROLOGY, May 2010, p. 4619–4629 Vol. 84, No. 9
0022-538X/10/$12.00 doi:10.1128/JVI.02406-09

Deubiquitinating and Interferon Antagonism Activities of Coronavirus Papain-Like Proteases▽

Mark A. Clementz,[1]† Zhongbin Chen,[2]† Bridget S. Banach,[1] Yanhua Wang,[2] Li Sun,[2] Kiira Ratia,[3] Yahira M. Baez-Santos,[3] Jie Wang,[4] Jun Takayama,[5] Arun K. Ghosh,[5] Kui Li,[4] Andrew D. Mesecar,[3] and Susan C. Baker[1]*

Department of Microbiology and Immunology, Loyola University Chicago Stritch School of Medicine, Maywood, Illinois 60153[1]; Division of Infection and Immunity, Department of Electromagnetic and Laser Biology, Beijing Institute of Radiation Medicine, Beijing 100850, China[2]; Department of Medicinal Chemistry and Pharmacognosy, University of Illinois, Chicago, Illinois 60607[3]; Department of Molecular Sciences, University of Tennessee Health Science Center, Memphis, Tennessee 38163[4]; and Department of Chemistry, Purdue University, West Lafayette, Indiana 47907[5]

Received 13 November 2009/Accepted 15 February 2010

Coronaviruses encode multifunctional proteins that are critical for viral replication and for blocking the innate immune response to viral infection. One such multifunctional domain is the coronavirus papain-like protease (PLP), which processes the viral replicase polyprotein, has deubiquitinating (DUB) activity, and antagonizes the induction of type I interferon (IFN). Here we characterized the DUB and IFN antagonism activities of the PLP domains of human coronavirus NL63 and severe acute respiratory syndrome (SARS) coronavirus to determine if DUB activity mediates interferon antagonism. We found that NL63 PLP2 deconjugated ubiquitin (Ub) and the Ub-line molecule ISG15 from cellular substrates and processed both lysine-48- and lysine-63- linked polyubiquitin chains. This PLP2 DUB activity was dependent on an intact catalytic cysteine residue. We demonstrated that in contrast to PLP2 DUB activity, PLP2-mediated interferon antagonism did not require enzymatic activity. Furthermore, addition of an inhibitor that blocks coronavirus protease/DUB activity did not abrogate interferon antagonism. These results indicated that a component of coronavirus PLP-mediated interferon antagonism was independent of protease and DUB activity. Overall, these results demonstrate the multifunctional nature of the coronavirus PLP domain as a viral protease, DUB, and IFN antagonist and suggest that these independent activities may provide multiple targets for antiviral therapies.

The front-line defense of a host cell against virus infection is the innate immune system, which utilizes multiple membrane and cytoplasmic sensors, such as toll-like receptors (TLRs) and RNA helicases, to detect pathogen-associated molecular patterns like viral RNA (3, 9, 31, 47, 54). Activation of these sensors by viral RNA intermediates sets off a cascade of signaling events that ultimately turn on transcription factors, such as NF-κB, ATF2/c-Jun, IRF-7, and IRF-3. These activated transcription factors translocate to the nucleus and upregulate transcription of interferon (IFN) mRNAs. The translation and subsequent secretion of IFNs activates cells to upregulate interferon-stimulated genes (ISGs) to establish an antiviral state hostile to viral replication. Of importance for this study, many of the signaling events that link the sensors to the transcription factors are mediated by the activities of kinases and ubiquitinating enzymes that modify and activate critical intermediates in the cascade (7, 8, 20, 25). For example, signaling from RIG-I can proceed through MAVS/TRAF3/TANK to TBKI and inducible IκB kinase (IKKi), which ultimately phosphorylate IRF-3. Recent studies indicate that both TRAF3 and TANK are modified by lysine-63-linked polyubiquitination and can be inactivated by DUBA, a cellular deubiquitinating (DUB) enzyme (28). Thus, ubiquitinating enzymes and DUBs are critical players in modulating the innate immune response.

For positive-strand RNA viruses that replicate in the cytoplasm of the cell using double-stranded RNA intermediates, the cytoplasmic innate immune sensors and subsequent signaling cascades represent a minefield that must be either neutralized, navigated by stealth, or both. Recent studies have revealed that viral proteases can act as "multitaskers" during viral replication by not only processing viral polyproteins but also cleaving/inactivating key players in the innate immune response. For example, the hepatitis C virus NS3-4A protease cleaves the viral replicase polyprotein and inactivates the key signaling proteins TRIF and MAVS (36, 38, 42, 46). Picornavirus 3C protease is essential for processing the replicase polyprotein and inactivating NF-κB and RIG-I (2, 49). In these studies, the catalytic function of the viral proteases was essential for the inactivation of host factors involved in signaling the innate immune response. Recently the coronavirus papain-like protease domains have also been identified as modulators of the innate immune response; however, the mechanisms of inhibition are not entirely clear (13, 16, 70).

Coronaviruses are enveloped viruses with large RNA genomes (28 to 32 kb) that cause disease in humans ranging from common colds (human coronavirus [CoV] 229E [HCoV-229E] and OC43) to croup and pneumonia, seen mostly in very young and old populations (HCoV-NL63 and -HKU1), to severe acute respiratory syndrome (SARS) coronavirus (SARS-CoV) with 10% mortality (53). Upon entry, coronavirus genomic

* Corresponding author. Mailing address: Department of Microbiology and Immunology, Loyola University Medical Center, Bldg. 105, Rm. 3929, 2160 South First Avenue, Maywood, IL 60153. Phone: (708) 216-6910. Fax: (708) 216-9574. E-mail: sbaker1@lumc.edu.
† These authors contributed equally to this work.
▽ Published ahead of print on 24 February 2010.

RNA is translated to produce two large polyproteins, pp1a and pp1ab. These polyproteins are processed by viral cysteine proteases, papain-like (PLPs/PLpro) and picornavirus 3C-like (3CLpro), to generate mature nonstructural proteins (nsp's) that assemble with host cell membranes to form double membrane vesicles (DMVs) (18, 19, 61). These DMVs are the site of viral RNA synthesis producing double-stranded intermediates and genomic/subgenomic mRNAs. Interestingly, robust replication of SARS-CoV was shown to trigger low but detectable levels of beta interferon (IFN-β) (13, 62, 63). The low-level IFN response to a vigorously replicating RNA virus suggests that SARS-CoV either evades or inactivates the innate immune response. Indeed, recent studies indicate that SARS-CoV encodes multiple proteins, such as nsp1, protein 3b, protein 6, and the nucleocapsid protein that modulate multiple pathways of the innate immune response (17, 27, 30, 48, 68). In addition, we showed that the SARS-CoV papain-like protease (PLpro) domain acts as an interferon antagonist that blocks the phosphorylation and subsequent nuclear translocation of IRF-3 (13). We also showed via X-ray structural studies that the SARS-CoV PLpro domain is similar to cellular deubiquitinating enzymes (57), and we and others demonstrated that PLpro is both a protease and a DUB (4, 39, 40). Initially, we hypothesized that either the protease or DUB activity would be required for modulating the innate immune response, but we found that inactivation of the catalytic cysteine residue of PLpro, which ablates both proteolysis and deubiquitinating activity, decreased but did not abrogate PLpro's ability to block activation of interferon (13). These results are consistent with a protease/DUB-independent mechanism that contributes to interferon antagonism. Frieman and coworkers also showed that catalytic mutants of PLpro retained interferon antagonism, and they reported that deletion of the PLP ubiquitin-like (Ubl) domain upstream of the catalytic site resulted in a loss of antagonism (16). Studies by Zheng et al. of the PLP domain of murine hepatitis virus (MHV) suggested that viral DUB activity may be required for interferon antagonism, although they reported that MHV PLP2 catalytic cysteine mutants became less efficient at, but did not eliminate, blockade of the interferon response (70). Therefore, further studies are required to clarify the role of coronavirus protease/DUB activity in PLP-mediated interferon antagonism.

In this study, we analyzed the DUB and IFN antagonism profiles of the papain-like proteases of human coronavirus NL63 and SARS-CoV (group 1 and group 2 coronaviruses, respectively). We show that HCoV-NL63 PLP2 is a deubiquitinating and deISGylating (ISG15-removing) enzyme. HCoV-NL63 infection, like that of SARS-CoV, triggers a weak type I IFN response in human airway epithelial cell cultures. We also evaluated the role of PLP2 and PLpro enzymatic activity in interferon antagonism. By generating dose-response profiles of IFN antagonism, we found that the papain-like proteases do not require enzymatic activity to inhibit type I IFN induction. Using a pharmacological approach, we found that the inhibition of PLpro did not alter the antagonism of IRF-3-dependent reporters but did affect an NF-κB- dependent reporter. Overall, we show that multifunctional coronavirus PLPs target the activities of key transcription factors involved in the induction of type I interferons and thereby hinder the activation of the innate immune system.

MATERIALS AND METHODS

Cells and HCoV-NL63. HeLa cells, HEK293 cells, and HEK293-TLR3 (stable expression of human TLR3 receptor) cells were cultured using Dulbecco's modified Eagle's medium containing 10% (vol/vol) fetal calf serum, supplemented with penicillin (100 U/ml) and streptomycin (100 μg/ml). The HCoV-NL63 (P8) virus and LLC-MK2 cells were kindly provided by Lia van der Hoek (University of Amsterdam, Amsterdam, Netherlands) and propagated as described previously (12). A plaque-purified isolate of HCoV-NL63 was kindly provided by Christian Drosten and propagated in CaCo2-TC7 cells (21). This virus stock was used to infect human airway epithelial cells as described previously (1).

Plasmid DNA. pcDNA3.1-Flag-Ub was kindly provided by Adriano Marchese (Loyola University Medical Center). IFN-β-Luc was kindly provided by John Hiscott (Jewish General Hospital, Montreal, Canada). pISRE-Luc has been previously described (35). pRL-TK *Renilla* luciferase reporter was purchased from Promega. N-RIG-Flag, NF-κB-Luc, and nsp2/3-GFP were kindly provided by Ralph Baric (University of North Carolina). pcDNA3-myc6-mISG15 was kindly provided by Min-Jung Kim (Pohang University of Science and Technology, Pohang, Republic of Korea). pcDNA3-Ube1L and pcDNA3-UbcH8 were kind gifts from Robert M. Krug (University of Texas).

PLP1 and PLP2 core domain synthesis, cloning, and site-directed mutagenesis. To obtain high expression in eukaryote cells, the codon usage of the HCoV-NL63 PLP1 core domain (amino acids 1018 to 1277 of HCoV-NL63) and PLP2 core domain (amino acids 1570 to 1884) were optimized based on human codon usage frequency, and the potential splicing sites and poly(A) signal sequences were removed and cloned into pcDNA3.1-V5/HisB at the BamHI and EcoRI sites as an in-frame fusion with the V5 peptide. The native viral sequence for the remainder of nsp3 (including the transmembrane domain downstream of PLP2) was cloned into pcDNA3.1-PLP2(N) using the existing EcoRI site and XhoI to generate transmembrane (TM)-containing PLP2 (PLP2-TM) in frame with the V5 peptide. To generate specific mutations in the catalytic residues (C1062 and H1212 in PLP1 and C1678 and H1836 in PLP2), mutagenic primers were incorporated into newly synthesized DNA using the QuikChange II XL site-directed mutagenesis protocol (Stratagene, La Jolla, CA) according to the manufacturer's instruction. Mutated nucleotides are indicated in bold. PLP1 C1062A was amplified using the forward primer 5′ AAC AAC GCC TGG ATC AGC ACC ACC CTG GTG CAA CTG 3′ and reverse primer 5′ GAT CCA GGC GTT GTT GTC GCT CTG GTC CAG CAC CCG 3′. PLP1 H1212A was amplified using the forward primer 5′ AGC GGC GCC TAC CAG ACC AAC CTG TAC AGC TTC AAC 3′ and reverse primer 5′ CTG GTA GGC GCC GCT GCC CTT CAC GCC CAG GTA CAC 3′. PLP2 C1678A was amplified using the forward primer 5′ AAC AAC GCC TGG GTG AAC GCC ACC TGC ATC ATC CTG 3′ and reverse primer 5′ CAC CCA GGC GTT GTT GTC GGT GGT GCC CAG CAC CCG 3′. PLP2 H1836A was amplified using the forward primer 5′ AAC GGC GCC TAC GTG GTG TAC GAC GCC GCC AAC AAC 3′ and reverse primer 5′ CAC GTA GGC GCC GTT GTC GAA GCT GCC GCT GAA GG 3′. The primers used for mutagenesis were designed according to the modified methods of Zheng et al. (71). All introduced mutations were confirmed by DNA sequencing.

Assay of deubiquitinating activity in cultured cells. The effect of HCoV-NL63 PLP1 and PLP2 on ubiquitinated proteins in cultured cells was assessed as described previously (14). Briefly, HeLa cells cultured in 60-mm dishes were cotransfected with 0.4 μg of pcDNA3.1-Flag-Ub plus appropriate amounts of constructs containing PLP1, PLP2, or the corresponding catalytic mutants. Transfection was performed with Lipofectamine 2000 per the manufacturer's instructions. The empty vector pcDNA3.1/V5-HisB was used to standardize the total amount of DNA used for transfection. After 48 h, cells were harvested by adding 250 μl 2× LBA, containing 20 mM *N*-ethylmaleimide (NEM) (Calbiochem) and 20 mM iodoacetamine (Sigma). Cell lysates were then analyzed for ubiquitin (Ub)-conjugated proteins by Western blotting with anti-Flag M2 antibody (1:10,000) (Sigma). Proteins were separated via SDS-PAGE, followed by transfer to a polyvinylidene difluoride (PVDF) membrane in transfer buffer (0.025 M Tris, 0.192 M glycine, and 20% methanol) for 2 h at 4°C. The membrane was blocked using 5% dried skim milk in Tris-buffered saline (TBS) (0.9% NaCl, 10 mM Tris-HCl, pH 7.5) plus 0.1% Tween 20 (TBST) for 2 h at room temperature. The blot was probed with the indicated antibody overnight at 4°C. The membrane was washed in TBST three times for 20 min (each). Following the washes, the membrane was incubated with peroxidase-conjugated secondary antibody (donkey anti-rabbit or goat anti-mouse IgG horseradish peroxidase [HRP]) (Amersham) at a dilution of 1:10,000 for 2 h at room temperature. The membrane was then washed three times with TBST and detected with Western Lightning Chemoluminescence Reagent Plus (PerkinElmer LAS Inc.). To confirm the expression levels of PLP1, PLP2, and the mutants, anti-V5 antibody

(Invitrogen) was used to detect the V5-tagged proteins. Calnexin was detected with anti-calnexin monoclonal antibody (MAb) (BD Transduction Lab) as a protein loading control.

NL63 PLP2 cleavage of K48- and K63-linked ubiquitin chains. The NL63 PLP2 wild-type protein was purified as previously described (4, 12), and ubiquitin chains were purchased from Boston Biochem (K48-Ub_6 [catalog no. UC-217] and K63-Ub_6 [catalog no. UC-317]). Proteolytic cleavage of K48-linked or K63-linked ubiquitin chains was carried out under the following conditions: 0.01 μg of purified PLP2 was incubated with 2.5 to 5 μg of K48-Ub_6 or K63-Ub_6 at 25°C in a 10- to 20-μl volume containing 50 mM HEPES, pH 7.5, 0.1 mg/ml bovine serum albumin (BSA), 100 mM NaCl, and 2 mM dithiothreitol (DTT). A control reaction was incubated under identical conditions with the exclusion of enzyme. At specified time points, the reactions were quenched with the addition of SDS-PAGE sample loading dye to a 1× concentration (25 mM Tris, pH 6.8, 280 mM β-mercaptoethanol, 4% glycerol, 0.8% SDS, 0.02% bromophenol blue) and heat treated at 95°C for 5 min. The samples were analyzed by electrophoresis on a 15% SDS-PAGE gel and stained with Coomassie dye.

Assay of deISGylating activity in cultured cells. The effect of HCoV-NL63 PLP2 on ISGylated proteins in cultured cells was assessed as described previously (69). Briefly, HEK293 cells cultured in 60-mm dishes were cotransfected with 0.5 μg of pcDNA3-myc6-mISG15, 0.25 μg of pcDNA3-Ube1L, and 0.25 μg of pcDNA3-UbcH8 plus appropriate amounts of constructs containing PLP2 or the corresponding catalytic mutant with a total of 2 μg of plasmid DNA for each transfection. The empty vector pcDNA3.1/V5-HisB was used to standardize the total amount of DNA used for transfection. Transfection was performed with Lipofectamine 2000 per the manufacturer's instructions. After 30 h, cells were harvested by adding 250 μl 2× LBA containing 20 mM *N*-ethylmaleimide (Calbiochem) and 20 mM iodoacetamine (Sigma). Cell lysates were then analyzed for ISG-conjugated proteins by Western blotting with monoclonal anti-myc antibody (1:2,000; MBL Companies, Japan) as described above. To confirm the expression levels of PLP2 and the mutants, anti-V5 antibody (1:5,000; Invitrogen) was used to detect the V5-tagged proteins. Actin was detected with antiactin MAb (Beyotime Institute of Biotechnology, China) as a protein loading control.

Enzyme-linked immunosorbent assay for IFN-β secretion in HAE culture supernatants. Human airway epithelial (HAE) cultures were generated as previously described (1). Cultures were inoculated with 100 μl of 10^5 PFU/ml HCoV-NL63, 2,000 hemagglutinating units (HAU)/ml Sendai virus (SeV), or medium for 1 h at 37°C, after which the inoculum was removed and apical washes with 200 μl of F12 medium (Gibco) were performed at indicated times. The IFN-β concentration was determined by a commercial enzyme-linked immunosorbent assay (ELISA) (PBL Biomedical Laboratories) according to the manufacturer's instructions. Data were analyzed and plotted using the GraphPad Prism 5.0 software program.

Luciferase reporter gene assay. To determine if PLpro and/or PLP2 modulates IFN expression in host cells, the IFN-β-Luc reporter, consisting of the IFN-β promoter upstream of firefly luciferase, was transfected into HEK293 cells along with PLpro, ΔUbl-PLpro-Sol, ΔUbl-PLpro-TM, PLP2, PLP2-TM, or the C1678A and H1836A PLP2 catalytic mutants in the soluble or transmembrane versions. pRL-TK, encoding *Renilla* luciferase under the control of the herpes simplex thymidine kinase promoter (low to moderate *Renilla* expression), was used for normalization of transfection efficiency. HEK293 cells were transfected by Lipofectamine 2000 or LT1 transfection reagent (MirusBio) according to the manufacturer's instructions and incubated for 24 h. Cells were then mock infected or infected with Sendai virus (Cantell strain; Charles River Laboratories) at the dose of 100 HAU/ml for 16 h or transfected with N-RIG-Flag for 24 h to activate the RIG-I-dependent IFN pathway. To detect TLR3-dependent IFN expression, HEK293-TLR3 cells were transfected with IFN-β-Luc and PLP2 for 24 h. Cells were then treated with poly(IC) for 6 h as described previously (13). Firefly luciferase and *Renilla* luciferase activities were assayed using the Dual-Luciferase reporter assay kit (Promega) and a luminometer.

Drug inhibition of SARS-CoV PLpro. HEK293 cells were transfected with plasmids encoding PLpro-TM (13), IFN-β-Luc, ISRE-Luc, NF-κB-Luc, pRL-TK, nsp2/3-GFP substrate, and/or N-RIG-Flag. The pcDNA3.1/V5-HisB vector was used to standardize the DNA concentration for transfection. Dimethyl sulfoxide (DMSO) vehicle control or 100 μM GRL-0617S (56) was added at the time of transfection. Tumor necrosis factor alpha (TNF-α) (10 ng/ml) from Roche was used to stimulate the NF-κB-Luc reporter (6 h of stimulation). Cell lysates were prepared per the manufacturer's instruction using 1× passive lysis buffer (Promega), and luciferase activity was measured using the Dual-Luciferase reporter assay kit (Promega) and a luminometer. Cell lysates were also mixed 1:1 with 2× sample buffer and subjected to Western blotting as described above. PLpro-TM was detected with anti-V5 (Invitrogen), and nsp2/3-GFP and nsp3-GFP were detected with rabbit anti-green fluorescent protein (anti-GFP) (Invitrogen).

RESULTS

NL63 PLP2 but not PLP1 has deubiquitinating activity. Previously we showed that HCoV-NL63 replicase nonstructural protein 3 (nsp3) encodes two papain-like proteases, PLP1 and PLP2, that process the amino-terminal end of the replicase polyprotein (Fig. 1A). In addition, we have shown that PLP2 can process K48-linked polyubiquitin chains, suggesting that this protease has deubiquitinating activity (12). Both the polyprotein cleavage and K48-linked polyubiquitin chain processing are dependent on a cysteine residue in the catalytic triad of this cysteine protease (12). To determine if one or both of these NL63 PLPs can remove ubiquitin conjugated to cellular proteins, HeLa cells were transfected with plasmid DNA encoding PLP1 or PLP2 along with pcDNA3.1-3×Flag-Ub, and the effect of expression of PLP1 and PLP2 on the extent of ubiquitinated cellular proteins was assessed via Western blotting with anti-Flag antibodies. We found that increasing expression of PLP2 resulted in a dramatic reduction in the level of Ub-conjugated proteins (Fig. 1B). We noted that PLP2 appears to have global DUB activity, since no particular cellular substrates were spared. As expected, this PLP2 DUB activity is dependent on an intact catalytic cysteine residue 1678, and mutation of this residue to alanine resulted in the loss of DUB activity (Fig. 1C). In contrast, PLP1 did not show any significant reduction of Flag-Ub conjugates at the concentrations tested (Fig. 1D). These results indicate that NL63 PLP2, like SARS-CoV PLpro, has potent DUB activity that can remove ubiquitin conjugates from many cellular substrates.

NL63 PLP2 processes lysine-63-linked in addition to lysine-48-linked polyubiquitin. Cellular proteins can be covalently modified with ubiquitin at one or multiple lysines through an isopeptide bond that links the carboxy terminus of ubiquitin to a lysine on the target protein. Ubiquitin itself contains seven lysines that can be further conjugated to the C terminus of another ubiquitin molecule, forming different types of polyubiquitin-linked chains on the targeted protein. The two most common types of polyubiquitin chains are linked through ubiquitin lysine 48 (K48) and lysine 63 (K63). These modifications play key regulatory roles in protein degradation and pathway signaling and have been associated with controlling several pathways of innate and adaptive immunity (7). Previous studies indicated that SARS-CoV PLpro processes both K48- and K63-linked ubiquitin (39, 40). To assess if HCoV-NL63 PLP2 has isopeptidase activity that will deconjugate K63-linked ubiquitin in addition to K48-linked isopeptidase activity, purified PLP2 enzyme was incubated with hexameric K48-linked and K63-linked polyubiquitin chains. SDS-PAGE analysis of the cleavage products shows that PLP2 can cleave the substrates *in vitro* (Fig. 2), and with prolonged incubation times, both chains can be reduced to monoubiquitin (data not shown). These data show that both major forms of polyubiquitin can be recognized and degraded by HCoV-NL63 PLP2.

PLP2 possesses deISGylating activity. Several viral DUBs, including SARS-CoV PLpro, can also deconjugate Ub-like moieties such as ISG15 (39, 40). Conjugation of ISG15 has been shown to be important for protection against viral infection

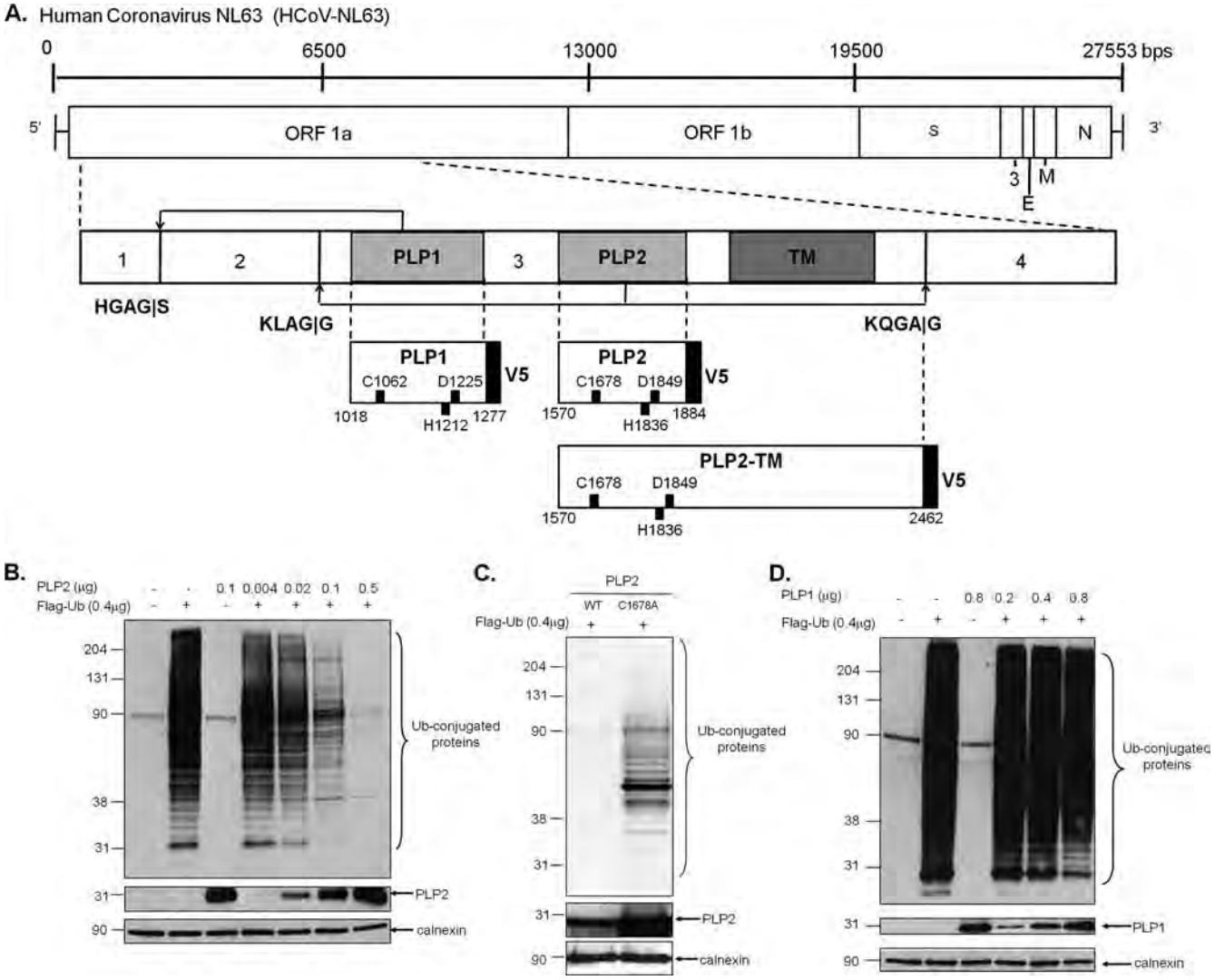

FIG. 1. HCoV-NL63 PLP2, but not PLP1, has a dose-dependent global deubiquitinating activity in cultured cells. (A) Schematic diagram of the NL63 genomic RNA and the resulting polyprotein 1ab, which contains three viral proteases. PLP1 and PLP2 cleavage sites are indicated, as are the resulting nonstructural proteins. The V5-tagged constructs of PLP2 used in this study are listed, and the catalytic residues numbering from ORF 1a are shown. DNA encoding HCoV-NL63 PLP2 (B), PLP2 C1678A (C), or PLP1 (D) was transfected into HeLa cells along with pcDNA3.1-3×Flag-Ub. Cell lysates were prepared at 24 h posttransfection and analyzed for Flag-Ub-conjugated proteins by Western blotting with an anti-Flag antibody. Mouse anti-V5 was used to confirm the expression of PLP1 and PLP2, and anticalnexin antibody was used to detect calnexin, which serves as a protein loading control. Molecular weight markers shown on the left of each gel are in thousands.

(15, 33, 34). We assessed whether HCoV-NL63 PLP2 can deISGylate cellular c-myc-tagged ISG15 (c-myc-ISG15) conjugates. HeLa cells were transfected with increasing amounts of plasmid DNA encoding PLP2 along with c-myc-ISG15 and the ISG15 conjugation machinery Ube1L and UbcH8 to enhance ISGylation of host cell proteins. The ability of PLP2 to deISGylate cellular proteins was then assayed via Western blotting with anti-myc antibody. We found that expression of increasing amounts of PLP2 was associated with a dramatic reduction in the levels of ISGylated cellular proteins (Fig. 3A), in agreement with a previous report (50). The deISGylating activity was dependent on intact catalytic residues C1678 and H1836, since mutation of these residues to alanine resulted in the loss of deISGylating activity (Fig. 3B). Thus, HCoV-NL63 PLP2 is a potent DUB/deISGylating enzyme that acts on many modified cellular substrates.

IFN-β release from human airway epithelial (HAE) cell cultures. HAE cultures are a useful model system for studying human respiratory viruses, including HCoV-NL63, since they mimic human bronchial epithelium, which is the primary site of infection (1, 60). HAE cell cultures were infected with HCoV-NL63 or Sendai virus, and apical wash samples were collected at 24, 48, 72, 96, and 144 h postinfection. The presence of secreted IFN-β in the apical wash was measured by ELISA. Mock-infected cultures released no detectable IFN-β, whereas cultures inoculated with a potent IFN inducer, Sendai virus, released more than 400 pg/ml of IFN-β. In contrast, inoculation of HAE cultures with HCoV-NL63 stimulated low but

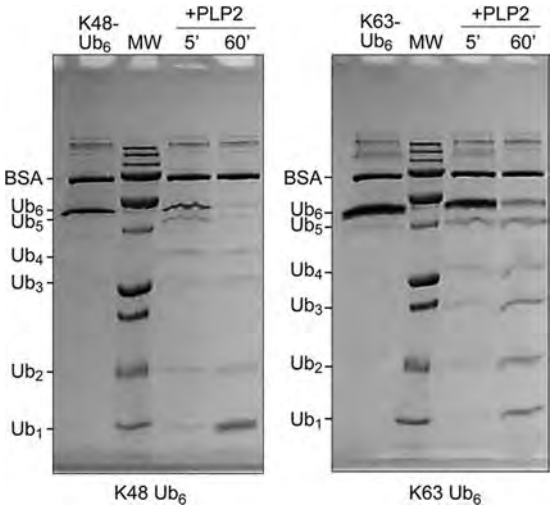

FIG. 2. Processing of K48- and K63-linked ubiquitin chains by PLP2. NL63 PLP2 was incubated with K48-linked (left) or K63-linked (right) Ub_6 chains for the indicated time points before being analyzed by SDS-PAGE. Uncleaved Ub_6 is run in the first lane of each gel. The expected sizes of the Ub species are indicated to the left of all gels. Molecular weight (MW) markers include 250,000-, 100,000-, 75,000-, 50,000-, 37,000-, 25,000-, 20,000-, 15,000-, and 10,000-molecular-weight bands.

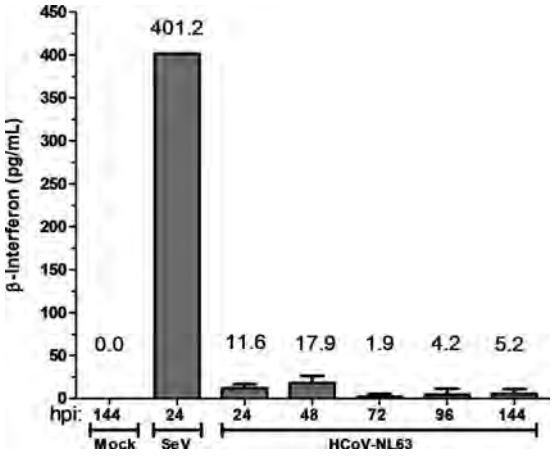

FIG. 4. Evaluating interferon-β secretion from human airway epithelial (HAE) cell cultures following HCoV-NL63 infection. Apical washes were collected from HAE cultures at 24, 48, 72, 96, and 120 h postinfection, and secreted IFN-β was measured by ELISA. Supernatant from HAE cells infected with Sendai virus (SeV) for 24 h was used as a positive control.

detectable levels of IFN-β from 24 to 144 h postinfection (Fig. 4). These results are reminiscent of the reports of low but detectable levels of IFN-β produced from SARS-CoV-infected cells (13, 63) and indicate that either HCoV-NL63 is a weak inducer of the IFN-β response or, like SARS-CoV, HCoV-NL63 encodes potent IFN antagonists.

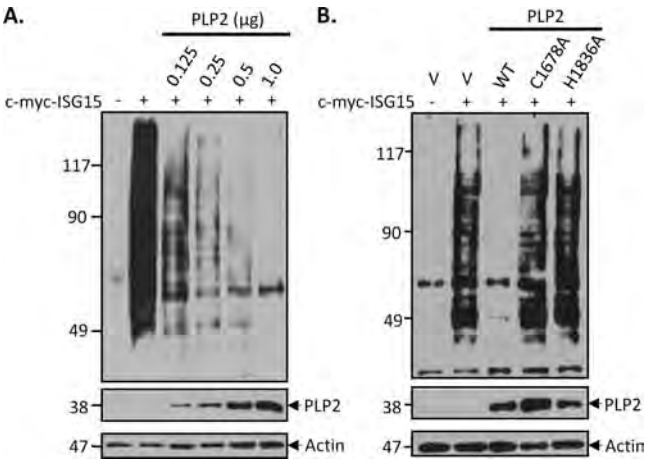

FIG. 3. NL63 PLP2 has global deISGylating activity in cultured cells. HEK293 cells were transfected with pcDNA3-myc6-mISG15, pcDNA3-Ube1L, and pcDNA3-UbcH8 plus indicated amounts of the PLP2 expression construct (A) or PLP2 expression construct and the corresponding catalytic mutants (B). To ensure that the total amount (2 μg/transfection) of plasmids for transfection was equal under every condition, empty vector pcDNA3.1/V5-HisB (v) was used to standardize the total amount of DNA. After 30 h, cells were harvested, and cell lysates were analyzed for ISG-conjugated proteins by Western blotting with monoclonal anti-myc antibody. Expression levels of V5-tagged PLP2 and mutant enzymes were detected with anti-V5 antibody. Actin was detected with antiactin MAb antibody as a protein loading control.

PLP2 inhibits both RIG-I- and TLR3-dependent IFN-β expression. To determine if PLP2 is an IFN antagonist, we transfected HEK293 cells with plasmids encoding HCoV-NL63 PLP2 or SARS-CoV PLpro along with IFN-β–luciferase and *Renilla* luciferase reporters for 24 h. Then, the RIG-I-dependent pathway leading to IFN-β expression was activated by Sendai virus infection for 16 h or by a dominant active N-terminal portion of RIG-I (N-RIG). We found that activation of the IFN-β promoter by Sendai virus (Fig. 5A) or N-RIG (Fig. 5B) was inhibited in the presence of either NL63 PLP2 or SARS-CoV PLpro. To determine if HCoV-NL63 PLP2 inhibits its TLR3-mediated activation of IFN-β production, PLP2 and the reporters were transfected into HEK293-TLR3 cells, and then the TLR3-mediated pathway was activated by addition of poly(IC) to the cell culture medium. We found that activation of the IFN-β promoter by the TLR3-mediated pathway was significantly inhibited by HCoV-NL63 PLP2 and SARS-CoV PLpro (Fig. 5C). These results demonstrate that the IFN antagonism mediated by coronavirus PLPs is conserved in two distinct viruses, although there is only 19% amino acid identity between the catalytic domains of HCoV-NL63 PLP2 and SARS-CoV PLpro in this region of nsp3 (4).

Mutation of the catalytic residues does not abolish HCoV-NL63 PLP2 IFN antagonism. To further elucidate the interferon antagonism profile of PLP2, a dose-dependent IFN antagonism profile was generated. Concurrently, to determine if IFN antagonism is dependent on catalytic activity, plasmid DNAs encoding PLP2 or the C1678A (devoid of enzymatic activity) and H1836A (severely reduced) catalytic mutants were transfected with the IFN-β and pRL-TK reporters into HEK293 cells, and IFN-β reporter activity was assessed. N-RIG was used to stimulate IFN-β induction. We found that, like the PLP2 wild type, both PLP2 C1678A and PLP2 H1836A exhibit dose-dependent inhibition of IFN-β promoter activity; however, the catalytic mutants were less efficient than wild-type PLP2 (Fig. 6A). Expression of the proteases was verified

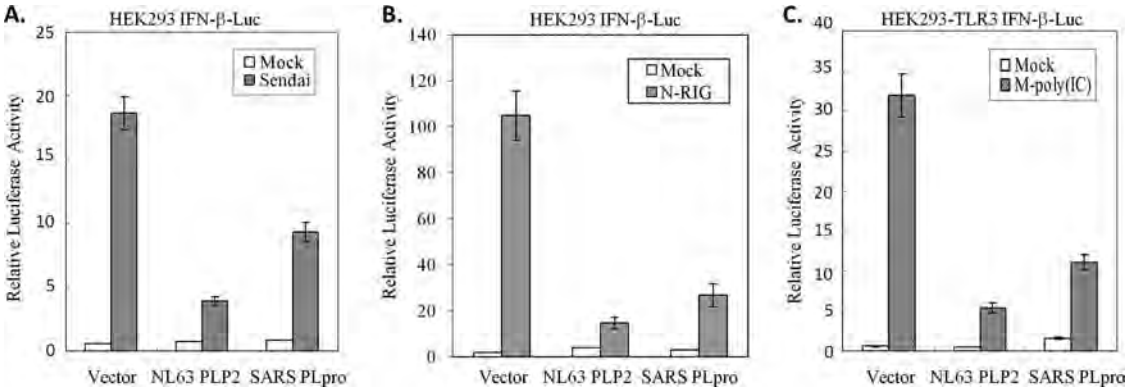

FIG. 5. PLP2 inhibits both RIG-I- and TLR3-dependent IFN-β induction. (A) HEK293 cells were transfected with IFN-β-Luc, pRL-TK, and either 300 ng of HCoV-NL63 PLP2 or 300 ng of SARS-CoV PLpro. At 24 h posttransfection, cells were either mock infected or infected with Sendai virus for 16 h. Following infection, cell lysates were prepared and assayed using the Dual-Luciferase reporter assay. (B) HEK293 cells were transfected with IFN-β-Luc, pRL-TK, 200 ng N-RIG, and either 300 ng of HCoV-NL63 PLP2 or 300 ng of SARS-CoV PLpro. At 24 h posttransfection, cell lysates were prepared and assayed using the Dual-Luciferase reporter assay. (C) HEK293-TLR3 cells were transfected with IFN-β-Luc, pRL-TK, and either 300 ng of HCoV-NL63 PLP2 or 300 ng of SARS-CoV PLpro. At 24 h posttransfection, cells were either mock treated or treated with poly(IC) for 6 h. Following poly(IC) treatment, cell lysates were prepared and assayed using the Dual-Luciferase reporter assay. Error bars indicate standard deviations from the means for triplicates.

by Western blotting (Fig. 6B). These results indicate that enzymatic activity of PLP2 is not strictly required for inhibition of antiviral IFN expression.

The transmembrane (TM) form of PLP2 is also an IFN antagonist. The PLP domains are part of a larger nsp3 protein in SARS-CoV and HCoV-NL63 that is membrane bound. Previously we showed that the biologically relevant transmembrane-containing form of SARS-CoV PLpro, termed PLpro-TM, is a potent IFN antagonist (13). To determine if the membrane-tethered version of HCoV-NL63 PLP2 can function as an interferon antagonist, the NL63 TM sequence was cloned into the PLP2 construct in frame with the V5 epitope tag, and the resulting construct was designated PLP2-TM. HEK293 cells were transfected with PLP2-TM or the catalytic mutant PLP2-TM C1678A or PLP2-TM H1836A, along with the IFN-β and pRL-TK reporters. N-RIG was used to stimulate IFN-β induction. We found that PLP2-TM and the catalytic mutants were able to inhibit N-RIG-induced IFN-β reporter activity in a dose-dependent manner, although like the soluble version of PLP2, the catalytic mutants were less efficient than the wild type (Fig. 7A). Expression of the proteases was verified by Western blotting (Fig. 7B). These data corroborate our previous results indicating that the catalytic site is not essential for IFN-β antagonism by HCoV-NL63 PLP2.

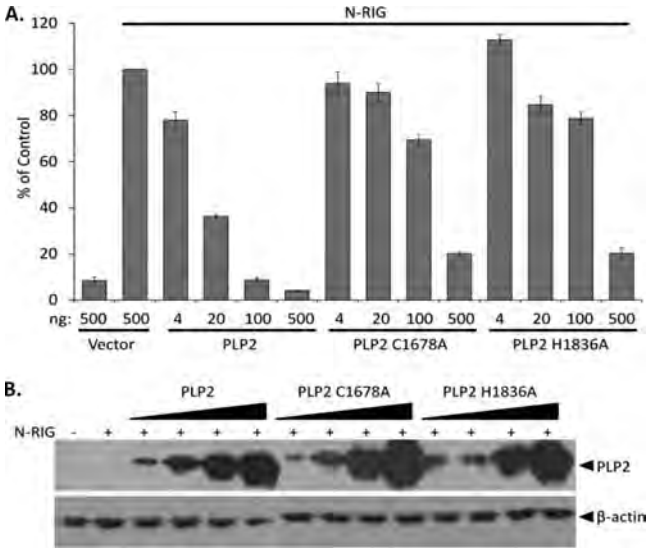

FIG. 6. HCoV-NL63 PLP2 and the catalytic mutants inhibit RIG-I-mediated IFN induction in a dose-dependent manner. PLP2 and the C1678A and H1836A catalytic mutants were cotransfected with IFN-β-Luc and pRL-TK reporters into HEK293 cells. A dominant active N-terminal portion of RIG-I was used to stimulate IFN-β induction. At 24 h posttransfection, cell lysates were harvested and assayed for luciferase activity via the Dual-Luciferase reporter assay. Values are expressed as percentages of N-RIG-stimulated luciferase controls set to 100. Error bars indicate standard deviations from the means for triplicates. (B) The cell lysates described above were mixed with 2× sample buffer and subjected to 12.5% SDS-PAGE. Following transfer to nitrocellulose, the membrane was blotted with mouse anti-V5 to detect the proteases and antiactin as a loading control.

PLpro IFN antagonism is not dependent on the ubiquitin-like domain. In addition to the downstream TM domain, a previous study suggested that the upstream ubiquitin-like domain (Ubl) plays a role in the IFN antagonism of SARS-CoV PLpro, since deletion of this domain in the soluble version of PLpro results in a loss of IFN antagonism (16). Currently, no analogous domain has been identified in HCoV-NL63 PLP2. To determine the role of the Ubl domain in the more biologically relevant transmembrane form of PLpro, we generated identical Ubl deletions (ΔUbl) of PLpro in both the soluble and transmembrane forms and performed a dose-response profile of IFN antagonism. In contrast to results of the study by Frieman and coworkers, we found that ΔUbl-PLpro-Sol was as potent as wild-type PLpro in inhibiting N-RIG-induced IFN-β reporter activity, as was ΔUbl-PLpro-TM (Fig. 8B). Expression of the proteases was verified by Western blotting (Fig. 8C). These results indicate that the Ubl domain of PLpro has no effect on antagonism of type I IFN induction.

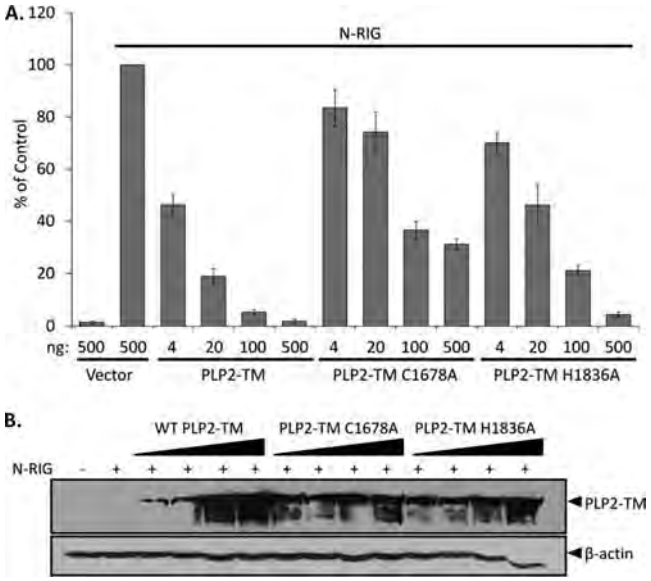

FIG. 7. The transmembrane form of HCoV-NL63 PLP2 and catalytic mutants inhibit RIG-I-mediated IFN-β induction in a dose-dependent manner. The native downstream hydrophobic domain was cloned into the PLP2 plasmid, and the catalytic cysteine or histidine residue was mutated to alanine. (A) HEK293 cells were transfected with the indicated amounts of PLP2-TM, PLP2-TM C1678A, or PLP2-TM H1836A along with the IFN-β-Luc and pRL-TK reporters. N-RIG was used to stimulate IFN-β induction. At 24 h posttransfection, cell lysates were harvested and assayed for luciferase activity via the Dual-Luciferase reporter assay. Values are expressed as percentages of N-RIG-stimulated luciferase controls set to 100. Error bars indicate standard deviations from the means for triplicates. (B) The cell lysates described above were mixed with 2× sample buffer and subjected to 12.5% SDS-PAGE. Following transfer to nitrocellulose, the membrane was blotted with mouse anti-V5 to detect the proteases and antiactin as a loading control.

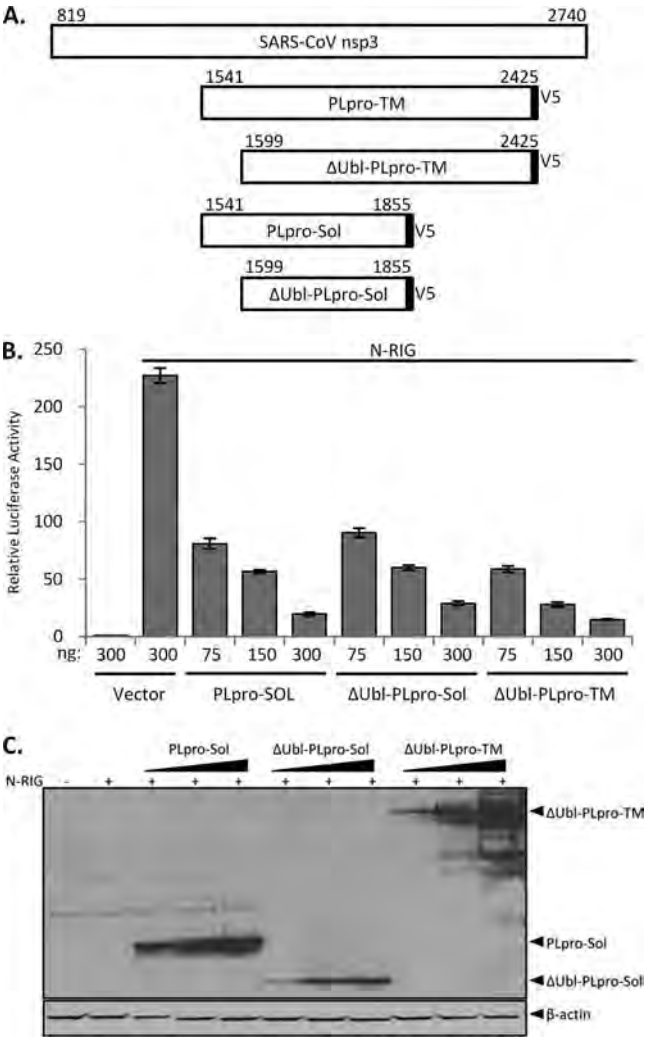

FIG. 8. The ubiquitin-like domain of SARS-CoV PLpro is not required for IFN antagonism. (A) Schematic diagram of nsp3 and the various V5-tagged deletion constructs. Numbers above the constructs indicate the amino acid numbers counting from ORF 1a. (B) HEK293 cells were transfected with the indicated amounts PLpro-Sol, ΔUbl-PLpro-Sol, or ΔUbl-PLpro-TM along with the IFN-β-Luc and pRL-TK reporters. A dominant active N-terminal portion of RIG-I was used to stimulate IFN-β induction. At 24 h posttransfection, cell lysates were harvested and assayed for luciferase activity via the Dual-Luciferase reporter assay. Values expressed are relative to results for cells transfected with the reporters alone. Error bars indicate standard deviations from the means for triplicates. (C) The cell lysates described above were mixed with 2× sample buffer and subjected to 12.5% SDS-PAGE. Following transfer to nitrocellulose, the membrane was blotted with mouse anti-V5 to detect the proteases and antiactin as a loading control.

Inhibition of SARS-CoV PLpro by protease inhibitor GRL-0617S has no effect on IFN-β or IFN-stimulated response element (ISRE) reporter activity but abrogates inhibition of NF-κB reporter activity. The mutagenesis data for PLP2 suggest that the catalytic residues (and thus catalytic activity) are not required for interferon antagonism, and Devaraj et al. reached a similar conclusion for SARS-CoV PLpro (13). To further evaluate the role of protease/DUB activity in interferon antagonism of wild-type PLpro, we added a protease inhibitor (GRL-0617S) that has been developed and shown to specifically and selectively block protease and DUB activity of SARS-CoV PLpro (56) and assessed the ability of PLpro to inhibit activation of IFN-β-Luc, ISRE-Luc, or NF-κB-Luc reporter activity. HEK293 cells were transfected with plasmid DNA encoding the transmembrane form of PLpro-TM (amino acids 1541 to 2425 of SARS-CoV ORF 1a), previously shown to be a potent IFN antagonist (13), and pRL-TK along with the IFN-β, ISRE, or NF-κB reporter, and an nsp2/3-GFP substrate. At the time of transfection, the cells were treated with 100 μM GRL-0617S (10 times the 50% effective concentration [EC_{50}]) or DMSO (vehicle control). At 24 h after transfection, cell lysates were generated and evaluated for induction of the reporters and proteolytic processing of the nsp2/3 substrate. We found that inhibition of protease activity by GRL-0617S had no effect on the IFN-β reporter (Fig. 9A) and little to no effect on the ISRE reporter, which is dependent on IRF-3 (Fig. 9B). We did detect an alleviation of PLpro-mediated inhibition of the NF-κB reporter by GRL-0617S (compare Fig. 9A and 9B with 9C). These results indicate that protease/DUB activity may be important for PLpro-mediated inhibition of NF-κB activity but not essential for inhibition of IRF-3 activity. To demonstrate efficacy of the protease inhibitor, cell lysates used in the reporter assay were assessed for nsp2/3-GFP substrate

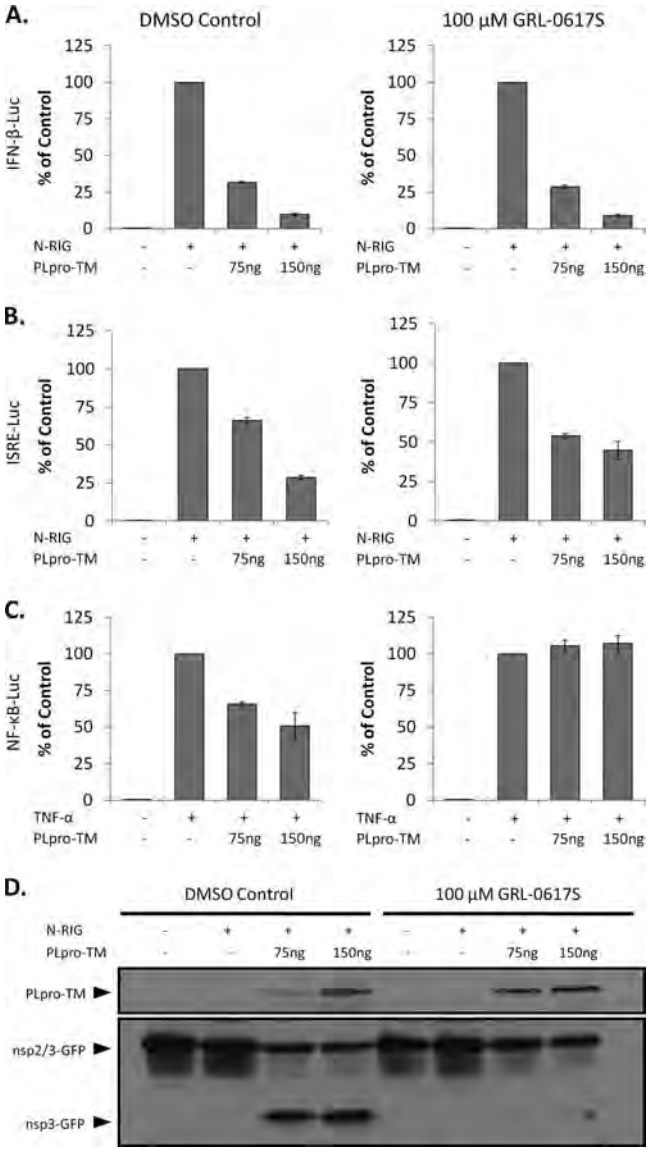

FIG. 9. SARS-CoV PLpro inhibits IFN-β and ISRE but not NF-κB reporter activity in a dose-dependent manner in the presence or absence of a protease inhibitor. HEK293 cells were transfected with the indicated amounts of PLpro-TM, pRL-TK, nsp2/3-GFP, and either IFN-β-Luc (A), ISRE-Luc (B), or NF-κB-Luc (C). N-RIG was used to stimulate IFN-β and ISRE. TNF-α (10 ng/ml) was used to stimulate the NF-κB-Luc reporter. DMSO vehicle control or 100 μM GRL-0617S was added at the time of transfection. At 24 h posttransfection, cell lysates were harvested and assayed for luciferase activity via the Dual-Luciferase reporter assay. Values are expressed as percentages of N-RIG- or TNF-α-stimulated luciferase controls, set to 100. Error bars indicate standard deviations from the means from triplicates. (D) The cell lysates described above were mixed with 2× sample buffer and subjected to 12.5% SDS-PAGE. Following transfer to nitrocellulose, the membrane was blotted with mouse anti-V5 to detect PLpro-TM and rabbit anti-GFP to detect the nsp2/3-GFP substrate and the nsp3-GFP cleavage product.

cleavage. The nsp2/3-GFP substrate contains a region of nsp2/nsp3 (including the cleavage site) fused in-frame with GFP and was previously shown to be a substrate for PLpro (16). As shown in Fig. 9D, the nsp3-GFP cleavage product was readily detected in cell lysates that contain PLpro in the absence of GRL-0617S. In contrast, the processing of nsp2/3-GFP and liberation of nsp3-GFP was almost completely abrogated in the presence of the drug. Overall, these data provide further support that there is a catalysis-independent component to type I IFN antagonism by the papain-like proteases of human coronaviruses.

DISCUSSION

In this study, we describe the multifunctional nature of the papain-like protease domains of NL63 and SARS coronaviruses. These coronavirus PLP domains act as viral proteases, deubiquitinating/deISGylating enzymes, and are able to antagonize innate immune induction of type I interferon. We found that PLP interferon antagonism is enhanced by, but is not strictly dependent on, the catalytic activity of the enzyme. Inhibition of coronavirus protease and DUB activity by mutagenesis or pharmacological means did not abrogate interferon antagonism. Therefore, these distinct PLP activities provide multiple targets for antiviral therapies.

The recognition of the DUB/deISGylating activity of SARS-CoV PLpro and HCoV-NL63 PLP2 provides new opportunities to investigate how the virus is modifying the host cell environment. Posttranslational modification of proteins by ubiquitin and ubiquitin-like (Ubl) molecules, such as SUMO, ISG15, and Nedd8, plays a critical role in the regulatory processes of virtually all aspects of cell biology (14, 15, 20, 22, 25, 29, 34, 41, 55). These modifications, though covalent, are highly reversible. Deubiquitinating enzymes can deconjugate Ub and Ub-like moieties and thus modulate the activities of ubiquitinated proteins. There are about 100 DUBs encoded in the human genome, and most of the known DUBs are cysteine proteases, characterized by a Cys-His-Asp catalytic triad (51). Several RNA viruses encode cysteine proteases to generate mature viral proteins necessary for replication, and many have been found to be multifunctional proteins. Like SARS-CoV PLpro and HCoV-NL63 PLP2, the protease of a nairovirus, Crimean Congo hemorrhagic fever virus (CCHFV), and the proteases of arteriviruses, including equine arteritis virus (EAV) and porcine respiratory and reproductive syndrome virus (PRRSV), have DUB and deISGylase activity (4, 15, 39). The contribution of these enzymatic activities to inhibition of type I IFN induction is currently poorly understood. A vast array of proteins involved in the type I IFN signaling cascade are activated by ubiquitination. Induction of IFN-β, for example, requires the activation of IRF-3 and NF-κB (45, 55). Ubiquitination is known to be intimately involved in the activation of NF-κB. Polyubiquitination of receptor-interacting protein (RIP), TNF receptor-associated factor 6 (TRAF6), and TNF receptor-associated factor 2 (TRAF2) activates these signaling intermediates, which leads to the polyubiquitination of IκB. IκB, which binds to and holds NF-κB inactive in the cytoplasm, is degraded via the proteasome, thereby freeing NF-κB to translocate to the nucleus and induce IFN-β transcription (20). Here we have shown that HCoV-NL63 PLP2 has a profound and global deconjugation effect on ubiquitinated cellular conjugates, suggesting that the DUB activity of PLP2 may modulate NF-κB activation. In addition, we demonstrate that protease inhibitors, which block coronavirus

DUB activity, abrogate the moderate inhibition of NF-κB reporter activity imposed by transient, ectopic expression of PLpro. These results support a role for coronavirus DUBs in modulating the NF-κB response during coronavirus replication. However, further investigation is needed to delineate the physiological effect of coronavirus PLPs on NF-κB signaling, since SARS-CoV PLpro did not inhibit virus- or double-stranded RNA (dsRNA)-induced activation of two well-characterized NF-κB-dependent genes, encoding interleukin 6 (IL-6) and A20, when it was stably expressed in HeLa cells in a tetracycline-regulated fashion (13).

The effect of ISGylation of cellular proteins on the antiviral response is far less understood. It is known that ISG15 conjugation is required for protection against lethal Sindbis virus infection of IFN-α/β receptor knockout mice (15). Also, ISGylation has been shown to influence the activation of the JAK/STAT pathway, involved in type I IFN signaling (44). Intriguingly, IRF-3 also undergoes ISGylation during viral infections, which was found to enhance innate antiviral responses by inhibiting virus-induced IRF-3 degradation (43). We found that HCoV-NL63 PLP2 globally deconjugates ISG15 similarly to its deconjugation of Ub, and this activity depends on the catalytic sites of PLP2. Although the contribution of the deISGylation activity of PLP2 to IFN antagonism remains to be further investigated, deISGylation of IRF-3 is unlikely to be a significant contributing factor, since the PLP catalytic mutants devoid of deISGylation activity still effectively inhibited IFN induction.

Using human airway epithelial cells, which represent a cell culture model for respiratory infection, we found that IFN-β release induced by HCoV-NL63 was weak but measurable. This finding is similar to weak IFN induction by the far more pathogenic human coronavirus SARS-CoV, suggesting that antagonism of type I IFN is a common trait of coronavirus infection (13, 58, 63). In addition to PLpro, SARS-CoV encodes several other IFN antagonists. ORF 3b, ORF 6, and nucleocapsid inhibit type I IFN induction via inhibition of IRF-3 phosphorylation and its subsequent nuclear translocation (30). ORF 6 and nsp1 have been shown to inhibit IFN signaling by interfering with the activity of STAT1 (17, 27, 48). Mouse hepatitis virus also encodes several IFN antagonists, including nsp1, nucleocapsid, and PLP2 (58, 68, 70). Thus, there is clear evolutionary pressure to encode and maintain multiple IFN antagonists. It has yet to be determined if nsp1 and nucleocapsid from HCoV-NL63 are IFN antagonists as well.

Using reporter assays, we found that HCoV-NL63 PLP2 can antagonize type I IFN induction independently of catalytic activity. Catalytic mutants of PLP2 can dose-dependently inhibit IFN-β induction; however, this inhibition is reduced compared to equivalent amounts of wild-type PLP2. In addition, we note that the presence of the transmembrane domain confers enhanced IFN antagonism, particularly in the catalytic mutants. We speculate that the TM domain may facilitate either protein folding or interaction with cellular protein partners. Overall, the antagonism profile of HCoV-NL63 PLP2 is remarkably similar to that of PLpro of SARS-CoV. In fact, using a known specific inhibitor of SARS-CoV PLpro (GRL-0617S), we found that PLpro can effectively inhibit type I IFN induction despite a profound reduction in proteolysis, which corroborates the notion of a catalysis-independent mechanism for type I IFN antagonism. Previously we showed that SARS-CoV PLpro is able to inhibit the phosphorylation and nuclear accumulation of IRF-3 following Sendai virus infection (13). We found that HCoV-NL63 PLP2 was also able to inhibit the translocation of IRF-3 to the nucleus (data not shown); however, the mechanism of this inhibition is not yet clear. We are actively searching for cellular factors that associate with HCoV-NL63 PLP2 as well as SARS-CoV PLpro.

The crystal structure of SARS-CoV PLpro has identified a unique domain that has remarkable similarity to ubiquitin (57). Frieman and coworkers reported that removal of the Ubl domain in the soluble version of PLpro resulted in a loss of IFN antagonism (16). However, we note that the authors of that study assessed IFN antagonism using one concentration of PLpro. In this study, by performing a dose-response profile of IFN antagonism, we found that deletion of the Ubl domain from both the soluble and the transmembrane version of PLpro had no effect on IFN antagonism. Thus, it is critical to assess the effect of IFN antagonism across a range of protein concentrations to fully evaluate the activity of these proteases.

Many viruses have been shown to inhibit the transcriptional activity of IRF-3 in a wide variety of ways (9, 24, 52). Some viruses inhibit IRF-3 phosphorylation, dimerization, and/or translocation to the nucleus. Others can induce IRF-3 degradation or sequester the transcription factor (11, 23). The mechanism of inhibition that can lead to these phenotypes can occur directly on IRF-3 or may affect any of the vast array of proteins upstream of IRF-3 in the type I IFN induction cascade. For example, the VP35 protein of Ebola Zaire virus (EBOV) has been shown to impact IRF-3 activity by binding dsRNA, thus preventing detection by RIG-I (5, 6). In addition, VP35 was shown to interact with Ubc9 (SUMO E2 enzyme), PIAS1 (SUMO E3 ligase), and IRF-7, leading to SUMOylation of IRF-7 and transcriptional repression of the IFN-β promoter (10). Respiratory syncytial virus (RSV) encodes two proteins, NS1 and NS2, that act individually or cooperatively to inhibit the activity of IRF-3. It was reported that these proteins reduce the expression of key kinases involved in IRF-3 phosphorylation (TRAF3 and IκB kinase epsilon [IKKε]), but how NS1 and NS2 induce TRAF3 and IKKε degradation is still unclear (64). Coronavirus PLPs could be acting on an as yet unidentified cellular factor involved in the IFN induction cascade. For example, in a recent study by Schröder et al., a new protein, DEAD box protein 3 (DDX3), was found to be involved in the type I IFN cascade. DDX3 was identified by coimmunoprecipitation with an IFN antagonist from vaccinia virus (VACV) protein K7 (59). Alternatively, it is intriguing to speculate that coronavirus PLPs may function by sequestering polyubiquitin complexes or membrane-associated factors, such as STING/MITA (26, 67, 72). Previously we showed that the block must be downstream of TBK1 but at or upstream of IRF-3 since a constitutively active form of IRF-3 is not blocked by PLpro (13). Further studies are needed to elucidate the mechanism by which coronavirus PLPs modulate IRF-3 activity.

The multiple enzymatic activities of SARS-CoV PLpro and HCoV-NL63 PLP2 may all influence the host cell type I IFN response. The DUB activity of these proteins could modulate the activity of key players in the signaling cascade that are known to be activated by lysine-48- or lysine-63-linked poly-

ubiquitination. Our data suggest that catalytic activity may contribute to IFN antagonism but ablation of proteolysis does not abrogate IFN antagonism. Thus, coronavirus PLPs also possess a catalytic activity-independent mechanism that acts to inhibit IFN induction. We are currently working to delineate both the DUB and catalytic activity-independent mechanism by which coronavirus PLPs inhibit type I IFN induction.

The data presented in this study draw significant parallels between the single papain-like protease of SARS-CoV PLpro and the second papain-like protease of HCoV-NL63 PLP2. Despite modest sequence identity (~19%), these two proteases have similar enzymatic activities and can inhibit type I IFN induction independently of catalytic activity. Since coronavirus PLpro/PLP2 domains are required for viral replication, they are attractive targets for antiviral therapeutics. Indeed, inhibitors of SARS-CoV PLpro have been shown to block virus replication (56). Though less pathogenic than SARS-CoV, HCoV-NL63 causes significant morbidity in children, the elderly, and immune-compromised individuals and has been shown to be an etiological agent causing croup (65, 66). In addition, we now recognize that bats and other mammals can serve as reservoirs for potentially emerging pandemic coronaviruses (32, 37). Thus, further studies of these multifunctional coronavirus PLPs are needed to determine if both protease inhibitors and blockers of interferon antagonism can be developed to reduce replication and pathogenesis of human and zoonotic coronaviruses.

ACKNOWLEDGMENTS

We thank members of the Baker lab for helpful discussions.

The work was supported by NIH grant P01AI060915 (to S.C.B., A.K.G., and A.D.M.), DoD grant W81XWH-09-01-0391 (to Gerald Byrne), and grants from the National Natural Science Foundation of China (30870536 and 30972761 to Z.C.) and Beijing Municipal Natural Science Foundation (7092075 to Z.C.). M.A.C. and B.S.B. were supported by NIH training grant T32AI007508.

REFERENCES

1. **Banach, B., J. M. Orenstein, L. M. Fox, S. H. Randell, A. H. Rowley, and S. C. Baker.** 2009. Human airway epithelial cell culture to identify new respiratory viruses: coronavirus NL63 as a model. J. Virol. Methods **156:**19–26.
2. **Barral, P. M., D. Sarkar, P. B. Fisher, and V. R. Racaniello.** 2009. RIG-I is cleaved during picornavirus infection. Virology **391:**171–176.
3. **Barral, P. M., D. Sarkar, Z. Z. Su, G. N. Barber, R. DeSalle, V. R. Racaniello, and P. B. Fisher.** 2009. Functions of the cytoplasmic RNA sensors RIG-I and MDA-5: key regulators of innate immunity. Pharmacol. Ther. **124:**219–234.
4. **Barretto, N., D. Jukneliene, K. Ratia, Z. Chen, A. D. Mesecar, and S. C. Baker.** 2005. The papain-like protease of severe acute respiratory syndrome coronavirus has deubiquitinating activity. J. Virol. **79:**15189–15198.
5. **Basler, C. F., A. Mikulasova, L. Martinez-Sobrido, J. Paragas, E. Muhlberger, M. Bray, H. D. Klenk, P. Palese, and A. Garcia-Sastre.** 2003. The Ebola virus VP35 protein inhibits activation of interferon regulatory factor 3. J. Virol. **77:**7945–7956.
6. **Basler, C. F., X. Wang, E. Muhlberger, V. Volchkov, J. Paragas, H. D. Klenk, A. Garcia-Sastre, and P. Palese.** 2000. The Ebola virus VP35 protein functions as a type I IFN antagonist. Proc. Natl. Acad. Sci. U. S. A. **97:**12289–12294.
7. **Bhoj, V. G., and Z. J. Chen.** 2009. Ubiquitylation in innate and adaptive immunity. Nature **458:**430–437.
8. **Bibeau-Poirier, A., and M. J. Servant.** 2008. Roles of ubiquitination in pattern-recognition receptors and type I interferon receptor signaling. Cytokine **43:**359–367.
9. **Bowie, A. G., and L. Unterholzner.** 2008. Viral evasion and subversion of pattern-recognition receptor signalling. Nat. Rev. Immunol. **8:**911–922.
10. **Chang, T. H., T. Kubota, M. Matsuoka, S. Jones, S. B. Bradfute, M. Bray, and K. Ozato.** 2009. Ebola Zaire virus blocks type I interferon production by exploiting the host SUMO modification machinery. PLoS Pathog. **5:**e1000493.
11. **Chen, Z., R. Rijnbrand, R. K. Jangra, S. G. Devaraj, L. Qu, Y. Ma, S. M. Lemon, and K. Li.** 2007. Ubiquitination and proteasomal degradation of interferon regulatory factor-3 induced by Npro from a cytopathic bovine viral diarrhea virus. Virology **366:**277–292.
12. **Chen, Z., Y. Wang, K. Ratia, A. D. Mesecar, K. D. Wilkinson, and S. C. Baker.** 2007. Proteolytic processing and deubiquitinating activity of papain-like proteases of human coronavirus NL63. J. Virol. **81:**6007–6018.
13. **Devaraj, S. G., N. Wang, Z. Chen, Z. Chen, M. Tseng, N. Barretto, R. Lin, C. J. Peters, C. T. Tseng, S. C. Baker, and K. Li.** 2007. Regulation of IRF-3-dependent innate immunity by the papain-like protease domain of the severe acute respiratory syndrome coronavirus. J. Biol. Chem. **282:**32208–32221.
14. **Evans, P. C., H. Ovaa, M. Hamon, P. J. Kilshaw, S. Hamm, S. Bauer, H. L. Ploegh, and T. S. Smith.** 2004. Zinc-finger protein A20, a regulator of inflammation and cell survival, has de-ubiquitinating activity. Biochem. J. **378:**727–734.
15. **Frias-Staheli, N., N. V. Giannakopoulos, M. Kikkert, S. L. Taylor, A. Bridgen, J. Paragas, J. A. Richt, R. R. Rowland, C. S. Schmaljohn, D. J. Lenschow, E. J. Snijder, A. Garcia-Sastre, and H. W. Virgin IV.** 2007. Ovarian tumor domain-containing viral proteases evade ubiquitin- and ISG15-dependent innate immune responses. Cell Host Microbe **2:**404–416.
16. **Frieman, M., K. Ratia, R. E. Johnston, A. D. Mesecar, and R. S. Baric.** 2009. Severe acute respiratory syndrome coronavirus papain-like protease ubiquitin-like domain and catalytic domain regulate antagonism of IRF3 and NF-kappaB signaling. J. Virol. **83:**6689–6705.
17. **Frieman, M., B. Yount, M. Heise, S. A. Kopecky-Bromberg, P. Palese, and R. S. Baric.** 2007. Severe acute respiratory syndrome coronavirus ORF6 antagonizes STAT1 function by sequestering nuclear import factors on the rough endoplasmic reticulum/Golgi membrane. J. Virol. **81:**9812–9824.
18. **Goldsmith, C. S., K. M. Tatti, T. G. Ksiazek, P. E. Rollin, J. A. Comer, W. W. Lee, P. A. Rota, B. Bankamp, W. J. Bellini, and S. R. Zaki.** 2004. Ultrastructural characterization of SARS coronavirus. Emerg. Infect. Dis. **10:**320–326.
19. **Gosert, R., A. Kanjanahaluethai, D. Egger, K. Bienz, and S. C. Baker.** 2002. RNA replication of mouse hepatitis virus takes place at double-membrane vesicles. J. Virol. **76:**3697–3708.
20. **Haglund, K., and I. Dikic.** 2005. Ubiquitylation and cell signaling. EMBO J. **24:**3353–3359.
21. **Herzog, P., C. Drosten, and M. A. Muller.** 2008. Plaque assay for human coronavirus NL63 using human colon carcinoma cells. Virol. J. **5:**138.
22. **Hicke, L., and R. Dunn.** 2003. Regulation of membrane protein transport by ubiquitin and ubiquitin-binding proteins. Annu. Rev. Cell Dev. Biol. **19:**141–172.
23. **Higgs, R., J. Ni Gabhann, N. Ben Larbi, E. P. Breen, K. A. Fitzgerald, and C. A. Jefferies.** 2008. The E3 ubiquitin ligase Ro52 negatively regulates IFN-beta production post-pathogen recognition by polyubiquitin-mediated degradation of IRF3. J. Immunol. **181:**1780–1786.
24. **Honda, K., and T. Taniguchi.** 2006. IRFs: master regulators of signalling by Toll-like receptors and cytosolic pattern-recognition receptors. Nat. Rev. Immunol. **6:**644–658.
25. **Isaacson, M. K., and H. L. Ploegh.** 2009. Ubiquitination, ubiquitin-like modifiers, and deubiquitination in viral infection. Cell Host Microbe **5:**559–570.
26. **Ishikawa, H., and G. N. Barber.** 2008. STING is an endoplasmic reticulum adaptor that facilitates innate immune signalling. Nature **455:**674–678.
27. **Kamitani, W., K. Narayanan, C. Huang, K. Lokugamage, T. Ikegami, N. Ito, H. Kubo, and S. Makino.** 2006. Severe acute respiratory syndrome coronavirus nsp1 protein suppresses host gene expression by promoting host mRNA degradation. Proc. Natl. Acad. Sci. U. S. A. **103:**12885–12890.
28. **Kayagaki, N., Q. Phung, S. Chan, R. Chaudhari, C. Quan, K. M. O'Rourke, M. Eby, E. Pietras, G. Cheng, J. F. Bazan, Z. Zhang, D. Arnott, and V. M. Dixit.** 2007. DUBA: a deubiquitinase that regulates type I interferon production. Science **318:**1628–1632.
29. **Kirkin, V., and I. Dikic.** 2007. Role of ubiquitin- and Ubl-binding proteins in cell signaling. Curr. Opin. Cell Biol. **19:**199–205.
30. **Kopecky-Bromberg, S. A., L. Martinez-Sobrido, M. Frieman, R. A. Baric, and P. Palese.** 2007. Severe acute respiratory syndrome coronavirus open reading frame (ORF) 3b, ORF 6, and nucleocapsid proteins function as interferon antagonists. J. Virol. **81:**548–557.
31. **Koyama, S., K. J. Ishii, C. Coban, and S. Akira.** 2008. Innate immune response to viral infection. Cytokine **43:**336–341.
32. **Lau, S. K., P. C. Woo, K. S. Li, Y. Huang, H. W. Tsoi, B. H. Wong, S. S. Wong, S. Y. Leung, K. H. Chan, and K. Y. Yuen.** 2005. Severe acute respiratory syndrome coronavirus-like virus in Chinese horseshoe bats. Proc. Natl. Acad. Sci. U. S. A. **102:**14040–14045.
33. **Lenschow, D. J., N. V. Giannakopoulos, L. J. Gunn, C. Johnston, A. K. O'Guin, R. E. Schmidt, B. Levine, and H. W. Virgin IV.** 2005. Identification of interferon-stimulated gene 15 as an antiviral molecule during Sindbis virus infection in vivo. J. Virol. **79:**13974–13983.
34. **Lenschow, D. J., C. Lai, N. Frias-Staheli, N. V. Giannakopoulos, A. Lutz, T. Wolff, A. Osiak, B. Levine, R. E. Schmidt, A. Garcia-Sastre, D. A. Leib, A. Pekosz, K. P. Knobeloch, I. Horak, and H. W. Virgin IV.** 2007. IFN-stimu-

lated gene 15 functions as a critical antiviral molecule against influenza, herpes, and Sindbis viruses. Proc. Natl. Acad. Sci. U. S. A. **104:**1371–1376.
35. **Li, K., Z. Chen, N. Kato, M. Gale, Jr., and S. M. Lemon.** 2005. Distinct poly(I-C) and virus-activated signaling pathways leading to interferon-beta production in hepatocytes. J. Biol. Chem. **280:**16739–16747.
36. **Li, K., E. Foy, J. C. Ferreon, M. Nakamura, A. C. Ferreon, M. Ikeda, S. C. Ray, M. Gale, Jr., and S. M. Lemon.** 2005. Immune evasion by hepatitis C virus NS3/4A protease-mediated cleavage of the Toll-like receptor 3 adaptor protein TRIF. Proc. Natl. Acad. Sci. U. S. A. **102:**2992–2997.
37. **Li, W., Z. Shi, M. Yu, W. Ren, C. Smith, J. H. Epstein, H. Wang, G. Crameri, Z. Hu, H. Zhang, J. Zhang, J. McEachern, H. Field, P. Daszak, B. T. Eaton, S. Zhang, and L. F. Wang.** 2005. Bats are natural reservoirs of SARS-like coronaviruses. Science **310:**676–679.
38. **Li, X. D., L. Sun, R. B. Seth, G. Pineda, and Z. J. Chen.** 2005. Hepatitis C virus protease NS3/4A cleaves mitochondrial antiviral signaling protein off the mitochondria to evade innate immunity. Proc. Natl. Acad. Sci. U. S. A. **102:**17717–17722.
39. **Lindner, H. A., N. Fotouhi-Ardakani, V. Lytvyn, P. Lachance, T. Sulea, and R. Menard.** 2005. The papain-like protease from the severe acute respiratory syndrome coronavirus is a deubiquitinating enzyme. J. Virol. **79:**15199–15208.
40. **Lindner, H. A., V. Lytvyn, H. Qi, P. Lachance, E. Ziomek, and R. Menard.** 2007. Selectivity in ISG15 and ubiquitin recognition by the SARS coronavirus papain-like protease. Arch. Biochem. Biophys. **466:**8–14.
41. **Liu, Y. C., J. Penninger, and M. Karin.** 2005. Immunity by ubiquitylation: a reversible process of modification. Nat. Rev. Immunol. **5:**941–952.
42. **Loo, Y. M., D. M. Owen, K. Li, A. K. Erickson, C. L. Johnson, P. M. Fish, D. S. Carney, T. Wang, H. Ishida, M. Yoneyama, T. Fujita, T. Saito, W. M. Lee, C. H. Hagedorn, D. T. Lau, S. A. Weinman, S. M. Lemon, and M. Gale, Jr.** 2006. Viral and therapeutic control of IFN-beta promoter stimulator 1 during hepatitis C virus infection. Proc. Natl. Acad. Sci. U. S. A. **103:**6001–6006.
43. **Lu, G., J. T. Reinert, I. Pitha-Rowe, A. Okumura, M. Kellum, K. P. Knobeloch, B. Hassel, and P. M. Pitha.** 2006. ISG15 enhances the innate antiviral response by inhibition of IRF-3 degradation. Cell Mol. Biol. (Noisy-le-grand) **52:**29–41.
44. **Malakhova, O. A., and D. E. Zhang.** 2008. ISG15 inhibits Nedd4 ubiquitin E3 activity and enhances the innate antiviral response. J. Biol. Chem. **283:**8783–8787.
45. **Maniatis, T., J. V. Falvo, T. H. Kim, T. K. Kim, C. H. Lin, B. S. Parekh, and M. G. Wathelet.** 1998. Structure and function of the interferon-beta enhanceosome. Cold Spring Harb. Symp. Quant. Biol. **63:**609–620.
46. **Meylan, E., J. Curran, K. Hofmann, D. Moradpour, M. Binder, R. Bartenschlager, and J. Tschopp.** 2005. Cardif is an adaptor protein in the RIG-I antiviral pathway and is targeted by hepatitis C virus. Nature **437:**1167–1172.
47. **Meylan, E., and J. Tschopp.** 2006. Toll-like receptors and RNA helicases: two parallel ways to trigger antiviral responses. Mol. Cell **22:**561–569.
48. **Narayanan, K., C. Huang, K. Lokugamage, W. Kamitani, T. Ikegami, C. T. Tseng, and S. Makino.** 2008. Severe acute respiratory syndrome coronavirus nsp1 suppresses host gene expression, including that of type I interferon, in infected cells. J. Virol. **82:**4471–4479.
49. **Neznanov, N., K. M. Chumakov, L. Neznanova, A. Almasan, A. K. Banerjee, and A. V. Gudkov.** 2005. Proteolytic cleavage of the p65-RelA subunit of NF-kappaB during poliovirus infection. J. Biol. Chem. **280:**24153–24158.
50. **Nicholson, B., C. A. Leach, S. J. Goldenberg, D. M. Francis, M. P. Kodrasov, X. Tian, J. Shanks, D. E. Sterner, A. Bernal, M. R. Mattern, K. D. Wilkinson, and T. R. Butt.** 2008. Characterization of ubiquitin and ubiquitin-like-protein isopeptidase activities. Protein Sci. **17:**1035–1043.
51. **Nijman, S. M., M. P. Luna-Vargas, A. Velds, T. R. Brummelkamp, A. M. Dirac, T. K. Sixma, and R. Bernards.** 2005. A genomic and functional inventory of deubiquitinating enzymes. Cell **123:**773–786.
52. **Ozato, K., P. Tailor, and T. Kubota.** 2007. The interferon regulatory factor family in host defense: mechanism of action. J. Biol. Chem. **282:**20065–20069.
53. **Perlman, S., and J. Netland.** 2009. Coronaviruses post-SARS: update on replication and pathogenesis. Nat. Rev. Microbiol. **7:**439–450.
54. **Pichlmair, A., and C. Reis e Sousa.** 2007. Innate recognition of viruses. Immunity **27:**370–383.
55. **Platanias, L. C.** 2005. Mechanisms of type-I- and type-II-interferon-mediated signalling. Nat. Rev. Immunol. **5:**375–386.
56. **Ratia, K., S. Pegan, J. Takayama, K. Sleeman, M. Coughlin, S. Baliji, R. Chaudhuri, W. Fu, B. S. Prabhakar, M. E. Johnson, S. C. Baker, A. K. Ghosh, and A. D. Mesecar.** 2008. A noncovalent class of papain-like protease/deubiquitinase inhibitors blocks SARS virus replication. Proc. Natl. Acad. Sci. U. S. A. **105:**16119–16124.
57. **Ratia, K., K. S. Saikatendu, B. D. Santarsiero, N. Barretto, S. C. Baker, R. C. Stevens, and A. D. Mesecar.** 2006. Severe acute respiratory syndrome coronavirus papain-like protease: structure of a viral deubiquitinating enzyme. Proc. Natl. Acad. Sci. U. S. A. **103:**5717–5722.
58. **Roth-Cross, J. K., L. Martinez-Sobrido, E. P. Scott, A. Garcia-Sastre, and S. R. Weiss.** 2007. Inhibition of the alpha/beta interferon response by mouse hepatitis virus at multiple levels. J. Virol. **81:**7189–7199.
59. **Schroder, M., M. Baran, and A. G. Bowie.** 2008. Viral targeting of DEAD box protein 3 reveals its role in TBK1/IKKepsilon-mediated IRF activation. EMBO J. **27:**2147–2157.
60. **Sheahan, T., B. Rockx, E. Donaldson, A. Sims, R. Pickles, D. Corti, and R. Baric.** 2008. Mechanisms of zoonotic severe acute respiratory syndrome coronavirus host range expansion in human airway epithelium. J. Virol. **82:**2274–2285.
61. **Snijder, E. J., Y. van der Meer, J. Zevenhoven-Dobbe, J. J. Onderwater, J. van der Meulen, H. K. Koerten, and A. M. Mommaas.** 2006. Ultrastructure and origin of membrane vesicles associated with the severe acute respiratory syndrome coronavirus replication complex. J. Virol. **80:**5927–5940.
62. **Spiegel, M., A. Pichlmair, L. Martinez-Sobrido, J. Cros, A. Garcia-Sastre, O. Haller, and F. Weber.** 2005. Inhibition of Beta interferon induction by severe acute respiratory syndrome coronavirus suggests a two-step model for activation of interferon regulatory factor 3. J. Virol. **79:**2079–2086.
63. **Spiegel, M., K. Schneider, F. Weber, M. Weidmann, and F. T. Hufert.** 2006. Interaction of severe acute respiratory syndrome-associated coronavirus with dendritic cells. J. Gen. Virol. **87:**1953–1960.
64. **Swedan, S., A. Musiyenko, and S. Barik.** 2009. Respiratory syncytial virus nonstructural proteins decrease multiple members of the cellular interferon pathways. J. Virol. **83:**9682–9693.
65. **van der Hoek, L., K. Sure, G. Ihorst, A. Stang, K. Pyrc, M. F. Jebbink, G. Petersen, J. Forster, B. Berkhout, and K. Uberla.** 2005. Croup is associated with the novel coronavirus NL63. PLoS Med. **2:**e240.
66. **van der Hoek, L., K. Sure, G. Ihorst, A. Stang, K. Pyrc, M. F. Jebbink, G. Petersen, J. Forster, B. Berkhout, and K. Uberla.** 2006. Human coronavirus NL63 infection is associated with croup. Adv. Exp. Med. Biol. **581:**485–491.
67. **Xia, Z. P., L. Sun, X. Chen, G. Pineda, X. Jiang, A. Adhikari, W. Zeng, and Z. J. Chen.** 2009. Direct activation of protein kinases by unanchored polyubiquitin chains. Nature **461:**114–119.
68. **Ye, Y., K. Hauns, J. O. Langland, B. L. Jacobs, and B. G. Hogue.** 2007. Mouse hepatitis coronavirus A59 nucleocapsid protein is a type I interferon antagonist. J. Virol. **81:**2554–2563.
69. **Zhao, C., C. Denison, J. M. Huibregtse, S. Gygi, and R. M. Krug.** 2005. Human ISG15 conjugation targets both IFN-induced and constitutively expressed proteins functioning in diverse cellular pathways. Proc. Natl. Acad. Sci. U. S. A. **102:**10200–10205.
70. **Zheng, D., G. Chen, B. Guo, G. Cheng, and H. Tang.** 2008. PLP2, a potent deubiquitinase from murine hepatitis virus, strongly inhibits cellular type I interferon production. Cell Res. **18:**1105–1113.
71. **Zheng, L., U. Baumann, and J. L. Reymond.** 2004. An efficient one-step site-directed and site-saturation mutagenesis protocol. Nucleic Acids Res. **32:**e115.
72. **Zhong, B., Y. Yang, S. Li, Y. Y. Wang, Y. Li, F. Diao, C. Lei, X. He, L. Zhang, P. Tien, and H. B. Shu.** 2008. The adaptor protein MITA links virus-sensing receptors to IRF3 transcription factor activation. Immunity **29:**538–550.